Acoustic sensors

Jean-Michel Friedt

Habilitation à diriger les recherches

Université de Franche Comté

Spécialité : Sciences pour l'Ingénieur

Jean-Michel FRIEDT

Capteurs acoustiques

presentée le 21 juin 2010 devant le jury composé de

B. Cretin	**Président**
E. Gizeli	**Rapporteurs**
D. Rebière	
L. Reindl	
D. Royer	

Université de Franche Comté, Besançon, France

Habilitation

Franche Comté University

Engineering department

Jean-Michel FRIEDT

Acoustic sensors

Defense date: 06/21/2010

Committee in charge:

B. Cretin	Chairman
E. Gizeli	Reporters
D. Rebière	
L. Reindl	
D. Royer	

Franche Comté University, Besançon, France

Contents

Chapter 1

General introduction

The central topic of all the discussions in this manuscript is around *acoustic-sensor based* measurement systems. Throughout this document, "acoustic" means the propagation of a mechanical wave on, or within, a substrate. However, we will discuss many other physical principles applied for sensing techniques, whether optical, scanning probe microscopy, electrochemistry.

The substrate we use in most of the discussions is quartz, keeping in mind that piezoelectricity is the main effect used for energy conversion, yielding an electrical measurement related to acoustic effects:

- this piezoelectric, and hence anisotropic, material provides a rich environment for developing sensors with properties dominantly affected by one physical phenomenom, such as surface mass adsorption (gravimetric sensor), temperature, stress (physical sensors) depending on the sensor design
- various kinds of waves are propagated, again depending on design considerations, yielding a vast field of research since each wave will be better suited for sensing a given material property,
- the piezoelectric effect is either used for actuating (reverse piezoelectric effect) or sensing: we shall for example use a patterned homogeneous quartz substrate to propagate plane wave (quartz crystal resonator, surface acoustic wave resonator) or machined devices to provide nanometric resolution (tuning fork for shear force miroscopy). In the latter example, actuation and sensing combined in the same transducer reduces the volume of the experiment (as opposed for example to silicon cantilevers for AFM which require a laser, focusing lenses and a photodetector) and hence the opportunity to use the sensor in environments unreachable to more cumbersome experimental setups.

Beyond the transducer which includes the piezoelectric substrate patterned with electrodes, an emphasis is placed on the development of the associated instrument, whether for

qualification purposes (calibration) or to allow laboratories which are not dedicated to working with radiofrequency instruments to use these sensors.

This presentation will mostly follow an historic evolution of the research I performed first in Belgium in the Biosensors group of IMEC in Leuven under the supervision of A. Campitelli, and later in France within the FEMTO-ST institute, under the supervision of S. Ballandras, where I have been hosted while being employed by the SENSeOR startup company. The complexity of the sensors follows the availability of simulation tools needed to design more complex sensors as well as the access to technology dedicated to piezoelectric substrates:

- an acoustic delay line is defined by two interdigitated transducers separated by a gap called the sensing area. An acoustic wave is launched with one transducer using the inverse piezoelectric effect, and received on the other transducer after a single propagation over the acoustic path. The apparent simplicity of the transducer allows for simple, or more complex (apodization, chirp, unidirectional), design and manufacturing process with minimal clean room constraints, while the measurement analysis are in a first gravimetric approximation analyzed using a transmission line model,

- an acoustic resonator is defined by two Bragg mirrors surrounding one or two interdigitated transducer (IDT) in case of a surface acoustic wave device, or by strong acoustic reflections associated with the large acoustic impedance variation at the substrate-medium (air or water) interface in the case of a bulk acoustic wave. The Bragg mirror confines the acoustic wave within the acoustic cavity: the equivalent length of the IDT is given by the number of reflections of the acoustic wave within the cavity, also known as the quality factor of the device. The design of a resonator requires simulation tools to accurately model the reflection coefficient of the mirror and design a synchronous structure in which the energy of all reflections add coherently within the cavity. Such modelling tool have been developed by the *time and frequency group of FEMTO-ST* consisting of a combination of mixed matrix model (for combining the properties of the propagation path, IDT and mirrors) and finite element analysis (for modelling the propagation and reflection characteristics of each elementary domain). These tools are also used beyond the design step for the quantitative analysis of experimental data: the set of properties of the medium interacting with the propagating or confined acoustic wave is injected into the model and iterated until the simulations fit the experimental data. Using this approach, we demonstrate for example the separation of the gravimetric and viscoelastic contributions during biochemical species adsorption experiments. Accurate simulations are furthermore needed for the analysis of resonator data whose quality factor (either through dissipation during the acoustic propagation or loss of reflection efficiency in the Bragg mirrors) evolves in parallel with the resonance frequency shift.

The strategy along which all these topics are developed – whether thin organic film characterization or physical quantities measurement – is towards the *understanding* of the interaction of the probe signal (most often an acoustic wave) with the surrounding medium. This requirement might lead us towards the identification of thin film properties which are usually not found in the literature unless one accepts the assumption that bulk properties are valid in films of a few nanometers thick. Hence, the work on biosensors will mainly focus on sim-

ple interaction mechanisms (physisorption or simple and well understood chemical binding mechanisms) to emphasize the thin film mechanical properties characterization. *Identifying* physical properties of thin films requires the measurement of at least as many variable as there are parameters to be identified, ideally with enough time resolution to extract kinetics. The **multiphysical approach** I have developed throughout the biosensor application projects aims at combining enough complementary measurement methods (acoustic velocity and loss, optical resonance angle and wavelength, electrochemical potential, scanning probe topography) to extract unique layer parameters relevant to biosensor modelling, including thin film density, thickness, viscosity, conductivity, and roughness. Combining instruments requires an additional step of not only understanding of underlying physics, but also practical implementating the method, either by developing the associated instrumentation or reverse engineering commercial instruments in order to combine their measurement results. A large part of Chapter 2 will be devoted to results obtained using this multiphysics approach, with the final aim of combining on a same sample acoustic (layer density, thickness and viscosity), optical (layer permittivity and thickness) and scanning probe microscopy (topography, local electrochemical or optical properties) measurements.

From the previous considerations, two applications of acoustic sensors have been under investigation, the results of which are described here:

- acoustic delay lines for the characterization of thin organic films, originally prompted by the analysis of biochemical layer for direct protein detection (PAMELA 5th FWP European project). This initial study lead to the characterization of thin organic films, easier to access and handle in a physics laboratory, and the *in situ* characterization of the mass sensitivity of Love mode acoustic delay lines using electrodeposition (Chap. 2). Although all the necessary instruments are available for using the acoustic sensor for analyzing further electrochemical reactions, we now focus towards gas sensing due to application driven demands, although the underlying physics is more trivial. Our latest endeavor hence focuses on the improvement of embedded electronics for recording acoustic velocity and losses of delay lines: we aim at providing rugged instruments with the robustness of an open loop network analyzer (full characterization of each sensor prior to use on the field) while gaining the accuracy of closed loop oscillator designs.
- resonator for the remote sensing of physical quantities: piezoelectric substrates probed by electromagnetic pulses provide the unique characteristics of passive (no battery associated with the sensor) and wireless transducers. The improved energy conservation of piezoelectric substrate (*i.e.* improved quality factor) provides an efficient means of identifying the acoustic signal using a monostatic RADAR strategy since all the background clutter has dissipated while the resonator still emits the stored energy when the probe signal is centered on its resonance frequency. While the basic principle of this strategy is simple enough, the practical application in industrial environments – beyond the academic demonstration of the principle – induces many technical challenges, some of the most interesting from a physical point of view will be described in Chap. 3.

> "... it is well known that a vital ingredient of success is not knowing that what you're attempting can't be done."
> *Terry Pratchett, Discoworld vol. 3 (Equal Rites)*

Chapter 2

Direct detection biosensors for the characterization of thin organic layers

Analytical chemistry has long been concerned with the development of techniques and instrument for identifying physical properties of molecules. More recently, emphasis has shifted from the identification and detection of inorganic species towards sensing the biological world, with applications to environmental pollution, food and health monitoring. This new trend provides an opportunity to probe the physics of the interactions of biological species (proteins, cells) with surfaces. Indeed, biological evolution has led to unique molecules – antibodies – able to react specifically with a restricted set of other molecules – antigens. Such antibodies, once immobilized on the sensing area of a physical transducer which defines the sensitivity of the sensor, provide the necessary selectivity for detecting one biochemical species amongst the many others found in a natural environment (polluted stream, blood serum).

The fundamental aspect of a biosensor as opposed to the more traditional analytical chemistry methods is the *work on surfaces*. Binding the sensing layer to a surface (as opposed to directly working in solution) allows flushing several reagents over the sensor without loosing the sensing ability, since the sensing layer is bound to the surface of the sensor. The result of the interaction of the sensing layer with its bio-active environment, whether a change in mass, refractive index/dielectric index, temperature from the heat released from the reaction, is probed by an analytical technique. The role of microelectronics technology is to miniaturize this external probing technique in order to either allow parallelization of the sensing mechanism (such as fluorescence of DNA by using multiple pixels on a CCD sensor) or making the sensor more portable/rugged for embedded/mobile applications. Miniaturization also provides new opportunities which could not be envisioned at the macroscopic level, such as the application to biochemical reactions with cells of classical enthalpy measurements or protein crystal growth under conditions where capillary forces become predominant over gravity.

Furthermore, the *direct detection biosensors* we are interested in should be able to detect

an analyte in a "raw sample" (requiring only physical filtering) without preliminary preparation: in such a case, the sensor is used for continuous monitoring, raw sample analysis (saving on preparation time and reagent cost) or automated periodic analysis of the accumulated analyte on/in the sensing surface (for example irreversible antibody reaction or gas adsorption).

Some of the challenges expected to be addressed during biosensor developments are:

- biosensors aim at probing minute changes in surface properties in order to detect biochemical reactions. However, detecting minute changes such as tiny optical index or mass changes means that such sensors should be immune to the most disturbing physical parameters, such as temperature and mechanical vibrations.

- an extensive understanding of the physical sensing mechanism is required for a quantitative analysis of the results, a proper interpretation of the signal change and for rejecting unwanted contributions to the sensor response. Such biophysical changes include surface charge distribution, hydrophilicity of the surfaces, conformation changes of proteins leading to mechanical and electromagnetic property variations and surface charge distributions.

These mechanisms can be probed with the adequate combination of sensors in order to gather enough informations on the system under investigation to draw conclusions on its behavior as accurate as possible.

The aim of this work is to focus on the particular case of biosensors designed for protein detection and more generally for antibody-antigen reaction monitoring. While the technical challenges of working in liquid media as required for handling biological samples, the general concepts and instruments are applicable to gas detection. However, we purposely exclude the work in DNA detection and DNA arrays, as well as the body of work on enzyme detection, since electrochemicaly active molecules are probably best detected using electrochemical techniques which provide both quantitative analysis capabilities and identification schemes associated with, for example, voltages characteristic of some electroactive chemical groups in a cyclic voltametry measurement. The reader is encouraged to refer to reviews on these topics [1, 2, 3, 4].

Ultimately, the sensitivity of a biosensor is related to the number of chemical sensing sites bound on the transducer surface. Optimization of the design of the transducer as well as chemical functionalization procedures require an accurate knowledge of the density of bound molecules, and thus of the transduction principle. After reviewing the different kinds of measurement techniques, broadly grouped in measurement of mechanical property changes and dielectric property variations due to protein binding on surfaces, we will attempt to correlate the results of these various techniques to extract as accurately as possible descriptions of the physical processes underlying biological species binding to surfaces, chemically functionalized or not.

2.1 Molecular recognition principles

Binding molecules on a surface is covered by fields such as surface chemistry and organic chemistry for the synthesis of molecules with the appropriate properties. The purpose is linking the inorganic surface of the transducer and the biological species – antibody – used for the specific detection of a reagent, without significantly affecting the recognition capabilities of this molecule (Fig. 2.1). Some of the understanding concerning the denaturation associated with protein binding to surfaces from a chemistry point of view are provided in [5, 6, 7].

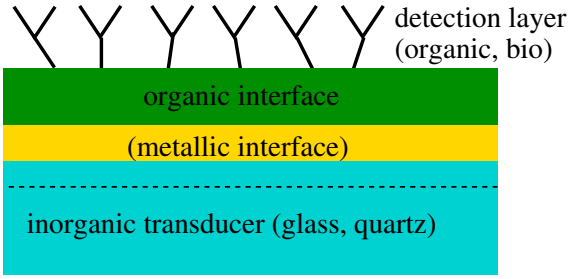

Figure 2.1: A direct detection (bio)sensor is made of a stack of layers, starting with the substrate of the transducer – quartz if the sensing principle is based on acoustic waves – possibly coated with a metallic layer if needed either for binding some chemistry or for the transduction mechanism (optical surface plasmon resonance requires a conducting layer). The aim of the organic interface chemistry is to link the detection layer – either organic or biological – to the inorganic transducer without significantly modifying the bulk properties of the sensing material. Sensing is either performed by binding antigenes to a specifically tuned antibody (selective detection), or by modifying the physical properties of the sensing layer under the influence of the compound to be detected (gas sensing). Our focus will be on characterizing the relationship between the quantities defining the behavior of the transducer and the physical properties of the adlayers which are modified by the presence of the analyte to be detected.

Most significantly, we shall remember that denaturation of proteins (or large organic molecules) occurs when binding them to hydrophobic surfaces, hence the need to coat the sensing surface with an hydrophilic intermediate linking layer allowing strong binding of the antibodies to the surface (possibly by covalent binding).

Available surface chemistries – depending on the kind of surface under investigation – are tuned for various requirements: anti-fouling coating are protein resistant and avoid unwanted or non-specific protein adhesion, silane provide an interface chemistry on oxides, thiols provide a surface chemistry on noble metals [8, 9], polymers provide 3D meshes with increased area but which move the antibodies further away from the surface [10], hence lowering the sensitivity of most of the sensors which will be depicted in this work. Polymers used for gas sensing are often physisorbed since the purpose here is to accumulate as many (light) gas molecules as possible, with a selectivity provided by the binding mechanism of the organic molecules with the gas molecules. Our investigations in this field have focused on demonstrating the use of SAW transducers to detect mass changes and possibly viscoelastic property changes (insertion loss variations) associated with gas adsorption in calixarenes (provided by A.W

Coleman, IBCP, Lyon, France). Other well known examples include non-selective organic solvent absorption in PDMS [11] and organic molecule destruction by ozone when this gas must be detected.

Different detection techniques have been developed which depart from the direct detection scheme. They are mainly provided for improving the detection limits: from direct detection to sandwich (enhancement methods) and competitive essay. Although additional steps are needed beyond the exposure of the sensing surface to the raw sample, we would still include these improved strategies in a direct detection scheme since after the sensing surface is exposed to the raw sample, the additional steps (adding nanoparticles to the bound proteins in a sandwich assay, filling the unreacted sites in a competitive assay) can be automated in a continuous monitoring strategy. The reversibily of such strategies is however more complicated to assess since more steps, and more reagents, act on the sensing surface. Although not part of this discussion, let us mention the magnetic bead sensing principle in which upconcentration is performed by magnetic nanoparticles floating in the sample under analysis. These particles are brought to the sensing surface by a magnetic field, followed by a release of the magnetic beads which have (or have not, depending on the surface functionalization characteristics) bound to the surface, and detected by a mass detection using, for example, an acoustic principle. This strategy includes a detected mass improvement through the added mass of the magnetic particle, upconcentration by bringing the magnetic beads in the solution close to the surface by a magnetic field, and possibly a reversibility strategy depending on the binding mechanism of the beads to the surface [12, 13].

2.2 Transduction principles

2.2.1 Mass variation detections

The most intuitive, if not the simplest mean of detecting a biological reaction occurring on a given surface, consists in detecting a mass change of the bound molecules [14] or cells. An obstacle to this detection method is the measurement *in liquid* of minute masses, in the hundreds of nanograms per square cm range. Following the original idea used in the microelectronics industry of monitoring thin film deposition by the frequency variation of a quartz crystal microbalance, the idea of using a resonating probe and monitoring frequency variations due to molecule adsorption has been developed very early.

We introduce the gravimetric sensitivity S of resonating devices working at frequency f_0 defined as

$$S = \frac{\Delta f}{f_0} \times \frac{A}{\Delta m}$$

where Δf is the frequency shift induced by the added mass Δm on sensing area A. Such a definition, which considers the relative frequency shift (or, at a given wavelength, velocity shift) allows comparison of sensors working in different frequency ranges. However, the assumption behind the use of this quantity as a reliable indicator of the capability of a transducer to detect minute masses is that the frequency shift of the resonator is solely due to

the added (deposited or adsorbed) mass, to the exclusion of other amplification or parasitic factors such as viscous interaction or ionic (double layer) density variations. We will see that this assumption is often erroneous for mechanical systems.

More recently, attempts to replace the quartz crystal microbalance with microscopic cantilevers with higher mass sensitivities have shown promising results if not yet as reliable as the QCM [15]. The behavior of such instruments can be monitored in two ways: either by measuring the (low frequency) deflection of the cantilever as is done in contact mode atomic force microscopy [16], or by recording resonance frequency shifts due to the bound biomolecules added mass and induced surface energy changes [17]. In the former case, the deflection is due to a modification of the surface energy on the side of the cantilever to which the molecules bind, leading to a stress and thus a bending of the beam [18, 19, 20, 21]. In the latter case, the improved sensitivity comes from the favorable mass ratio of the transducer to the detected molecule. indeed, the Sauerbrey equation (which is an analytical formulation of the mass sensitivity for resonators with variable boundary limits as will be seen later in section 2.2.1) associates the relative frequency shift $\Delta f/f$ to a mass adsorbed at the surface of the resonator Δm through the thickness change of the resonator. The resulting perturbation to the resonance condition, since multiples of half wavelengths $n\lambda/2$ are confined in the resonator thickness e, relates a thickness change Δe to a wavelength variation $\Delta\lambda = \frac{2}{n}\Delta e$ and hence a frequency change

$$\Delta f/f = \Delta\lambda/\lambda = \Delta e/e$$

by assuming as a first approximation that the added layer has the same properties than the bulk of the transducer, then

$$\Delta f/f = (\rho\Delta e)/(\rho e) = \Delta m/m$$

with m the *mass of the active part of the transducer*. Reducing the mass of the transducer to bring it close to that of the adsorbed mass should hence improve the sensitivity $S = \frac{A}{m} = \frac{1}{\rho e}$. Notice that the mass sensitivity is *independent on the overtone number* n. Practically, low e generate devices excessively sensitive to their environment with poor stability, and hence reduced detection limits since the baseline is no longer stable enough to distinguish mass adsorption to external disturbances. One approach to solving the sensitivity to external disturbances (temperature, hydrostatic pressure) is to perform *differential measurements*, in which a non-functionalized sensor monitors in parallel to the active sensor the influence of the environment on the signal. This unwanted disturbance is either digitally subtracted during a postprocessing step, or removed during the measurement in a closed loop oscillation configuration by monitoring the low frequency signal at the output of an RF mixer.

This analysis provides the basis for two aspects of this research: surface acoustic sensors provide better sensitivity than bulk acoustic resonators since the design of the former is compatible with an increase in frequency, hence a decrease in wavelength and shallower penetration depth e of the evanescent wave in the substrate. Secondly, Love mode acoustic sensors [22, 23, 24, 25, 26] are most sensitive thanks to the confinement of the acoustic energy within a thin guiding layer, yielding shorter a penetration depth than the evanescent wave found in other propagation modes. In all cases, *increasing the working frequency increases the sensitivity.*

Devices with low mass include cantilevers, but also thin film resonating devices (FBAR and Lamb-mode acoustic devices), both of which being excessively fragile to handle. Furthermore, these devices often exhibit acoustic modes which generate longitudinal waves in the viscous medium surrounding the transducer, a problem emphasized when working in liquid media. Dissipating energy in the environment during each oscillation is another way of expressing the fact that the quality factor is strongly reduced by viscous media. However, the stability of the baseline is directly linked to the quality factor: the ability of the resonator to store energy allows it to resist to the attempts of the environment to shift the resonance frequency, and hence the higher the quality factor the better the stability of the baseline of the acoustic transducer. In other words, any fluctuation faster than the *Leeson frequency* [27] $f_L = \frac{f_0}{2Q}$ is smoothed by the resonator [28, p.73].

Since generating longitudinal waves in the environment will necessarily result in unacceptable quality factor degradation and hence poor baseline, one strategy is quality-factor control to artificially compensate for energy loss by injecting energy *in phase* with the natural oscillation of the acoustic sensor. One interesting strategy with this approach is that a resonator is not solely used in a closed loop oscillator condition, but the analysis starts with an openloop characterization of the acoustic transducer while the oscillation is only an asymptotic behavior of the band-pass filter associated to the electronic circuit providing energy, when the losses are compensated for by the amplifier. We have applied this strategy for low-frequency tuning forks [29], although it appeared that such transducers are *too stiff* to act as useful sensors. The limit to the quality factor enhancement is the oscillator: when enough energy is injected in phase in the transducer, an oscillator starts [1] [29]. This technique is easily applied to low frequency (sub-MHz) devices, while we have not had the opportunity of testing an extension to radiofrequency (above 30-MHz) devices.

The detection limit of the sensor is obtained by including the noise on the frequency measurement in the sensitivity equation. Indeed, the smallest mass density $\Delta m/A$ that can be detected is associated to the smallest frequency variation Δf we can reliably detect. In an openloop configuration, we are not measuring an oscillator frequency f but a phase shift $\Delta\varphi$ at constant frequency. Hence, the detection limit is associated to the noise on the phase measurement, which we have observed to be typically 0.3 degrees on commercial network analyzers. This phase shift is associated to a frequency shift through the phase-frequency relationship, assumed to be locally linear and with a slope $\frac{d\varphi}{df} = 2 \times \pi \frac{L}{V}$ [30] with L the distance between the interdigitated transducers of a delay line and V the acoustic velocity. For a Love mode sensor with $L = 8$ mm and $V = \lambda f = 4750$ m/s, we find a slope of $\frac{d\varphi}{df} = 6 \times 10^{-4}$ degrees/Hz. Hence, a 0.3 deg. variation is equivalent to a noise level of Δf=500 Hz. One can obviously see here the poor resolution of the delay line probed in an openloop configuration, compared to a high-quality factor resonator which typically displays a baseline stability at least 10 times better. Nevertheless, the detection limit we deduce is

$$\boxed{\frac{\Delta m}{A} \geq \frac{\Delta f}{Sf} = 20 \text{ ng/cm}^2}$$

[1] note that the opposite, quality factor *degradation*, follows the same strategy and is used when a resonating transducer exhibits too slow a response delay to environmental effects, as for example when a resonator is used to keep a tip at a constant distance in scanning probe microscope setups.

We, as many other groups cited above, have exploited the basic delay line configuration for propagating a Love mode acoustic wave and monitoring biochemical reactions occurring on the surface by measuring the phase velocity [31, 32, 33]: in order to successfully perform these experiments, emphasis in the fabrication process was put on the development of a reliable, wafer scale packaging [34].

The quartz crystal microbalance (QCM)

The quart crystal resonator (QCR) – abusively called Quartz Crystal Microbalance under the assumption of purely gravimetric interactions of the adsorbed layer – has been used for years for monitoring inorganic thin film deposition under vacuum conditions. Beyond the basics, and hardly reliable, strategy of measuring the resonance frequency of the QCR, dipping in solution to perform a chemical reaction on the surface, drying and measuring the resonance frequency shift, recent instrument developments have demonstrated the use of QCR with one side (grounded to avoid electrochemical and double ionic layer interactions) in contact with liquid [35, 36]. This tool, now classically available in many surface chemistry laboratories, first gives access to the time-resolved evolution of a reaction on the surface of the sensing area, but has most significantly led to a vast body of literature concerned with modelling interactions of the acoustic wave with the surrounding fluid beyond the gravimetric effect, also known as the Sauerbrey relation. The viscoelastic interaction of polymers, thick protein films and rough surfaces has appeared as a major contribution next to the gravimetric effect, as will be discussed layer in this document. Unexpected results include frequency *increases* – opposite to the predicted decrease – upon DNA strand adsorption interpreted as coupled resonator interaction [37].

The original derivation of the mass detection mechanism by Sauerbrey [38, in german] is based on the idea that the acoustic wave propagating in the quartz substrate is traveling at constant velocity, and the boundary conditions define the wavelength and hence the resonant frequency of the sensor (by confining an odd number of half-wavelengths between the surfaces of the quartz wafer). Although this argument is acceptable for QCMs oscillating under vacuum, with only minor deviations to the predicted proportionality factor relating mass to frequency shifts, major discrepancies were quickly identified when these sensors were used in liquid [39, 40, 41]. The two kinds of experiments requiring liquid medium are electrochemistry [42] and biology [43]. The former provides a mean of calibration thanks to the independent reaction quantities provided by the charge flowing through the potentiostat.

The discrepancies are either attributed to water layers trapped within the biological layer under investigation, to viscous effects dependent on surface roughness [44, 45, 46, 47, 48, 49], to electrolyte conductivity/double layer variations [50, 51, 52, 53], or film viscoelastic properties [54]. The latter have been probed early on by several groups [55] using an impedance analyzer for open loop analysis of all the parameters of the QCM, or by monitoring the dissipation and keeping the amplitude of the oscillator fixed using an automatic gain control [56]. In the former case, the equivalent electrical model – the so called Butterworth-Van Dyke or BVD [57, 58] – of the QCR includes a capacitor (representing the electrical capacitance between the electrodes patterned on the opposite faces of the quartz wafer) in parallel with a resistance, a

capacitance and an inductance in series (the resistance representing the mechanical losses, the inductance the mass inertia and the capacitance the material stiffness). The quality factor is then inversely proportional to this resistance and is an indicator of the acoustic energy losses in the surrounding medium. New commercial probing tools are being developed by companies including Maxtek (now Inficon, New York, USA) and Q-Sense (Göteborg, Sweden) which provide the relevant parameters such as dissipation (i.e quality factor) [40] and resonance frequency, emphasizing the cause of these discrepancies which always lead to an overestimate of the deposited mass.

The reference system we refer to throughout this first half of the discussion is QSense's Quartz Crystal Resonator [2]. The reasons for selecting this instrument as reference are its excellent stability, its explicit purpose to tackle the issue of gravimetric *v.s* viscoelastic contribution to the observed resonance frequency shift by *measuring multiple overtones* as well as the *acoustic losses* (the so called dissipation, defined as the inverse of the quality factor), and finally the published models for an accurate analysis of the acquired data [59, 60].

While these source of discrepancies have been considered as hindrances to accurate measurements in the early uses of QCMs in liquids, the development of models appropriately simulating each effect actually provided added informations on the layers under investigation. Additional informations can be obtained by probing the QCM at various overtones since the dependency of the cause of the discrepancy with frequency is a precious indication of the sensing mechanism. Even though working at overtone provides added informations on the sensing mechanism, the sensitivity of a QCM is defined by the resonance frequency of its fundamental mode (usually in the 5 to 10 MHz range). Increasing the sensitivity of QCMs by increasing the resonance frequency (by decreasing the thickness of the quartz wafer supporting the shear oscillation) is limited by mechanical resistance constraints, limiting the maximum fundamental resonance frequency to 50 MHz up to now [61]. Indeed, from the Sauerbrey equation one deduces the proportionality between the sensitivity of the QCM and the square of the resonance frequency: $S_{QCM} = \frac{2f_0}{\rho c}$ where $\rho = 2650$ kg.m^{-3} is the density of quartz and $c = 3340$ m/s is the velocity of the shear wave in AT-cut quartz. The sensitivity of a 10 MHz QCM is thus 23 g.cm^{-2}. As was mentioned earlier, *overtones of a QCM exhibits the same sensitivity as the one calculated with the fundamental frequency*: using a nth overtone (n odd) is *not* equivalent in terms of sensitivity to using a wafer n times thinner to increase the fundamental frequency of the resonator by n. This analogy is emphasized in the comparison of the sensitivity of High Bulk Overtone Resonator (HBAR) and thin Film Bulk Acoustic Resonator (FBAR): while the latter exhibits large sensitivities above the 1000 cm^2/g range, the thin membrane make them less robust than HBARs, which provide an information as rich as QSense's overtone analysis but on a wider frequency range and with a robust setup since the thin piezoelectric layer is coated atop a (more or less thick) substrate with low acoustic losses.

Although the overtones all display the same mass sensitivity, analyzing at many different wavelengths a thin viscous film provides a rich set of data thanks to the shear wave evanescent

[2] www.q-sense.com

field penetration depth δ dependence with frequency f:

$$\delta(f) = \sqrt{\frac{\eta_l}{\pi f \rho_l}}$$

where η_l is the dynamic viscosity and ρ_l the density of the layer (for water, η_l=0.01 g.cm−1.s^{-1} and ρ_l=1 g.cm^{-3}. For f = 15, 25 and 35 MHz, δ is respectively equal to 145, 113 and 95 nm, much further than the biological layer thickness we are interested in). This dependence has been used to quantify the nature of the layer interaction with the acoustic field: in the case of a gravimetric (Sauerbrey-like) interaction, the frequency shift associated to the added mass scales with the overtone number, while in the case of a predominantly viscous interaction, the frequency shift scales as the *square root* of the overtone number [62]. Hence, beyond the use of the damping for qualifying the nature of the interaction as promoted by QSense, the scaling law of the frequency shift with the overtone number is a useful indicator as well, expected to be much richer in the case of HBARs where available overtone numbers can reach up to the hundreds rather than the 5th or seventh overtone at best with QSense's instrument. Such analysis has been performed for protein layer as well but never published: long, fibrillar proteins (collagen, fibrinogen) form thick (100 nm) layers swollen with solvent and display viscous interactions (with frequency shifts scaling with the square root of the overtone number) while small globular proteins (IgG, S-layer) form thin (sub-10 nm) layers whose interaction with the acoustic field induces a frequency shift scaling with the overtone number (Fig. 2.2).

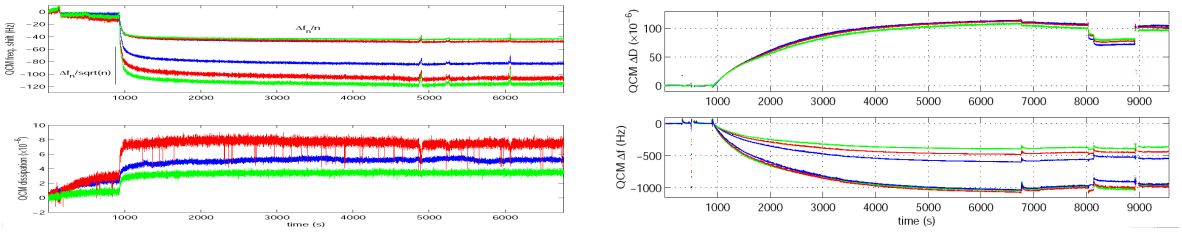

S-layer 30 μg/ml collagen

Figure 2.2: Left: QCR measurement at 3 overtones (number 3, 5 and 7) of an S-layer adsorption. The frequency shifts scale as the overtone number and not as the square root of the overtone number, a sure indication of a rigid gravimetric interaction confirmed by the slight damping factor increase. Right: 30 μg/ml collagen adsorption on a gold surface processed to become hydrophobic (methyl-ended thiols), displaying a frequency shift scaling as the square root of the overtone number and with a strong damping increase during the reaction. Converting this data set to an adsorbed mass using the Sauerbrey equation yields results with little relationship to the physical properties of the layer.

Surface acoustic waves (SAW)

A different kind of mass detection sensors are the surface acoustic wave (SAW) based sensors [63, 23].

While SAW have been known for a long time, the most common propagation type used in electronics application – the Rayleigh wave – is ineffective in probing reactions in liquid

media because of the presence of an out-of-plane longitudinal component which is strongly damped when the surface of the sensor is in contact with a liquid [64]. Other kinds of surface acoustic waves [65] include acoustic plate modes [66, 67], flexural plate waves and the Love mode [68, 69, 70, 71, 72, 73, 74]. The latter is characterized by the confinement of the acoustic energy of the propagating wave in a thin waveguide, leading to energy trapping at the sensing interface and improved sensitivity. In the case of SAW sensors, the wavelength is defined by the transducer electrodes – interdigitated transducers (IDT) commonly made of a thin aluminum layer patterned on the quartz substrate for generating the acoustic wave by reverse piezoelectric effect, and the propagation velocity is the varying parameter depending on the mass load on the propagation path. Hence, the resulting parameter monitored during the reaction is either a phase shift in open loop configuration, or an oscillation frequency in closed (phase locked loop) configuration. In all cases the acoustic wave devices here operate at frequencies equal to or above 100 MHz.

Our interest will be the identification of physical properties of thin adsorbed organic films, and an assessment of the validity of the gravimetric measurement classically performed in vacuum and usually extended to liquid media. We shall focus on guided Love mode acoustic sensors which combine a plurality of advantages for our purpose:

- the sensing area between the IDTs is a passive region which is not necessarily patterned with electrodes: these devices are hence suitable as "active" windows for use with optical sensors, or after coating with a conducting area are easily used during electrochemical reactions,
- the shear acoustic scalar wave only interacts with the viscoelastic surrounding medium through an evanescent wave and hence minimal losses allow for a measurement to be performed even with liquid media (water, biological buffers)
- the simple openloop measurement configuration in which an S_{21} transmission measurement is always available provides a stable mean of measuring properties of unknown layers – with useful debugging signals even with large insertion losses – as opposed to a closed loop oscillator which is harder to debug for strong viscoelastic loads

SAW devices offer, compared to QCM, the advantages of an improved sensitivity [67] and an open backside allowing the combination with additional optical sensors. The most commonly used transduction principle – IDTs – induces a transfer function $H(\omega)$ of the acoustic transducer which is modelled as the Fourier transform of the IDT shape. This model is easily justified by considering that the voltage applied to the IDT instantaneously generates an electric field in the piezoelectric substrate and hence a mechanical wave, which propagates at a finite velocity. The time delay between the contributions of each IDT pair is formally equivalent to a Fourier transform [75, p.58]:

$$\boxed{H(\omega) = \sum_0^N (-1)^n A_n \exp(-i\omega t_n)}$$

with t_n the finger position and, in case apodization is used, A_n the coverage ratio of adjacent fingers [76].

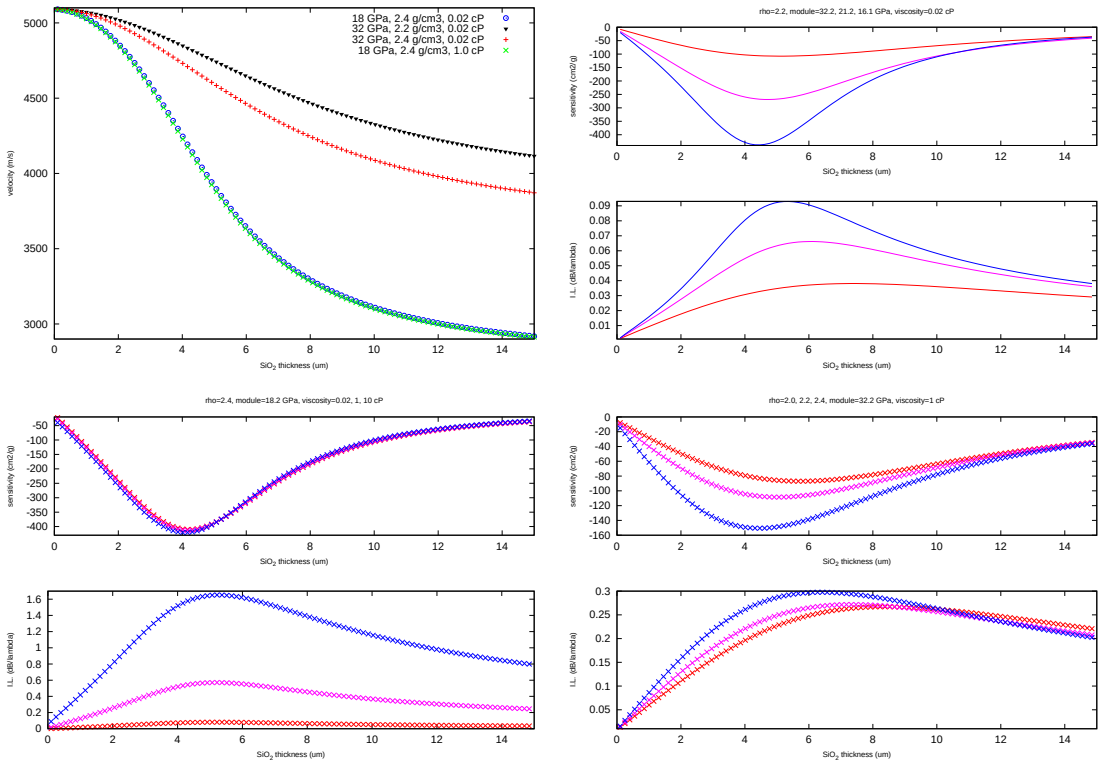

Figure 2.3: Top left: velocity of the Love mode acoustic wave as a function of the guiding layer thickness when working at a fixed frequency of 123 MHz. These velocities were computed for a sensing layer covered with air (0.02 cP), water and a fluid 10 times more viscous than water. Notice that the velocity v is hardly affected by the viscosity, but it strongly dependent on the shear modulus c_{66} since $v = \sqrt{c_{66}}\rho$ with ρ the density of the guiding layer. For thick guiding layer, the acoustic mode velocity is asymptotically equal to the velocity of the shear wave in the guiding medium. Decreasing velocities curve are associated to decreasing shear moduli, and increasing densities. Top-right: gravimetric sensitivity Sas a function of the shear modulus, for a fixed guiding layer density of 2.2 g/cm^3 and air above the sensing area. The experimental measurements of $S = 180 \pm 20$ and $S = 400 \pm 20$ cm^2/g are both met for a shear modulus of about 18 GPa. Increasing mass sensitivity absolute value and increasing insertion losses are associated to decreasing shear moduli, from 32 to 16 GPa. Bottom-left: gravimetric sensitivity as a function of the viscosity, for a shear modulus of 18 GPa and a density of 2.2 g/cm^3. Although the viscous layer above the sensing area affect the dispersion relation, the mass sensitivity is hardly affected. Nevertheless, we always calibrate our sensor in liquid media to match practical applications of protein and polymer detection. The insertion loss is strongly affected by the viscosity of the liquid above the sensing area. Increasing losses are associated to increasing viscosities. Bottom-right: influence of the layer density on the gravimetric sensitivity, for the tabulated shear modulus of silicon dioxide 32 GPa and water above the sensing area. The experimental sensitivity cannot be met with such a shear modulus and densities within reasonable values. The higher the density, the higher the mass sensitivity absolute value.

This relationship is as important as the optical Fourier transform of diffracting optical systems – again demonstrated through the same formalism of time delayed sources whose contribution at each point in space is provided by the same formalism – and shows how these optical and acoustic systems are used for frequency domain filtering and how to design the response through a Fourier transform of the spatial distribution of the IDTs.

While SAW devices seem to be less affected than QCM by viscous interactions with the surrounding liquid [77], variations in ionic content or conductivity [78] of the liquid medium over the sensing area induces major disturbances in the measurement even when the metal coated sensing area is grounded. As an example of direct detection of proteins by Love mode devices, Harding *et al* claim to identify the frequency shift induced by the added mass from 5 ng/ml anti-sheep IgG [79] while Saha *et al* reliably detect IgG concentrations as low as 1 μg/ml bound to proteins G [74]. Since in the SAW sensor, the sensing area is not an electrically active area but only provides the propagation path of the acoustic wave generated by the IDTs, coating the sensing area and referencing the voltage of this electrode (grounded) or keeping a floating potential provides the means for differential analysis and distinguishing the ionic double layer contribution from the gravimetric contributions. More generally, a differential analysis of SAW delay lines with different sensing area coatings is mandatory for subtracting correlated effect (stress, temperature) and emphasizing the relevant measurement (adsorbed mass).

Quantitative analysis of the SAW response requires the accurate modelling of the gravimetric and viscoelastic contribution to the phase (or frequency) signal measured as the propagating acoustic wave interacts with the surrounding fluid. For a bare Love-mode SAW sensor fabricated by coating monocrystalline quartz with PECVD silicon dioxide, the only non-tabulated free parameters are the amorphous silicon dioxide density and shear modulus, which are known to widely vary depending on the PECVD process. As an example, L. Francis used a specially developed process for depositing low density, highly porous SiO_2 and hence increase the gravimetric sensitivity. Fig. 2.3 exhibits some of the modelling performed using a mixed-matrix approach in which the silicon dioxide density is varied from $\rho = 2.0$ to 2.4 g/cm^{-3}, and the shear modulus from the tabulated bulk value of 31.2 GPa to 16.1 GPa, a reasonable value for thin deposited films a few micrometers thick. We observe that the density hardly affects the mass sensitivity in such a reduced range, but the lower range of the shear modulus provides results consistent with the experimental measurements of $S = 180 \pm 20$ cm^2/g and $S = 400 \pm 20$ cm^2/g for silicon dioxide thicknesses of 2.5 and 4 μm respectively (experimentally measured using the liquid-phase electrodeposition procedure described in [62]). Although the simulations resulting in Fig. 2.3 correctly predict the mass sensitivity, the insertion losses for a 100 λ long transducer as the one we use experimentally is here overestimated. Indeed, two sets of parameters will either fit correctly the mass sensitivity (low shear modulus) or the insertion losses (tabulated parameters of silicon dioxide, with a shear modulus of 32.2 GPa), but not both simultaneously. Experimentally, the 20 to 25 dB insertion losses observed in air are due to the low piezoelectric coupling coefficient of quartz, and for 6 dB to the lack of directional transducers (half of the energy is radiated outward by each IDT). The strong overestimate of the losses at low shear modulus when the sensing area is exposed to liquid is due to the excessive wave confinement close to the viscous liquid and hence the excessive predicted loss. The cause of this discrepancy – either the insertion loss or the sensitivity are correctly predicted, but not both simultaneously – is still under

investigation.

One additional limitation of the model is the prediction of the *acoustic losses in the guiding layer*. In the case of resonators, the imaginary part of the shear modulus is taken as the real part divided by the quality factor, so that the model fits the experiment. This strategy is not applicable in the case of delay lines: the losses exhibited in Fig. 2.3 are the result of the viscous dissipation of the shear evanescent wave in 0.02 cP air, 1 cP water and an undefined 10 cP liquid which could be a water-glycerol mixture.

Although the velocity of the wave, confined in the SiO_2 layer, is hardly affected by the viscous interaction of the wave with the liquid, the velocity *shift* due to viscous drag is significant and can affect the quantitative interpretation of frequency shift as solely due to a gravimetric effect. A strong indicator of the influence of viscosity is the measurement of insertion losses – the delay line equivalent of the resonator quality factor (or damping when using QSense's naming convention), which increase dramatically and make the sensor useless for the most viscous fluids due to the long sensing area (100-wavelengths). This topic was discussed in details in [80]. Since the mixed matrix model provides a velocity v as a function of layer stack parameters (quartz-silicon dioxide-viscous fluid), the numerical values of the gravimetric sensitivity S were computed as the derivative of the phase velocity Δv as a function of the guiding layer thickness variation Δt, divided by the guiding layer density ρ and acoustic wave velocity v

$$S = \frac{\Delta v}{\Delta t} \times \frac{1}{\rho v}$$

Indeed, following the Sauerbrey equation derivation, the sensitivity is given by the velocity variation due to a thin film adsorption upon the guiding layer which acts as a disturbance to the acoustic wave propagation. The higher this disturbance – here observed as a velocity variation – the higher the sensitivity. This mixed matrix model is in agreement with the transmission line model presented by L. Francis in his PhD, and here includes in addition the viscous contribution to the velocity shift.

Sensor calibration

While the Sauerbrey relation provides an estimate of the mass sensitivity of bulk acoustic resonators through limit condition variations, no such analytical formula exists for surface acoustic wave resonators or delay lines. Both devices are affected by acoustic velocity variations which are only accessible through transmission line or mixed matrix models. An alternative approach is to calibrate the SAW sensor by depositing a known mass and monitoring the resulting signal shift. Under the assumption of a purely gravimetric effect, the mass sensitivity is computed from these data.

While thin metallic film deposition in vacuum and photoresist spin-coating [71] has been classically used for mass calibration [70], we wished to develop the means to *reversibly* deposit *variable amounts* of a reference compound on the surface of a SAW sensor *in liquid medium* to assess the mass sensitivity while the acoustic wave interacts with the viscoelastic medium

as one boundary condition. The implemented method is based on electrodeposition of copper and silver since both metals are well known with well defined electrochemical potentials and stable solutions for electrochemistry from copper sulfate and silver nitrate solutions [62].

Unexpected interpretation complications included

- the underpotential deposition of copper on gold, which on the one hand delays the bulk copper film formation during the reduction step since a first single atom film must cover the gold surface before the bulk reaction starts. On the other hand, underpotential deposition appears as an opportunity to obtain the "true" (as opposed to geometric) area of the sensor as a discrepancy between the expected mass of a single copper atom layer covering the geometric area and the observed signal. Considering that the atomic weight of Cu is m_{Cu}=63.5 g/mol and its density is ρ_{Cu}=8920 kg.m^{-3}, the molar volume is m_{Cu}/ρ_{Cu}=7.1 cm^3/mol. Hence, this mechanistic view of the atom yields an estimated atomic size of $d_{Cu} = \sqrt[3]{\frac{\rho_{Cu}}{N \times m_{Cu}}} = 0.22$ nm diameter with N Avogadro's number. Hence, a single atomic layer weights $\rho_{Cu} d_{Cu} \simeq$200 ng.cm^{-2}. We have seen earlier that with a detection limit of around 20 ng.cm^{-2}, a single Cu atomic layer is easily measured, as observed experimentally [81]
- the unexpected roughness of electrodeposited copper yields unwanted viscoelastic contributions to the calibration signal which has been assessed using QCM-D measurements. Silver grows as a conformal layer to the gold working electrode and hence does not exhibit this roughness effect which enhances the viscoelastic contributions [48].

Our own contribution in this field has been the qualification of copper and silver electrodeposition for estimating the mass sensitivity of surface acoustic delay lines [81] with the simultaneous measurement of surface roughness at the nanometric level using a scanning probe microscope, and the viscoelastic to mass contributions to the signal as a function of the deposited metal [62].

SAW delay lines as active transparent substrates

Considering the acoustic sensor as an active "window" [3], our focus is the combination of the Love mode transducers with other techniques for simultaneously measuring different properties of a same layer and accumulating enough information to separate the contribution of individual properties. As an example of this principle, the combination of acoustic and optical methods provides an interesting example: at a single wavelength, the acoustic wave is affected by a mass ($\rho \times h$ where ρ is the density of a layer and h its thickness) and viscosity η which induces both a frequency shift [82] and an insertion loss increase. An optical method

[3] here, active is opposed to the passive glass slide classically used to support chemical reactions under a microscope or optical setup such as UV-visible spectrometers, with no sensing functionality. SAW sensors provide similar optical performances and an open sensing area available for most chemical functionalization techniques, while the acoustic wave propagation provides the added benefit of measuring the mass of adsorbed species or viscoelastic properties of the medium

is sensitive to an optical thickness $n \times h$ with n the optical index of the layer. Each method individually does not give access to a fundamental property of an organic compound, n or ρ, and in each experiment the particular layer thickness h. Only a combination of the methods probing the same layer – under some assumptions – provides enough data to separate each variable contributing to the observed signals. We will specifically focus on the following combinations:

- *scanning probe microscopy and acoustic* methods, whether using bulk acoustic wave resonators or surface acoustic wave delay lines. The initial objective was to use a scanning probe microscope to identify the thickness of the layer, a task complicated by the soft nature of organic layers in liquid media. Identifying the thickness and adsorbed mass should yield an estimate of the layer density. Furthermore, the spatial resolution of scanning probe techniques provides the means to assess the assumption of homogeneity of the adsorbed layer at the acoustic wavelength scale.
- *evanescent wave optical and acoustic* methods, and more specifically surface plasmon resonance (SPR) and surface acoustic methods.

Multiple technical challenges are met in the combination of acoustic sensor with scanning probe microscopy or optical techniques. We will discuss some of the solutions we have developed and the obtained results. We will first review some of the current status of the direct detection biosensor techniques before presenting in detail the actual contributions to the field.

Delay line v.s. resonators

We have selected acoustic delay lines as acoustic transducers for monitoring (bio)chemical reaction for its ease of design and the absence of electrodes on the sensing area (as opposed to resonators). However, we must still identify the means to probe the acoustic wave properties, namely its velocity and losses along the propagation path. Two ways are classically identified:

- the closed loop configuration, in which the delay line acts as a filter to a wideband amplifier, and oscillation is achieved by solving the Barkhausen conditions, *i.e.* a gain of the amplifier greater than the loss of the filter and a total phase shift multiple of 2π.
- the open loop configuration, in which an externally generated signal is injected into the probed acoustic device, and both acoustic velocity and insertion losses are observed for instance as the outputs of an I/Q demodulator. This solution is attractive since it allows debugging a poor response (selecting whether the insertion loss is too high or the selected working frequency is not in a linear phase *v.s* frequency region) while providing the same level of measurement accuracy *assuming the frequency source is more stable than acoustic velocity fluctuations in the delay line.* Hence, the stability issue is moved from the closed loop amplifier noise level, to the local oscillator reference. The latter includes both the (low) frequency resonator (typically a 5 to 20 MHz resonator) and associated reference oscillator electronics (including the phase locked loop and direct digital synthesizer) to reach the delay line working frequency.

Selecting one mode or the other should provide similar detection limits and sensitivity under the assumption of gravimetric effects, since the sole effect of mass loading is decreasing the acoustic velocity. However, the narrowband resonator response is not only associated to a velocity shift but also to the Bragg condition of the mirror cavity configuration. Furthermore, the delay line, with its small phase *v.s* frequency slope ($2\pi L/v$, with L the distance between IDTs and $v = f_0 \times \lambda$ the acoustic wave velocity for a device whose frequency response is centered around f_0 and the wavelength is defined by the IDT pattern at λ) displays a poor baseline stability compared to the high quality factor (high phase *v.s* frequency slope equal to $\frac{\pi \times Q}{f_0}$ rad/Hz).

2.2.2 Improving the detection limit using dedicated electronics

As has been discussed multiple times so far, our aim is to provide a full sensing setup, including not only the transducer but also the associated embedded electronics. This requirement is especially true when combining several methods since each laboratory, hosting part of the needed equipment, lacks the other aspects of the combination. Since we will illustrate acoustic methods combination with optical and scanning probe microscopy techniques, we will focus on automating the acoustic measurement in order to provide mobile instruments for running such experiments in laboratories providing the complementary technique. While network analyzers and frequency counters are readily available as table top laboratory instruments, our purpose here is to analyze the developments needed to include such instruments in dedicated electronics.

While the amplification circuitry to achieve oscillation is basically rather trivial using modern monolithic amplifiers to feedback the output of a 4-port transducer on its input, obtaining acceptable phase noise performances requires appropriate shielding and the use of low noise components. Furthermore, the measurement challenge is moved towards the frequency counter: achieving the performances and bandwidth of commercially available counters (the HP53131A will be used as our reference) is no trivial task [83, 84].

On the other hand, I believe that open loop – network analyzer like – instruments are the most flexible approach for either fully automating the use of acoustic sensors of inexperienced users (industrial or military applications) since they allow for the full characterization of the transducer performances. In that case, the two challenges lie in the flexible yet precise RF source, and on the other hand with the measurement of the acoustic wave propagation properties. The synthesis we focus upon is a fully software controlled Direct Digital Synthesizer (DDS) – such as Analog Devices AD9954 – with a baseband output up to 133 MHz, and the ability to probe acoustic sensors up to 533 MHz using some of the spurious signal associated with DDS. In terms of phase and magnitude detection, we have long been satisfied with integrated I/Q demodulators such as Analog Devices AD8362, which provides the same resolution and accuracy than commercial network analyzers (0.3 degrees at 125 MHz). We attribute such poor performances in terms of phase measurement to the wide bandwidth of these components developed initially for wideband digital communication: the AD8362 will process phase variations up to 1 MHz. By developing dedicated phase detectors with lower bandwidth – still compatible with (bio/electro)chemical time constants in the hundreds

of milliseconds range – we improved the resolution by more than a factor 30. Once such improvement has been observed, automating the measurement process becomes a matter of identifying the right working point by choosing the working frequency close to the lowest insertion loss still providing a phase signal within the analog to digital converter working range (typically 90^o phase difference between the reference and the measurement in order to allow for large amplification factors followed by analog to digital conversion). Furthermore, while the surface adsorption occurs, the acoustic wave velocity changes until the phase condition reaches one of the boundaries of the analog to digital conversion range. When such conditions occur, the automatic feedback controls the working frequency in order to bring the phase back close to 90^o, so that the digitized signal is again brought close to 0. Performing this feedback during faster reactions such as those found during electrochemical reactions proved challenging: some assumptions had to be made, including the phase $v.s$ velocity relationship in order to compute frequency steps which would quickly bring the phase back within analog to digital conversion range, without slow tracking while searching for the optimal working frequency.

2.2.3 Improving the detection limit using differential measurements

A meaningful signal is only relevant with respect to a baseline noise level. We have discussed the improved baseline stability of resonators with respect to delay lines for signals further away from the carrier than the Leeson frequency. Nevertheless, close to the carrier frequency (*i.e.* long term fluctuation which are no longer damped by the resonator quality factor), environmental changes still affect slow drifts in the signal. Since the (bio)chemical reactions we are interested in typically occur in the minutes to hours time scales, such slow fluctuations significantly affect the baseline stability. We have hence focused on differential measurements to subtract correlated noise sources: two similar devices are realized on a same substrate, only one of which is chemically functionalized while the other, still being subject to the same environmental conditions, is assumed not to react chemically. While this strategy is efficient for gas sensing (lack of the appropriate polymer on the surface will not yield gas phase adsorption on the base inorganic surface of the transducer) and moisture detection (transition from gas to liquid phase on the sensor while the reference is isolated in a dry air packaging), it is more difficult to use for biological species since the lack of functionalization usually allows for non-specific molecule binding. On the other hand, anti-fouling coatings are challenging to characterize and might significantly affect the acoustic wave propagation properties (and hence temperature coefficient of frequency change) with respect to the functionalized sensitive transducer. Finally, the experimental use of a differential measurement demonstrates that even though the reference and measurement devices are fabricated at short distances on a same substrate, their acoustic properties is never exactly the same. Hence, we have demonstrated some frequency change compensation in limited temperature ranges, and reduction of the hydrostatic and viscoelastic induced frequency shifts, while never being able to fully remove these effects.

Again the differential measurement strategy is different whether discussing a closed loop operation: in case of two (reference and measurement) oscillators, differential measurement is most easily performed using a RF mixer followed by a low-pass filter. However, experience shows that identifying one oscillator not running or running at the wrong frequency is difficult

with such a setup. Similarly, using the two outputs running through two (reference and measurement) delay lines to feed a single I/Q demodulator for relative phase and magnitude detection makes debugging difficult in case the sensor is not working properly, Our latest development thus focuses on the real time characterization of multiples devices – whether oscillator or delay line – and digital signal processing for accurate identification of the acoustic device parameters. Using such a configuration, each transducer is characterized individually before fancier signal processing is performed to extract as much signal as possible from the recorded data. The differential measurement setup reduces by one to two orders of magnitude the temperature coefficient of frequency: on AT-quartz with 2.5 μm thick silicon dioxide guiding layer, the initial relative frequency shift associated with temperature of 1 to 2 ppm/K (linear approximation in the 20 to 55 ^{o}C and 55-100 ^{o}C ranges respectively) become 0.1 ppm/K in the 30 to 100 ^{o}C range during differential frequency processing, with several zero-derivate frequency *v.s* temperature points (Fig. 2.4).

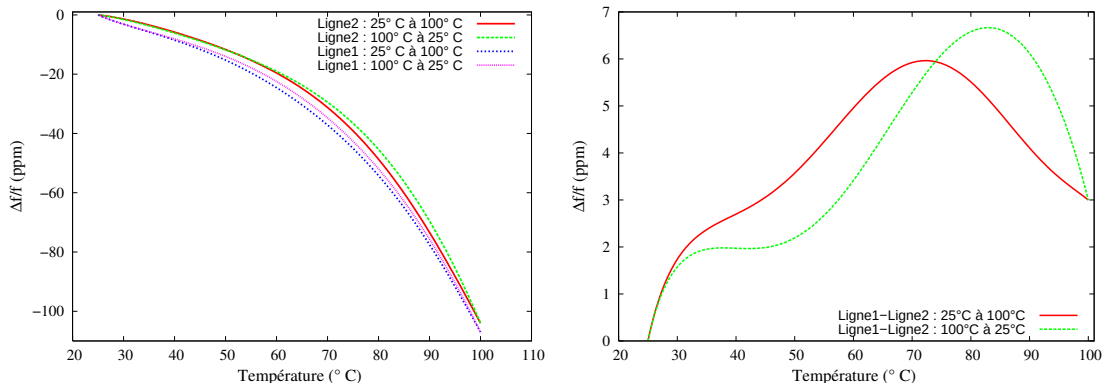

Figure 2.4: Left: raw frequency *v.s* temperature measurements for two Love mode delay lines on a same substrate, while increasing and decreasing the temperature of the temperature-controlled chuck. Right: differential measurement by post-processing the raw measurements (subtraction of the phases of both delay lines at fixed frequency) for each temperature measurement. In this particular case, two temperature-compensated regions are visible around 40 ^{o}C and 70 ^{o}C.

2.2.4 Evanescent wave based methods: Surface plasmon resonance (SPR), waveguide

Index of refraction, dielectric constant

We have focused so far on acoustic methods for measuring mechanical parameters of thin adsorbed film. We have used shear evanescent wave in order to achieve acceptable insertion losses by avoiding longitudinal wave propagation in the liquid, but more important in order to confine the meaningful signal to a small volume above the propagating surface. The typical penetration depth of a shear acoustic wave at 125 MHz in water is 50 nm.

Another parameter related to the adsorption of proteins on surfaces is the local change of the dielectric index (which is related to the optical index by the theoretical relationship

$n = \sqrt{\varepsilon}$, valid for non-polar materials [85]) of the thin adsorbed film with respect to the bulk medium (solvent). Tables providing the optical index of a wide range of metals as a function of wavelength are available in Refs [86, 87, 88]. Since a biosensor is only monitoring reactions occurring *at the surface of a sample*, the dielectric probing method must be as insensitive as possible to bulk changes while focusing on surface effects: evanescent wave based effects have thus been efficiently used in this application [89].

As opposed to bulk measurements of proteins in solution (such as by fluorescence emission of labeled antibodies – Enzyme-Linked ImmunoSorbent Assay (ELISA)), the idea behind the use of evanescent wave based methods is, as was done for acoustics, to confine the electromagnetic wave acting as a probe to the surface to which the biological layer to be analyzed is bound.

SPR [90, 91] is based on the generation of an *evanescent wave on a metallic surface*: in the commonly used Kretschmann configuration [92], a laser at wavelength λ travels through a transparent substrate of optical index n_{prism} and is reflected on a thin metallic layer with dielectric index $\varepsilon_1 = \varepsilon_1' + i \times \varepsilon_1''$ at incidence angle θ. If the wavevector of the incoming laser $k = \frac{2\pi}{\lambda} n_{prism} \sin(\theta)$ matches the surface plasmon resonance wavevector of the metal $k_{sp} = \frac{2\pi}{\lambda}\sqrt{\frac{\varepsilon_1'\varepsilon_2}{\varepsilon_1'+\varepsilon_2}}$, an evanescent wave propagates parallel to the sensing surface and penetrates the overlying dielectric (dielectric index: ε_2) by a depth (at which the electric field intensity is $1/e$ of the field on the surface) $\delta_{SPR} = \frac{\lambda}{2\pi}\sqrt{\frac{\varepsilon_1'+\varepsilon_2}{\varepsilon_2^2}}$. This value is in the tens of nanometers for noble metals [93], *i.e.* of the same order of magnitude than those found for surface acoustic wave transducers. This evanescent wave is strongly dependent on any layer deposited on top of the metallic layer supporting the SPR, including thin dielectric layers formed of proteins. SPR is based on the monitoring of a reflected laser intensity dip due to the ohmic losses in the metal when the wavevector matching condition is met. The free parameters for matching the wavevector condition are the wavelength of the incoming light source and the angle of incoming angle. Since the unknown values of the dielectric layer being probed are its thickness and its optical refraction index, varying only one of the free parameters (angle or wavelength) does not enable full characterization of the layer [94, 95].

The choice of metal and wavelength determine the sensitivity of the transducer [96, 97]. Only noble metals for which the real part of the dielectric index is greater (in absolute value) than that of the surrounding dielectric medium can be used as a surface coating on which the plasmon is generated [93, 98, 99] – notice the similarity with the acoustic Love mode guiding layer condition. At long optical wavelengths (> 600 nm) for which the sensitivity of the instrument is the highest [100, 97], the choice of metals is restricted to gold, copper and silver.

The less common surface plasmon spectroscopy (SPS) which varies both the incoming light source angle and the wavelength (Fig. 2.5) provides access to both dielectric layer thickness and refractive index [101, 102]. Both optical index of the unknown layer being probed and its thickness can then be simultaneously be determined. This technique has so far only been used with thin organic layers [103, 104, 100] and for the determination of optical properties of thin metallic [105] or dielectric inorganic films [106] but presents promising capabilities for

identifying protein properties [107, 97].

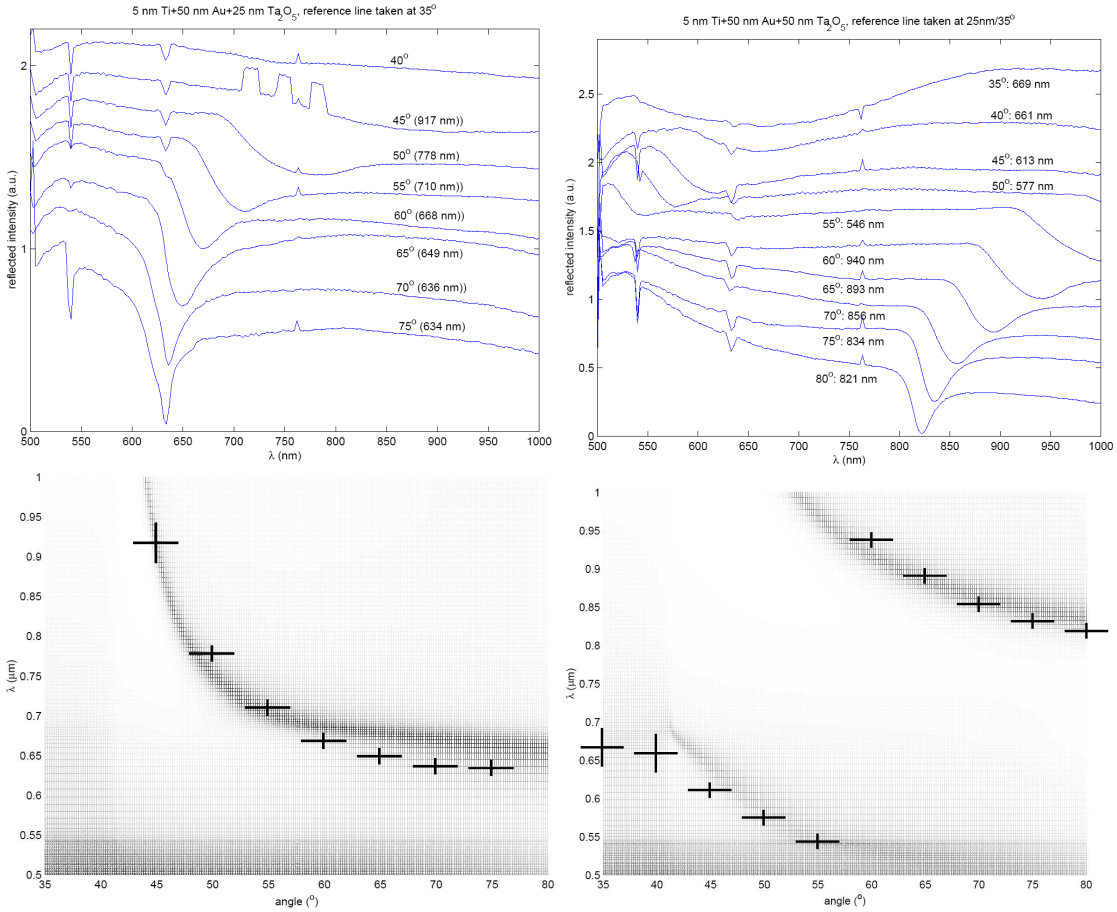

Figure 2.5: Experimental Surface Plasmon Spectroscopy obtained by using a conventional UV-Visible spectrometer, exploiting its convergent beam to generate a plasmon on a Ta_2O_5 coated gold layer on glass. Varying both the angle and the wavelength provides the means to set a unique pair of thickness t and permittivity n, as opposed to single wavelength surface plasmon resonance which only provides $n \times t$. Each wavelength sweep at a given angle presented here takes about 10 minutes to acquire, so the total duration for obtaining each graph is about one hour, incompatible with time dependent phenomena. Unpublished data.

Further refinements of the evanescent wave interaction include SPR imaging for arrays in which various antibodies are spotted to provide unique responses to an analyte, hence improving the selectivity through signal processing, as was demonstrated for cell-substrate contact imaging [108]. The lateral extension of the surface plasmon, which limits the spot size in arrays aimed at SPR imaging (for example for protein arrays) is given by the characteristic length $L_x = \frac{1}{2k_x''}$, dependent on the wavenumber $k_x'' = \frac{2\pi}{\lambda}\left(\frac{\varepsilon_1'\varepsilon_2}{\varepsilon_1'+\varepsilon_2}\right)^{\frac{3}{2}} \times \frac{\varepsilon_1''}{2\varepsilon_1'^2}$ at wavelength λ, typically in the micrometer to tens of micrometer range [93].

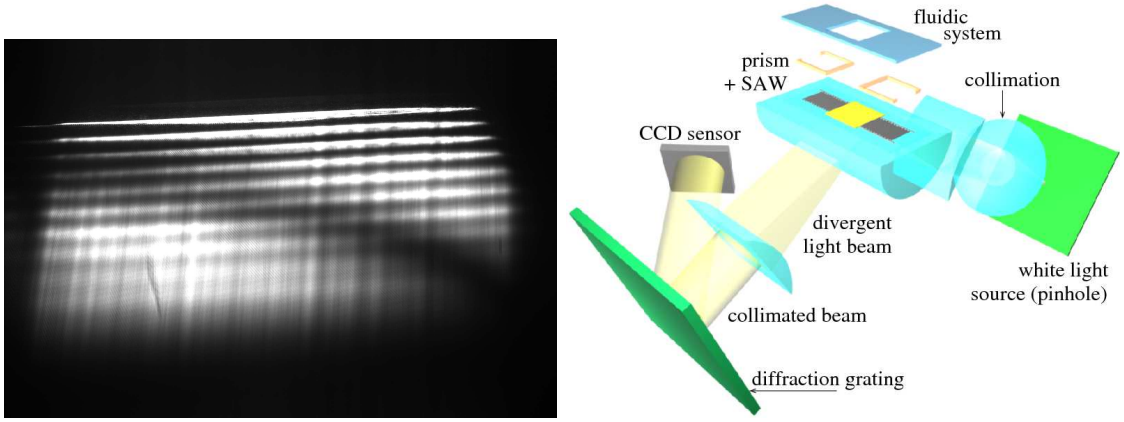

Figure 2.6: Left: white light SPR providing with sub-second time steps the full dispersion curve of the plasmon including the contribution of the coating. Right: schematic of the experiment for monitoring at 25 images/seconds the full dispersion relation of the SPR (700-900 nm). The fringes along the ordinate – variable wavelength – axis visible on the left image are attributed to interferences due to the birefringence of quartz. The abscissa is the incoming beam angle. Unpublished experiment performed with B. Sadani and J. Salvi, optics department, FEMTO-ST. Unpublished data.

Nanoparticle-based sensors

We have seen how an electromagnetic evanescent wave is generated on a thin planar metallic layer when the incoming wavevector of the light beam matches the wave vector of the surface plasmon resonance. A similar phenomenon happens during the interaction of an incoming light beam with nanometer-sized metallic beads [98, 109]. While the color [110, 111] – ranging from dark red to bright yellow – of nanometer sized noble metal beads is a trivial indicator of the interaction of these particles with visible wavelength light, a precise modeling of the UV-VIS spectrum is challenging [112, 113, 114] and requires adding particle to particle and particle to substrate interactions to the classical Mie scattering theory [115]. The transmission spectra are dependent on the size and shape of the particles [116, 117, 118]. Like SPR, the resulting UV-VIS spectrum is strongly dependent upon the thickness and optical index of an adsorbed dielectric layer on these metallic beads [119, 120]. This sensitivity is used for the development of biochemical sensors [121, 122, 123, 124, 125, 126, 127, 128]. In this application both the resonance wavelength at normal incidence angle and absorbance are measured in transmission mode as the noble metallic nanoparticles are coated with a film of the dielectric material under investigation. We have demonstrated the use of such a “simple” setup (covalent binding of gold filled and hollow spheres on quartz slides) for protein detection [129]. Although the bulk processing of quartz substrate in gold nanoparticle baths is an attractive approach from a manufacturing process point of view, an issue with the random distribution of metallic nanoparticles on a surface is the reproducibility when manufacturing the sensor: an alternative approach closer to the classical microelectronics cleanroom processing methods is to pattern a diffraction grating which displays similar sensitivity to adsorbed dielectric material [130].

Sensor calibration

Apart from the engineering difficulty in building the integrated optical setups (and most importantly of injecting light in the sensor and reading the output intensity), one issue is the calibration of these sensors. Unlike the mass sensor, metal electrodeposition can hardly be used since the interaction of an evanescent wave with an additional conducting layer is strongly non-linear and requires extensive simulations to be interpreted [131]. Furthermore, most optical systems monitor the variation of a single parameter, either resonance angle or resonance wavelength. Monitoring only one of these parameters leaves an uncertainty on the deposited mass since either the optical index of the layer or the thickness of the layer remain unknown. The commercially most successful evanescent-wave based instrument (Biacore) has been calibrated by comparing its output with the signal read from radiolabeled biological species [132], and the linear relationship between equivalent refraction unit change (RIU) and adsorbed mass demonstrated for small globular protein. Hence, great care should be taken when using the provided relationship (thick organic films, surfactant).

The only technique to the best of our knowledge to allow the identification of both the optical index and the thickness layer in liquid media is VASE [133] (Variable Angle Spectroscopic Ellipsometry), with the experimental difficulty of eliminating – or determining – the optical polarization rotation due to birefringence in the stressed input and output windows as well as possible optical index variations of the liquid medium the light beam has to shine through the liquid medium. QSense AB provides a fluidic cell for its QCR compatible will fixed angle ellipsometry, referred to as the Module 401 [134].

The issue of calibrating optical methods is fundamental when comparing the results with acoustic methods. These two techniques actually provide the common information on film thickness and independent informations on mechanical properties and density in the former case, dielectric properties in the latter case. In the few cases where comparisons have been done between the optical and acoustical sensors, wide discrepancies have been observed in the deduced thickness (and hence mass since the macroscopic area of the sensor is assumed to be known), most certainly because of an inadequate inclusion of trapped water effects (which increase the sensed mass and decrease the effective optical index, Fig. 2.7).

Optical wave confinement to the surface finds additional applications in the characterization of the surface to be used for biosensors: evanescent wave based fluorescence and second harmonic generation (SHG).

Interferometric methods

This analysis of evanescent wave would be incomplete without mentioning integrated Mach Zender classically used as optical switches and modulators [135]. The optical waveguide is achieved by metallic atom diffusion in a high optical index medium such as lithium niobate. The use of this substrate yields the obvious combination of optic and acoustic sensor for probing adsorbed molecules. Although all the equipment and knowledge are available within our research institute at FEMTO-ST, no opportunity has yet appeared to perform such an

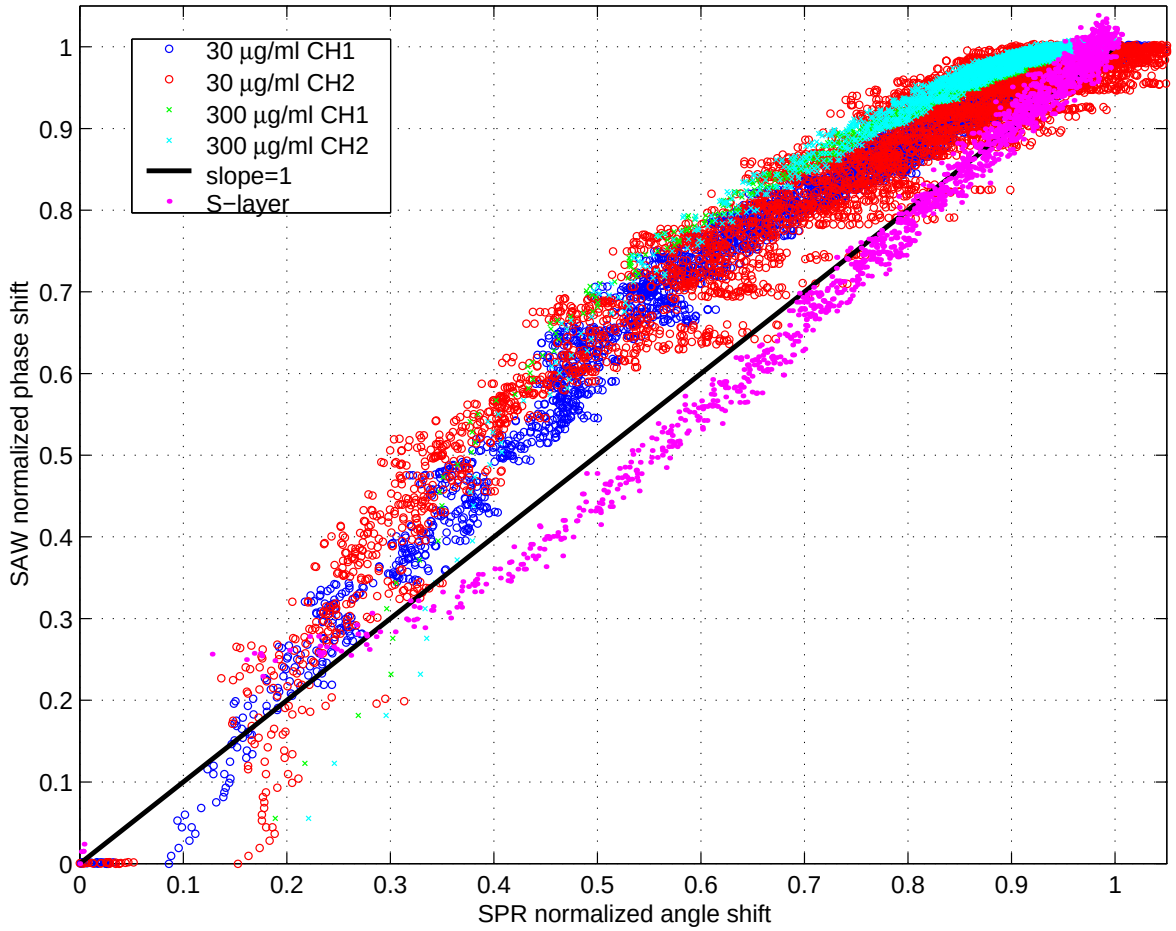

Figure 2.7: Evolution of the normalized acoustic signal as a function of the normalized (SPR) optical signal. Were the two techniques to provide the same information, all points would like on the $y = x$ line, as seen for the (rigid) S-layer. The case of fibrillar proteins clearly exhibits an overestimate of adsorbed mass by the acoustic method (or an underestimate by the optical method). Unpublished data.

experiment which is resource consuming in terms of cleanroom manufacturing [136]

Beyond the integrated Mach Zender interferometer, other optical methods possibly compatible with acoustic methods are the waveguide sensor [137, 138, 139, 140] and its extension known as the resonant mirror [141, 142]. In a principle similar to SPR, but with solely dielectric layers rather than with an electromagnetic wave induced collective electron motion, the incoming light is channeled in a low optical index layer sandwiched between two high optical index layers. As with any thin film technique, manufacturing such device requires intensive use of cleanroom technology. Although these instruments appear attractive in terms of dimensions since they are manufactured at a chip scale level, the complete optical setup, and especially the light injection and detection in the thin layers, is bulky and difficult to align.

2.2.5 Impedimetric measurements

The same arguments as presented above for optical sensors apply to electromagnetic sensing of the surface: the most efficient sensor would attempt to confine the electromagnetic energy close to the surface where the reaction is occurring. Such close confinement can be achieved by designing interdigitated electrodes separated by a distance of the same order of magnitude as the depth of electromagnetic field penetration. Technological limitations currently limit the dimensions of these patterns to a few hundred nanometers. An attractive option to compensate for the lack of resolution of optical lithography techniques to reach the dimensions of the proteins is the binding or sputtering of discontinuous metallic beads or islands [143, 144] whose conductivity and impedance properties change upon binding of biological species. On the opposite extreme, a much more simple two-plate capacitance setup exhibits high sensitivity to the binding of proteins on the appropriate interface chemical layer [145, 146]. In that case, both impedance spectroscopy [147] and amperometric [148] measurements are used. The IMEC biosensor group had an activity in this field for developing IDT transducers on polymer with 500 nm periodicity: we never managed to achieve reproducible results on these devices which appeared challenging to manufacture and even more difficult to handle during the chemical functionalization step. PDMS packaging was specifically developed for this application (Fig. 2.8).

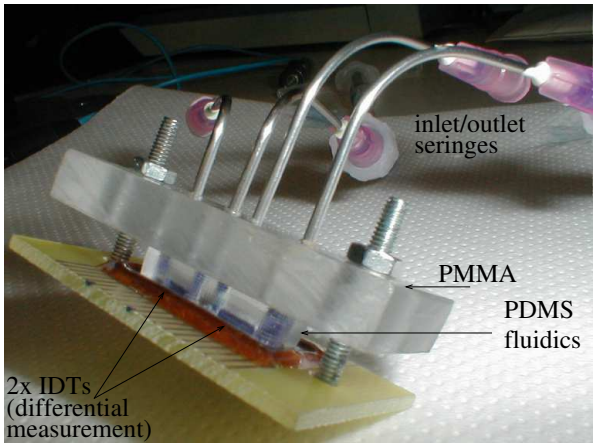

Figure 2.8: Packaging example for a dual-IDT setup (Au IDTs on silicon) used for spectroscopic impedance analysis. The PDMS cell provides a tight seal between the inlet and outlet syringes and the silicon substrate, while the PMMA piece generates uniform pressure over the whole area of the PDMS seal. The challenge for transferring this technology to the SAW sensor is that in the latter case, the acoustic signal has to propagate with minimal attenuation under the seal designed to prevent the liquid from reaching the IDTs.

2.2.6 Scanning probe microscopy

Scanning probe microscopy in liquid medium [149], and most especially atomic force microscopy (AFM), has been considered as potentially very useful for probing at the nanometer

level the reactions occurring on surfaces [150, 151]. Comparing topographic images provided by scanning probe microscopy, taken at different times during the adsorption reaction, provides at best images which require extensive interpretation, or at worst results unusable or in wide disagreement with other sensing mechanisms [152]. Molecular resolution can be achieved by AFM and informs on the layout of the protein film on the surface [153, 154, 155, 156], most usually on large proteins such as fibrinogen. Part of the experimental challenge in such experiments is achieving atomically flat surface on significant area of the sample: for example, high temperature or hydrogen flame annealing of gold is incompatible with the lower Curie temperature of piezoelectric substrates used for acoustic sensing. Data processing on the resulting images is eventually used to extract quantitative informations on the layer under investigation, such as relative volume of protein on the surface [157] or surface roughness as estimated by a fractal dimension [158].

Although straight AFM imaging rarely provides quantitative information on biological samples [159, 160, 161, 162, 163, 164], the analysis of the force distance-curve obtained by the probe can bring new insights at the nanometer level on the interaction between biological species (either bound to the tip or to the surface) and the layer under investigation [165]. Indeed, using AFM-related methodologies, quantitative binding force measurements between molecules have been obtained [166], or more rough repulsion/attraction force estimates depending on the layer charges have been monitored [167, 168]. Such measurements find applications in the development of surfaces which are either attractive or repulsive to biological species, and should be consistent with the claims of Cooper *et. al* of breaking binding bonds using high vibration amplitudes of QCR [169].

The need we expressed in the beginning of this discussion concerning the functionalization of the transducer surface in order to efficiently bind receptor molecules and define the kind of interaction with the unknown molecules is still valid for scanning probe microscope tips. This aspect is demonstrated with the ability to change the kind of interaction – from hydrophobic to hydrophilic on the tip side – by changing the surface chemistry [170, 171, 172]. One challenge we have met in our own attempts to functionalize AFM tips is the assessment of the aging of the functionalization layer as the probe scans the surface of the sample: strong coating of silicon tips with metal, resistant to wear during contact mode scanning, is difficult to achieve. When the metalization is not deteriorated during the imaging steps, the distribution of the molecules and their diffusion along the surface – a process well know in the dip-pen patterning method – is itself a challenging task only a few groups have been able to tackle appropriately [173].

Beyond the atomic force (and in this case chemical binding force) mapping, a special case for enhancing the signal from proteins and identify their binding property is the imaging of electroactive species by scanning tunneling microscopy [174]. Scanning Electrochemical Microscope [175, 176, 177] and Kelvin probes [178] have demonstrated amazing mapping of ionic pore transport processes [179, 180, 181, 182] down to the single channel resolution.

2.3 Biosensor metrology: how do the techniques compare ?

2.3.1 Comparison of SAW and SPR

We have seen two major sets of techniques based in one case on mechanical property changes due to the added biological film, and on dielectric or optical index property variations in the second case. The results of these two measurement techniques can be compared and common parameters such as the layer thickness and water content related for added information on the layer under investigation. QCM measurement setups have been combined with the following optical techniques: ellipsometry [183, 184, 185], SPR [186, 187, 188, 189], interferometry [190].

Biosensors are based on the monitoring of physical signals resulting of reactions occurring on surfaces: these signals depend on the surface density of sensing sites. On the other hand the property of interest for the user of the instrument is the bulk concentration of the protein to be detected. A major issue to be solved is to understand the conversion mechanism from a transducer signal to a surface site density to a bulk concentration. This conversion depends on the physical principle of the transducer and on its parametric sensitivities to temperature, hydrostatic pressure, acceleration, on the chemical binding properties of the receptors to the sensing surface and their affinity to the analyte to be detected (association and dissociation constants of the sensing molecule to the surface and with the analyte) and on the fluidics supplying the analyte to the sensing area (diffusion control or strong mixing). Since any of these parameters will affect the detection limit, a realistic simulation for predicting the capability of a transducer is difficult and requires accurate physical parameters to be included in the model. One issue here is the very wide variety of physical properties of protein layers that can be found in the literature: optical index range from 1.45 to 1.454 [191, 185, 192] while densities range from 1.2 to 1.45 g.cm^{-3} [184, 193, 185, 192]. We have thus developed an instrument combining SPR (based on the Holland Biomaterials Ibis SPR instrument) and SAW for simultaneously probing the properties of a layer adsorbing on the gold-coated quartz surface using the two techniques [194], as well as the associated signal processing techniques (SPR signal fit for improved resolution, modelling the acoustic and optical signal to generate tabulated responses to various layer properties and hence identify from the experimental data what physical parameters represent correctly the properties of the layer). Such an experiment provided the data needed to identify the discrepancy between the measurements obtained from the two techniques when monitoring thick, solvent swollen, organic layers (Fig. 2.7).

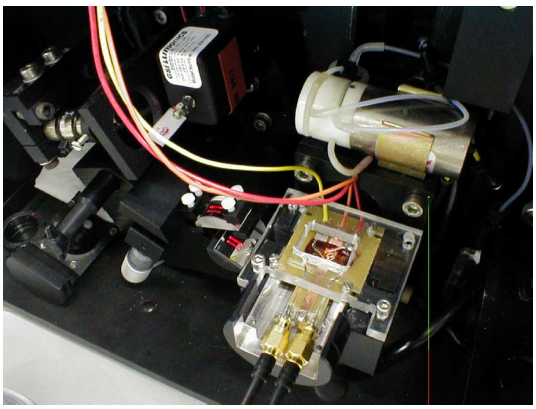

Picture of the SAW/SPR combination setup

Water content in the protein film will modify the value of these physical parameters depending on experimental conditions. A wide range of possible water content is reported [132] –

from 30 to 78%. This water content can be expected to depend on protein conformation [184], which is itself function of ionic concentrations in the surrounding medium, pH ... We have ourselves characterized the water content of a polymer which evolves from an hydrophobic (shrinking configuration towards the hydrophobically treated gold surface) to an hydrophilic (swelling configuration) as a function of temperature: poly(N-isopropyl-acrylamide) - PNIPAAm [195]. In this analysis, we were able to demonstrate, to the best of our knowledge a unique contribution to the understanding of the conformation of this polymer physisorbed to a surface, an evolution of the water content in the layer from about 5% to 15%, with significant changes in the viscosity (1.5 to 4 cP) and thickness (from 20 to 60 nm) of the adsorbed layer.

Certainly the best known example of calibration of a direct sensor is the use of radiolabeled proteins to determine the SPR signal to protein surface coverage of the commercial Biacore (Pharmacia Biosensor AB, Uppsala, Sweden) instrument [132]. Since this calibration was done on a limited range of proteins, care should be taken when using the data processing strategy implemented in the Biacore system data acquisition software to compute protein surface coverage [196, 197]. Biacore uses two units, the Response Unit (RU) and the Refractive Index Unit (RIU). The RU (which is equal to 10^{-6}RIU) is defined so that 1000 RU is equal to 0.1 millidegree – the more usual quantity used when simulating SPR response being the angle shift of the incoming laser with respect to the gold-coated side of the prism surface. The conversion to surface coverage provided by this commercial instrument is that 0.1 millidegree corresponds to a protein layer of 0.1 ng.mm^{-2} [132]. Comparing results from different manufacturers of SPR instruments is further complicated by the fact that they all work at different wavelengths, selected due to technological constraints: Texas Instruments uses integrated semiconductor chips centered around 840 nm (infrared diodes well know to a semiconductor manufacturer), Biacore uses commercially available diodes centered at 760 nm while Holland Biomaterials uses in its Ibis instrument a semiconductor laser at 670 nm. These longer wavelength than the usual HeNe 633 nm laser are selected since the longer the wavelength, the sharper the SPR signal. The assumptions behind this conversion include the optical index of the dielectric layer adsorbed on gold (which defines the conversion from a given layer thickness to an angle shift and hence to RU) and the density of this layer (which converts a given thickness to an adsorbed mass). As an illustration of these approximations, Fig. 2.9 exhibits a simulation comparing the angle shift associated with the coating of the gold surface with a 10 nm thick layer with optical index 1.45 or 1.454 (which is the range of values found in the literature). The former case yields an angle shift of 813 m^o while the latter is 0.837 m^o. Notice that the angle shift is not simply a matter of optical thickness – due to the evanescent nature of the SPR wave – since a layer 10.4 nm thick with optical index 1.40 provides the sample optical thickness than a 10 nm thick layer of optical index 1.45, but only yields an angle shift slightly larger than the 10 nm thick layer. The second assumption needed when converting the thickness to a surface mass density is the volume density of the layer: a 10 nm thick layer provides 8.3 ng/cm^2 if the density is 1.2 and only 7.1 ng/cm^2 at 1.4 g/cm^3. In this example, 1000 RU=0.1^o would be associated, assuming a linear relationship between angle shift and layer thickness (as verified by simulations) with a thickness of 1.2±0.03 nm and hence a surface density of 100 ng/cm^2=1 ng/mm^2 *if the volume density of the layer is 1.2.* These two assumptions, optical index and density of the adsorbed layer, will be discussed later (section 2.3).

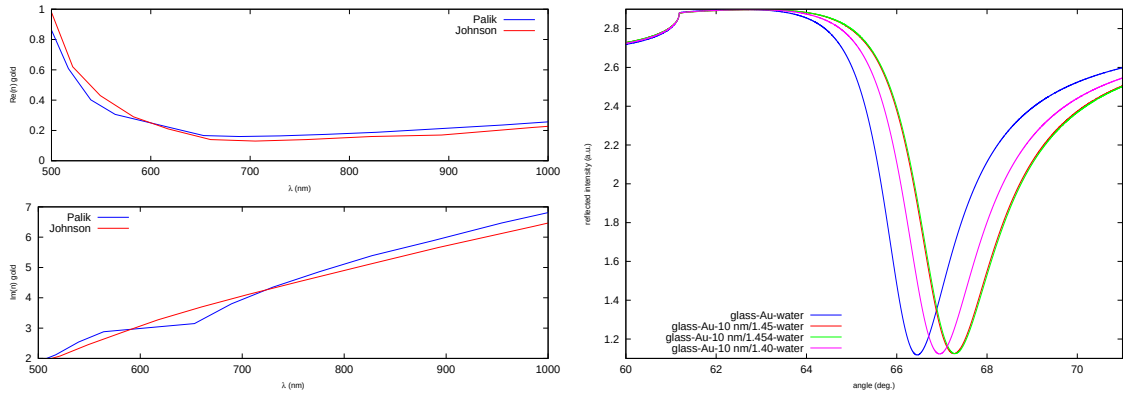

Figure 2.9: Left: comparison of two tabulated datasets (Ref. [86, 88]) of the complex optical index of gold, a fundamental parameter when modelling surface plasmon resonance behavior to adsorbed layers [198]. Right: evolution of the reflected intensity *v.s* incoming laser angle (and hence wavevector) at fixed wavelength (760 nm). This simulation was performed using $n_{Au} = 0.14 + i \times 4.58$, $n_{glass} = 1.518$ and $n_{water} = 1.33$, varying the optical index of the adsorbed layer while keeping its thickness fixed at 10 nm. The gold layer supporting the plasmon was taken as 45 nm thick. Software implementation of [131] provided by R. Giust (optics department, FEMTO-ST).

AFM imaging of the surfaces on which the reactions occur might at first seem an attractive idea for gathering knowledge on the reactions occurring on the surface, such as film homogeneity, thickness or protein orientation on the surface. However, most reports of AFM images of protein layers displaying molecular resolution require specially prepared surfaces, either ultra-flat gold or titanium or atomically flat mica. None of these surfaces are compatible with another measurement technique such as SPR [199] or QCM [200, 201]. Hence, the combination of AFM with two direct detection approaches often leads to disappointing results due to the surface roughness of the gold layer on which the reaction is occurring (50 nm thick evaporated gold layers on optically polished quartz samples with less than 1 nm peak to peak roughness display peak to peak roughnesses in the 3 to 5 nm range).

While the combination of SAW sensors with integrated optical waveguide sensors should be technically feasible since both techniques use a same material as substrate (lithium tantalate) and bring new informations on the adsorbed layer in a way similar to SPR and SAW combination, such an instrument has not yet been built.

2.3.2 Atomic force microscopy combined with acoustic sensors

In order to compare complementary models at the sub-micrometric scale and the millimetric scale, we combine a scanning probe microscope and either a quartz crystal resonator (QCR) [202, 203] or a SAW delay line. The first technical challenge is the identification of a suitable scanning probe microscope in which the probe is in motion over the fixed sample (Fig. 2.10), as seen for example in Molecular Imaging's AFM. Furthermore, we wish to work in liquid to perform electrochemical reactions and analyze biological samples.

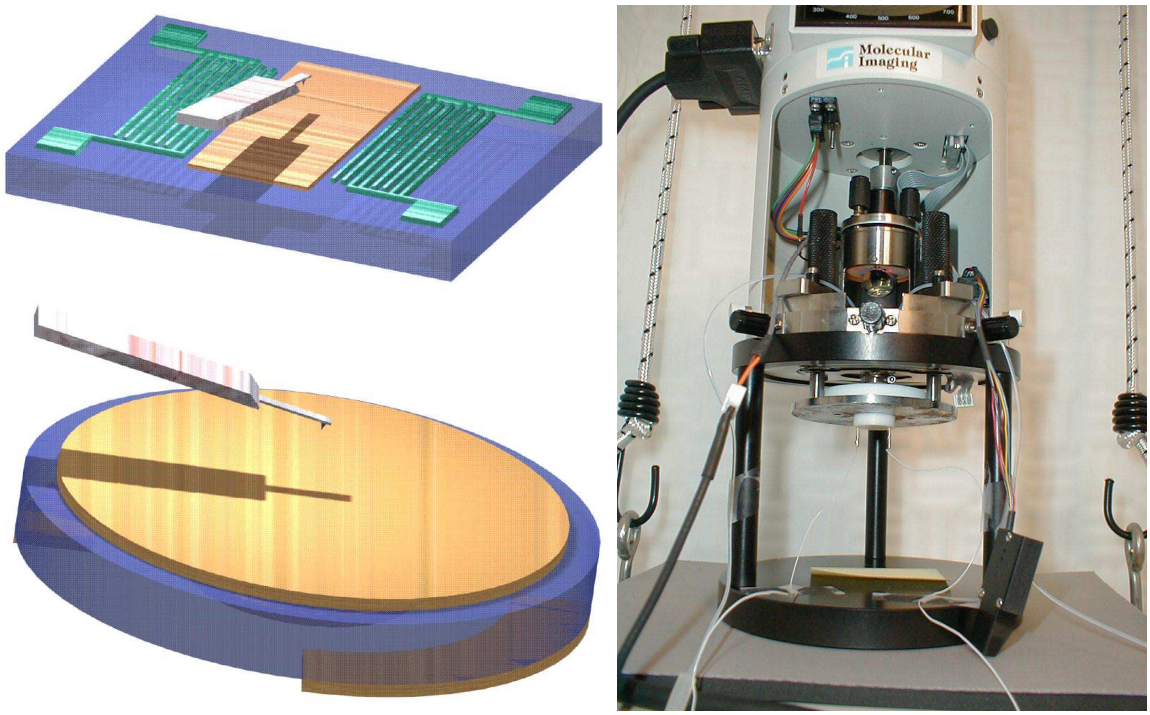

Figure 2.10: Molecular Imaging's AFM compatible with measurement of samples in liquid media. The tip, whose deflection is detected by optical means (reflected laser) is mobile while the sample holder is fixed. Artwork on the left by K.H Choi.

In the most common silicon AFM probe (as opposed to the shear force probe we will discuss later in section 2.4), a tip-ended cantilever is kept at a constant height over a sample. The tip height is typically a few micrometers, so that a thin layer of liquid is confined between the cantilever and the surface of the acoustic sensor, as well as between the tip holder (a few hundred micrometers above the surface) and the acoustic transducer. Beyond the classical model of a pure shear wave propagating in a QCR, the finite dimensions of the electrodes means that some longitudinal waves are generated in the liquid by the QCR. These propagative waves generate a standing wave pattern with interference conditions varying with the cantilever-acoustic sensor surface distance. We have observed that this standing wave pattern and the feedback of the longitudinal wave on the acoustic sensor is the source of additional noise on the resonance frequency measurement, especially in the fundamental mode of the QCR where the energy is poorly confined in the resonator [42]. This phenomenon is especially visible during the probe approach phase before any imaging actually occurs as we have observed during such experiments: bringing a vibrating QCR close to an AFM holder generates standing wave patterns with boundary conditions dependent on the probe holder-quartz surface [204]. Due to the lack of energy confinement in a delay line and hence lack of displacement magnification by the quality factor, this effect is not seen on acoustic delay lines.

Although the application of the AFM-acoustic sensor combination has been disappointing, partly due to the roughness of the PECVD silicon dioxide coating and even of the thin polycrystalline gold film on QCR, when applied to biological samples [152, 205], we have

found the complementarity of the nanometric scale imaging and acoustic response useful when applied to electrodeposition aimed at understanding the resonator response to loads with various geometries [81].

2.4 Shear force microscopy: beyond the AFM

The Atomic Force Microscope is the most basic form of scanning probe microscope: a thin (low stiffness) cantilever is swept over the surface and tip-surface interactions are detected either as low-frequency deflections of the cantilever or high resonance frequency shift. While historically the first AFM deflection was measured using a tunnelling current measurement setup (requiring fine adjustment of the tunnelling tip with respect to the AFM cantilever and low noise, low drift current measurement amplifiers), the most common deflection measurement techniques is nowadays the laser deflection technique: a laser is focused on the cantilever and reflected on a photodiode. Alternative optical techniques include interferometric measurements: in all cases the optical alignment process is tedious and time consuming, especially if the sample is coated with liquid.

Alternatively, the cantilever would include its own deflection sensor. While some of the most complicated cleanroom processes include not only a piezoresistive layer atop the cantilever but also the whole measurement electronics, using a cantilever made of a single-crystal piezoelectric material is possibly one of the most efficient way of actuating (voltage applied to the cantilever) the device and detecting its interaction with a surface (current sensing). Although cleanroom manufacturing of piezoelectric substrates is a complicated task, small piezoelectric cantilevers are readily available as quartz tuning forks for the watch industry [206]. Hence, the quartz tuning fork in used here as a compact, integrated scanning probe sensor which efficiently decouples the tip-surface distance control (vibration of the tip over the surface and measurement of the phase between excitation voltage and measured current as a function of interaction force) from the actual (electro)chemical function of the tip. Since the tip only aims at reducing the area of the probe-surface interaction but has no influence on the distance control, its chemical nature, orientation or electrical connection are free to be tuned to any kind of application [207]. Amongst the most intriguing applications of such devices are the Scanning ElectroChemical Microscope (SECM) [175, 208] in which the tip acts as a working electrode (electrochemical potential mapping or ion flux measurements), Magnetic Force Microscopy [209] or Scanning probe Near-field Optical Microscope [210, 211, 212]. In all these cases, our interest in combining the scanning probe tip with acoustic sensors is

- complementary scales of interaction (millimetric for the acoustic wave, nanometric for the scanning probe)
- complementary physical quantities (mechanical, dielectric, chemical)
- small size of the probe and the associated probe-surface distance feedback mechanism.

However, before claiming to replace AFM probes with shear force microscope cantilevers, one must assess the spatial resolution (associated with the vibration amplitude of the tip)

and accuracy of the measurement. In order to achieve these goals, we have focused on two aspects of shear force microscopy [213, 214, 215, 29, 216, 217, 218, 219]:

- improved sensitivity through dynamic quality control. The quartz cantilever is a very stiff sensor [220] whose performance can only be appreciated through its large quality factor yielding stable base line and hence accurate measurements. In order to magnify this aspect, we have been interested in "artificially" improving the quality factor by injecting in phase energy in the resonator. Since the quality factor is the ratio of the stored energy to the dissipated energy during each period, injecting energy in-phase with the oscillation will provide quality factor improvement. The limit to the improvement is the oscillator, where the energy injected overcomes the losses.
- analyze through interferometric methods [214] and digital imaging processing techniques [215, 216] the vibration amplitude as a function of input voltage but also modelling the nature of the vibration and selecting the acoustic mode providing the best sensitivity (by increasing the area covered by the tip during each oscillation period [4].

Using finite element analysis on the one hand, optical methods (speckle interferometry and stroboscopic imaging of the cantilever followed by subpixel-displacement detection) we have demonstrated that under classical conditions (sub-V amplitude excitation voltage), the vibration amplitude is in the 10 to 50 nm range, about an order of magnitude worse than AFM but about the same order of magnitude than the tip radius. While the detection of a physical phenomenon enhanced by the tip (localized surface plasmon, electrochemical current) might be detected with a better resolution by using a synchronous detection strategy, the distance feedback averages the mechanical forces of the sample acting on the probe. Most important for our application, we have become familiar with the realization of the shear force microscope heads and established that the volume of the probe is less than 10 mm^3, much less than that of an AFM head, and compatible with a measurement on a SAW surface packaged in an open-cuvette fluidics setup. Furthermore, the tip-sample interaction is obviously visible during the stroboscopic imaging process, and while tuning forks are attractive because they include in the same transducer the actuator and the sensor, the techniques we developed might be used for real time distance control with sub-nanometer accuracy. At the moment this processing is performed off-line due to the heavy computing load (2D Fourier transforms of each image), but the topic of including complex processing algorithms in reconfigurable processors for real time applications will be the topic of the last chapter of this presentation (section 4.4). The model of the tuning fork we have developed might be usable to match experimental force-distance curves with various models of tip-sample interactions, but such extensions of our work are still in progress and no usable result has been achieved yet.

2.5 Conclusion on chemical (bio)sensors

Having reviewed some of the transducers compatible with a direct detection application targeted towards molecules in liquid media, we have wondered how to quantitatively qualify the

[4] private communication with D. Courjon

physical properties of the organic layers adsorbed to the surfaces. In order to reduce the number of variables and achieve as many individual measurements as we have found parameters, we have focused on combining various techniques. Furthermore, analyzing simultaneously a given layer with several technique focused on a same spot allows for a comparison of the responses and a validation of the assumption made in extracting layer parameters from each measurement. During a further application step, multiple techniques provide unique signatures for each compound, an approach similar to that used in "artificial noses" except that we here replace an experimental classification of the responses of different layers to various compounds, by a physical modelling of the response of a given layer probed by different techniques.

In order to acquire informations at complementary scales, we have attempted to use scanning probe microscopy (AFM and shear force microscopy) for gathering topographic data at the nanometer scale complementary with the micrometric (SPR imaging) or millimetric (acoustic wave propagation) lateral resolution of optic and acoustic techniques. Although working on polycrystalline gold and PECVD-deposited silicon dioxide layers has proved difficult due to excessive background surface roughness, extensions towards the local chemical characterization with SECM or Kelvin probes should provide useful informations such as in-situ (bio)molecule surface coverage.

Hence, further work on biosensors will focus on the white light SPR combined with SAW sensors for improving the definition of the constants we use in our models of thin films, and possibly on the addition of a scanning probe technique as described above. Achieving these steps requires stabilizing cleanroom processes such as device manufacturing, thick layer PECVD deposition and etching, and liquid tight and robust open-cuvette packaging of the acoustic sensors.

Chapter 3

Acoustic sensors for remote sensing

Most of the work on wireless interrogation of acoustic sensors for the determination of a physical quantity focuses on the use of acoustic delay lines [221, 222, 223]. As opposed to the 4-port acoustic delay line described earlier, the configuration most commonly used is a 2-port configuration suitable for connecting an antenna, in which the same IDT is used to launch the wave and detect the energy reflected on mirrors patterned on the piezoelectric substrate. This configuration is probably commonly used because its spectral response is rich and provides many degrees of freedom for improving one particular aspect of the sensor (reference signal, identification with a large number of bits, coupling ...). For historical reasons related to industrial applications of these sensors in our study – burying the sensors in a polymer to monitor its temperature evolution for instance – and complying with radiofrequency (RF) emission standards, we have selected the less usual approach based on resonators [224]. The consequences in terms of performances, application fields, interrogation electronics but also limitations in terms of identification will be described here first with a summary of the available literature, followed by a description of our own contributions to this field.

3.1 Introduction

The most intuitive introduction to 2-port delay lines refers to its time-domain operation: a short electromagnetic pulse is converted into a short acoustic pulse launched on the piezoelectric substrate by a short set of IDTs (typically 10 to 20 fingers). While propagating on the surface, this acoustic pulse is reflected by impedance variations, whether due to mass loading (deposited electrode gratings) or obstacles (etched grooves). After being delayed by the propagation time, the reflected energy is converted back to an electromagnetic wave by the same IDT used previously. Hence, acoustic delay lines are defined by a rich set of features (reflected energy bursts) in the time domain, however necessarily associated to a wide spectral occupation. The time delay between pulses is associated with the physical quantity being measured as long as the acoustic velocity is affected by this quantity. The interrogation unit hence sees, as an answer to a single probe pulse of typically 100-ns long, a series of

reflected pulses separated by a time delay in the hundreds to microsecond range. Hence, the spectral bandwidth of such devices is typically a few tens of MHz, defined by the length of the transducer.

On the other hand, resonators are characterized by a narrow spectral bandwidth Δf, typically a few tens of kHz for a working frequency f_0 above 100 MHz. The corresponding quality factor $Q = f_0/\Delta f$ is achieved on devices with small (millimetric) dimensions thanks to the energy confinement in a cavity made of interdigitated transducers [225] surrounded by Bragg mirrors. The design of resonators is complicated since the design of mirrors with optimum reflection coefficients requires an accurate model including the influence of the geometry of the reflectors (metal thickness as a function of the metal nature, and metalization to period ratio).

Although resonators and delay lines are designed with different constraints and probing methods in mind – resonators are most easily described in the frequency domain and delay lines in the time domain – the conversion of the description of each behavior between time domain and frequency domain is always possible through the Fourier transform. The duality of the description of each behavior means that we find similar methods for probing each kind of transducer: either processing the time domain response of the transducer to a short pulse (impulse response yielding an exponential decay of the resonator signal or multiple reflections of the delay line) or the (frequency) spectral domain obtained by sweeping the probe signal frequency at a rate slow enough to achieve appropriate spectral separations of the contribution of each frequency (identification of the resonance frequency of a resonator or the time domain response of the delay line through an inverse Fourier transform). The probed bandwidth is defined by the kind of transducer under investigation: wideband or short time pulse for delay lines, narrowband or long time pulses for resonators.

Hence, selecting a delay line or a resonator as transducer is not a matter of acoustics (both responses are similar, under the assumption that the measured quantity is mainly due to an acoustic velocity variation and *not* associated with a synchronism condition – loss of the reflection on the Bragg mirrors) but of complying with radiofrequency emission standards and technological constraints. The use of delay lines has been demonstrated for a number of applications including chemical species concentration measurement [226, 227] and physical properties [228, 229] including temperature [230, 231, 232, 233, 234, 235], pressure [236, 237, 238, 239], stress [240], torque [241], and moisture level [223, 242, 243]. Another way of using acoustic transducers is as a converter from a low frequency response (as for example provided by silicon MEMS, Fig. 3.1) to the radiofrequency through capacitive pulling of the resonance frequency.

Due to their intrinsic wideband response, delay lines can comply with ISM radiofrequency emission regulations only in the 2450 MHz range and beyond. However, reaching such frequency requires an excellent technological control of the fabrication techniques, with optical lithography patterning of metallic structures with submicrometric dimensions on piezoelectric substrates: these constraints are less severe when aiming for lower frequencies. Furthermore, the penetration depth of the interrogation electromagnetic waves in dielectrics is more efficient at lower frequencies: low frequency devices are easier to probe when embedded in dielectric media such as soils or plastics. However, the dimensions of the antennas scales with

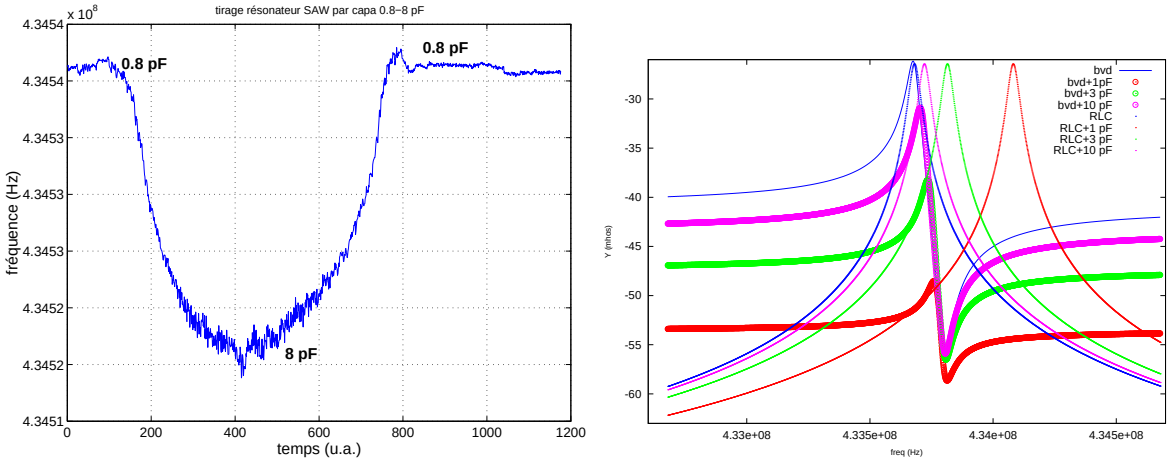

Figure 3.1: Left: wireless measurement of the capacitive pulling of a single resonance around 434 MHz with a variable capacitor tuned from 0.8 to 8 pF. Right: the optimum pulling capacitance is close to the parallel capacitance (classically called C_0 in the Butterworth-van Dyke model), but the pulling efficiency is limited by the antiresonance. This experiment was performed to simulate a humidity level detector, developed as a capacitor with varying value as a function of moisture level. The moisture sensor happened to be unsuitable for RF applications though. The Butterworth-van Dyke parameter used in these simulations are $C_1 = 1.85$ fF, $L_1 = 72.8$ μH, R_1=21 Ω and C_0=3.3 pF.

the frequency, and typical dimensions are a fraction of 70 cm at 434 MHz in vacuum and is reduced to only 12 cm at 2450 MHz.

The 80 MHz-wide, 2.45 GHz range band, cluttered with digital communication signals, is used for delay lines interrogation units. The European 1.7 MHz-wide, 434 MHz band, is used when interrogating resonators. These default selections are due to technical constraints: the former induces too many technological difficulties to reach reliable performances – mainly concerning the quality factor – when fabricating resonators, the latter is too narrow for interrogating delay lines of usable dimensions (<1 cm).

A more general concept is that we shall always perform *differential* measurements by exploiting two signals from a transducer – one being associated with the physical parameter to measure and the other one independent of this quantity and used as reference – allowing thus the rejection of correlated noise sources to only keep the measurement information [244, 245]. This technique is usually performed using resonators by patterning two transducers at different propagation angles on a same substrate (*i.e.* with different resonance frequency dependencies for the measured quantity) and, for delay lines, measuring the *phase difference* between multiple reflections on mirrors patterned on the substrate on which the acoustic wave propagates (Fig. 3.2).

Since they arguably are easier to design and to manufacture, the literature is mainly filled with presentations focusing on the use of delay lines, while only two industrial applications are based on interrogating resonators: Transense (and Vectron with its sensor department called Sengenuity) and SENSeOR. The strategies used for probing resonators by these two

companies are different as will be seen later.

3.2 Interrogating delay lines

3.2.1 Time delay measurement

Let us first consider the interrogation of delay lines [246, 247, 248, 249, 250, 251, 252]. The simplest strategy consists of generating a short radiofrequency pulse centered on the working frequency of the interdigitated transducer connected to the antenna, then of sampling the returned signal from the sensor, and finally identify the two-way time of flight duration (Fig. 3.2). The acoustic wave velocity is associated to the measured quantity, considering that the travel time of the electromagnetic wave in air is negligible, which is anyway eliminated by comparing the *relative* delay between reflectors on a same delay line. This relationship is usually approximated as a polynomial series, and locally linearized to provide a proportionality factor between the measured frequency and the physical quantity under investigation.

A first approach for identifying the delay is performed by identifying the position of the maximum of returned signal. This method, very sensitive to noise on the measured power, is improved by a polynomial fit of the envelope (hence reducing the influence of noise since the position of the maximum is associated with multiple received power measurements). An additional improvement consists in performing an intercorrelation of the received signal with the expected received signal (optimum matched detection filter), but intercorrelating two rectangles of width (duration) τ yields a triangle with base width 2τ, which only provides a rough propagation time delay estimate. Using a frequency sweep (chirp) for pulse compression is discussed in the next paragraph.

A significant improvement of the measurement resolution is achieved by measuring the *phase* of the received signal. In this case, the maximum received power (identified through a crosscorrelation) provides a rough estimate of the physical quantity – needed to solve multiple 2π phase rotation ambiguities – while the phase measurement relative to a local oscillator or from one reflection to another provides an accurate measurement of the propagation time. An absolute phase measurement does not make sense (since the local oscillator does not meet synchronization conditions with the wideband signal propagating on the acoustic device) but only *relative* phase measurements on echos from the transducer provide the means to compute the acoustic velocity and hence the physical quantity to measure. Furthermore, the absolute phase measurement is dependent on the distance of the delay line to the RADAR antenna: the distance effect is eliminated when performing a differential measurement.

Although reflection-mode delay lines have not been a central activity of the time and frequency department of FEMTO-ST, they provide a unique opportunity as active targets for classical RADAR systems [253]. We have hence developed a reflective delay line compatible with classically available Ground Penetrating RADARs (GPR) for use as a buried, passive and wireless temperature sensor. Since GPR usually work in the 50 to 500 MHz range as a compromise between modest antenna size and electromagnetic wave propagation depth, we

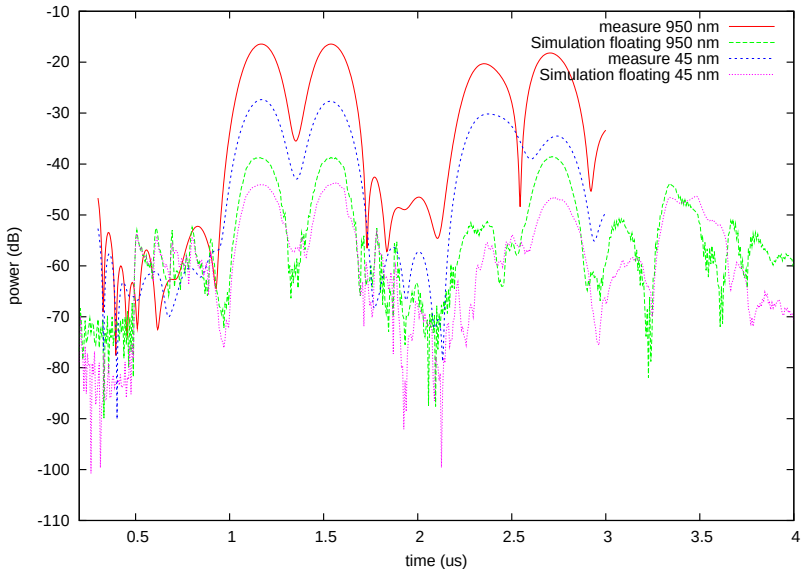

Figure 3.2: Comparison of the modelled – using a mixed matrix method – and experimental reflection response of a 100 MHz delay line made of 45 nm thick and 950 nm thick Al electrodes on $LiNbO_3$-(YXl)/128. While the absolute modelled magnitude is pessimistic compared to the experimental data, the relative peak magnitudes and position in time are accurately predicted. During the experiment displayed on the left, the sensor was moved from a distance of 1 m from the receiving antenna (2 m from the emitting antenna) to 50 cm at time 250 (trace 600): the delay reduction is observed on the two reflected signals but is no longer visible on the *differential signal* (phase difference between the two reflected pulses) used to compute the temperature. Models and delay line designs performed by S. Alzuaga (time-frequency department, FEMTO-ST). Unpublished data.

had to comply with the available instrument working at 100 MHz. The resulting delay line is a chip less than 1 cm^2 in dimensions, but the associated antenna is still about 1 m. Indeed, the electromagnetic wavelength of 3 m is reduced in a high permittivity medium, and the 300 m/μs velocity in vacuum is reduced to 170 μm in ice, the medium we wish to apply this technology to. At such a velocity, a half-wavelength dipole is 85 cm wide, made of two flexible wires 42.5 cm long each. We have, using such a setup, demonstrated the measurement of the temperature of the transducer with sub-K resolution (Fig. 3.3). However, we have also identified that a single electromagnetic pulse, as generated by RADARs during the imaging step, is inefficient in loading the delay line. Our current interest, having analyzed all the emission and reception stages of the commercial RADAR, is the development of a custom electronic system able to switch between RADAR imaging mode (single pulse) and SAW delay line monitoring (generating as many pulses as their are finger pairs in the transducer): the former mode for the classical sub-surface structure identification and sensor positioning, the latter for the actual physical quantity measurement.

This strategy is obviously applicable to other quantities than temperature, and most significantly for geophysical purposes the strain applied to load cell in a strain gauge configuration. Similarly, pressure sensors might find applications for measuring water pressure during thawing and freezing processes.

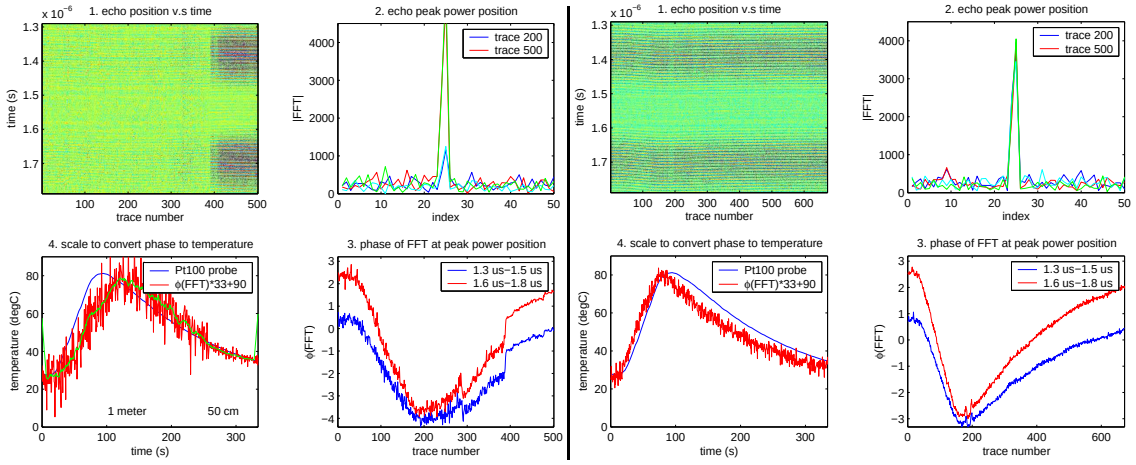

Figure 3.3: Two examples of reflective delay line temperature measurements using a 100 MHz MALA RAMAC instrument. The processing steps are first to record echos as is classically done during sub-surface structure search (top-left); the processing steps include broadband Fourier transform for identifying the reflected signal (top-right), followed by a phase extraction of the Fourier transform at the index previously identified (bottom-right). Finally, the calibration coefficients are applied to convert a time delay to a temperature, and a comparison is performed with a reference (Pt100) sensor (bottom-left). The delay lines were designed and manufactured by S. Alzuaga, time-frequency department, FEMTO-ST. Unpublished data.

3.2.2 Pulse compression

We have seen that one limitation of the crosscorrelation identification of the position of the echo of duration τ centered at a fixed frequency is that the crosscorrelation width is 2τ. A classical method for pulse compression by a factor B – yielding a crosscorrelation pulse width reduction by a factor B – is to generate a pulse shape allowing a distinction between the beginning and the end of the pulse. One way of achieving this result is to sweep the frequency during the emission to generate a so called *chirped sequence* [254, 255]. When a chirped signal sweeps a frequency span ΔF during a pulse duration τ, then $B = \tau\Delta f$ (Fig. 3.4). Beyond the improved accuracy on the time delay estimate, energy conservation implies that the shorter the crosscorrelation width, the larger the magnitude of the peak: this effect is *not* visible on Fig. 3.4 since all the magnitude curves were normalized so that the maximum amplitude is 1 (as opposed to a constant unit area). A large crosscorrelation peak magnitude implies that a signal can be extracted from a noisy measurement, hence compensating for the large insertion losses of delay lines and hence a poor radiofrequency link budget (section 3.2.4).

An alternate strategy to frequency sweeping to reach pulse compression is to use phase coding. Since the aim of pulse compression is to reduce the width of the crosscorrelation peak (for example by providing a signature to distinguish the beginning and the end of the pulse as was shown previously), the same result can be achieved by coding a sequence on the phase allowing the distinction of various parts of the pulse. This method is easier to implement than the frequency shifted chirp since the radiofrequency source is monochromatic

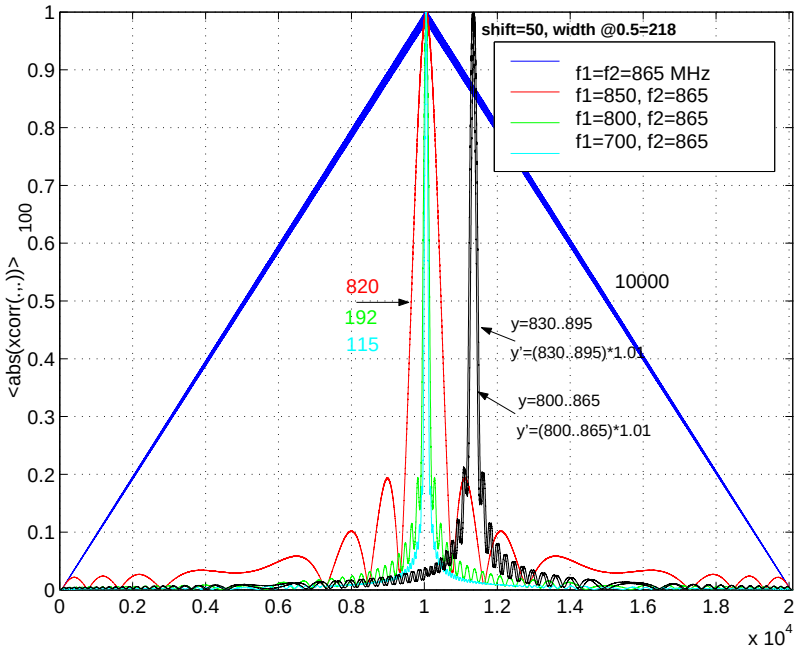

Figure 3.4: Simulation of the pulse compression of synthesized chirps using a variable frequency bandwidth Δf around 860 MHz, swept during a duration τ. These curves demonstrate that the crosscorrelation peak width is reduced by a factor $B = \Delta f \times \tau$. The synthesized signal is sampled with 0.1 ns steps during a 1 μs.

and a programmable phase shifter is located after the synthesis, before the emission power amplifiers. However, this strategy is also more sensitive to velocity variations and Doppler induced frequency shifts which introduces a new phase shift. The purpose of the phase coding is to efficiently distinguish various parts of the pulse: this result is best achieved using the so called *Barder code* encoding.

3.2.3 Frequency domain measurement

The advantage of the time domain approach is how easy it is to implement: generate a pulse, switch the duplexer from emission to reception channels (in a monostatic antenna configuration), and periodically sample the returned signal using a fast analog to digital converter in order to acquire the necessary data for a crosscorrelation calculation. Although computationally and memory intensive, the implementation is straight forward: since the acoustic propagation delay is typically of the order of a microsecond or more, the switching speed of the duplexer is not an issue. Sampling the returned signal is either performed at a baseband level or after shifting to an intermediate frequency using a mixer and low-pass filtering: in any case, a fast sampling rate is needed, greater than 10 Msamples/second (to reach a time resolution in the hundreds of nanoseconds range).

An alternative solution is the use of the duality of the time-frequency approaches and to sweep a wide enough frequency band (the fewer the number of fingers in the transducer, the wider the bandwidth, with typical pulse durations shorter than 100 ns, *i.e.* 10 MHz) around the central working frequency of the delay line. The time domain information is then recovered through an (inverse) Fourier transform. One can demonstrate theoretically and experimentally that the wider the frequency range swept, the more accurate the time domain peak position. This strategy is for example used when characterizing delay line transducers using a network analyzer with a time domain conversion option.

3.2.4 Conclusion on the delay lines

The main advantages of delay lines is their ease of design, and their robustness to manufacturing variations: while the reflection coefficient of the mirrors is dependent on the deposited metal thickness, the main measurement (relative phase of reflected pulses) is solely associated with acoustic propagation characteristics in electrode free areas of the transducer. Furthermore, the full characterization of a transducer used as sensor is performed very quickly: less than 5 μs are typically needed between pulse emission and returned signal sampling to obtain a first estimate of the measured physical quantity (we will see later that duration 1000 times longer are needed for resonators).

The main drawback of delay lines is their large insertion loss (typically more than 35 dB) and hence the reduced interrogation range. This drawback is partially compensated for by using pulse compression techniques described earlier in this document, which beyond improving the time domain accuracy on the crosscorrelation peak position, significantly improve the signal to noise ratio and hence the ability to extract some returned signal from the environmental electromagnetic noise in the radiofrequency link. Finally, delay lines cannot be monitored while complying with ISM regulations in frequency bands other than those above 2450 MHz, which we consider a major hindrance when aiming at an industrial use of these devices buried in dielectric media. We hence analyze the performances of an alternate solution: the acoustic resonator.

3.3 Interrogating resonators

As was discussed before with delay lines, identifying the resonance frequency of resonant acoustic devices [256, 257, 258, 259, 260, 261] is performed either through a Fourier transform after sampling the response of the transducer in the time domain [262] or a frequency sweep as implemented in the classical heterodyne analyzers [263, p.29].

From an electronics point of view, the resonator is characterized by its spectral simplicity: as opposed to a delay line whose response sums the contribution of numerous reflectors, possibly including some phase shift effects, the resonator ideally exhibits a Dirac-like shaped spectrum around the resonance frequency f_0, and practically a finite width Δf spectrum also described through the quality factor $Q = f_0/\Delta f$. The impulse response of such a device

in the time domain is an exponentially decaying oscillation at f_0 with a characteristic time constant (amplitude decay by a factor $1/e$ of its initial vibration amplitude as determined during the excitation phase) $Q/(\pi f_0) = 1/(\pi \Delta f)$ or, similarly, a decay in Q/π periods.

Connecting several resonators in parallel yields an impulse response which is a sum of all the individual contributions, but usually few resonators are excited at the same time because of their narrow spectral width. In case we are trying to comply with ISM band regulations, we focus on keeping the spectra of the excitation pulses within the authorized boundaries (about 434±0.85 MHz or 2450±40 MHz) and only 2 or 3 resonances can be simultaneously located within the lower frequency band. Working in the 434 MHz frequency band was decided following two considerations: at such a low frequency, the penetration depth of an electromagnetic wave in a dielectric medium (cf. the discussion on surface plasmon resonance earlier in this document) – either as a propagating wave with an attenuation due to the conductivity of the medium, or an evanescent wave – is increased at lower frequencies (longer wavelengths, keeping in mind to stay above the water absorption bands), but the coupling efficiency with an antenna of "reasonable" dimensions with respect to most industrial applications (dimensions of the order of ten to a few tens of centimeters) leads us not to work below a few hundreds of MHz, otherwise the antennas reach strongly subwavelength dimensions and only the near field magnetic coupling is efficient (as seen in 125 kHz or 13.56 MHz RFID silicon devices). Working at 434 MHz is hence a tradeoff between the RF link budget and propagation depths in dielectric media.

The two main strategies for probing such resonating devices are:

- generate through a wideband pulse all the available resonances, and separate each contribution at different resonance frequencies through a Fourier transform: the time domain sampled returned signal is converted to a frequency domain response where each contribution is best identified. The advantage of this strategy is a short interrogation duration (a single short pulse loads all the resonators simultaneously, typically within a few microseconds: the wider the bandwidth and the shorter the pulse duration). However, this strategy requires an important computing power in order to compute the Fourier transform, a fast and periodic sampling and a wideband emitted pulse. Furthermore, each resonator is only loaded with the fraction of the energy of the emitted pulse that covers its spectral response, and hence a given emitted power is distributed amongst all the resonators within the probed radiofrequency band.
- excite successively each narrowband frequency band within the probed range (Fig. 3.5). Each band must be narrower than Δf so that the accuracy of the measurement is only limited by the quality factor of the acoustic device and not by the spectral width of the probe pulse. When the probe pulse spectrum covers a fraction of the response of the acoustic resonator, the latter stores some energy which will be emitted once the emission signal stops. The advantage of this strategy is its low requirements in terms of computational power, the need for a single analog to digital conversion of each probed frequency (no periodic sampling) and to optimize the overlap of the spectral responses of the probe pulse and the resonator. However, at first glance the method is slower compared to the other strategies due to the large number of sampled frequencies (128 steps in our implementation) and the finite duration of each probe pulse which

must last at least $Q/(\pi f)$.

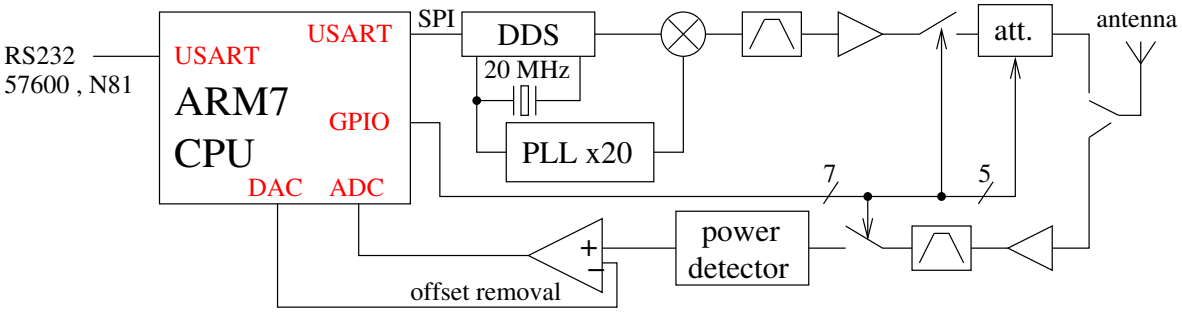

Figure 3.5: Schematic of the embedded interrogation unit we developed for probing the resonance frequency of passive resonators through a wireless link. `att.` is a variable, digitally programmable, attenuator from 0 to 31 dB, used to improve the interrogation dynamics at close range by reducing the emitted power. All sequences – triggering the RF switches for isolation, switching from emission to reception modes, tuning the emitted power, setting the offset after power detection – a synchronized by an ARM7 central processor unit [264].

The latter strategy requires a fast commutation of the duplexer for switching the monostatic antenna from the emitter to the receiver stages: less than Q/π periods of the resonator are available or at most about 1 μs at 434 MHz, and 36 times less at 2450 MHz, to reach the technological limits of the electronic components currently available. Switching off the emission source during the listening phase is the easiest strategy to implement and the one providing the best isolation, but also induces a strong spectral occupation since wideband parasitic emissions are associated with switching on and off the radiofrequency source. An alternate solution, classically known as the continuous wave (CW) RADAR, focuses on a strategy similar to that of an interferometer: a wave is continuously emitted by the reader's antenna, and a fraction of the energy is simultaneously routed towards a phase and magnitude (I/Q) detector. The contribution of the "arm" of the interferometer going through the antenna and radiofrequency link is disturbed by the impedance change of the resonator when present, inducing a phase and magnitude variation and a signal change at the output of the interferometer. Although functional and using much less bandwidth (and hence easing the compliance with ISM regulations), this strategy provides a poorer isolation than the commutation of the source and hence a shorter interrogation range. The duration of the interrogation is still limited by the quality factor of the resonator.

3.3.1 Oscillator

An alternate strategy to openloop probing of the SAW resonator (in which the probed device answers to a forced signal generated by an external source) is to use the acoustic device in an oscillator configuration [265, 266]: the resonator is looped *via* a wideband amplifier which compensates for its insertion losses and phase shift, according to the Barkhausen conditions [267, 28]. However, such a strategy is difficult to implement in a wireless configuration since any variation within the electromagnetic propagation path between the amplifier and

the resonator induces a phase shift and hence an oscillation frequency change (Barkhausen conditions) or, worse, an increase of the losses, yielding oscillation cancellation.

Finally, the forced regime electronics can be placed in a deep sleep mode between two measurements, as opposed to the oscillator whose wakeup time might be long before the signal becomes stable enough for a measurement (note that in the openloop configuration, this issue arises with the reference clock of the DDS). Finally, the complexity of the instrument is shifted from the frequency synthesis (DDS) to the frequency counter, with a global number of components and power consumption [268] roughly equal to that of the openloop strategy.

We have nevertheless pursued the oscillator strategy in a wired configuration in order to assess the ultimate performance of the transducer. Indeed, the analog phase control provided by the oscillation circuit is the most efficient strategy for using at best the high quality factor of our resonators. Since we only have dipole resonators available, we replace the amplifier feedback strategy with a negative resistance, Colpitts oscillator compatible with a use above 100 MHz. In this configuration, one electrode of the resonator is grounded, so that the resulting oscillator is usable not only in an isolated package for physical quantity sensing, but also for (bio)chemical sensing applications. The resulting frequency stability is in the hertz range at one second integration time, and because of the poor thermal insulation (and large temperature coefficient of these temperature sensors), the Allan deviation keeps on rising with longer integration times (Fig. 3.6).

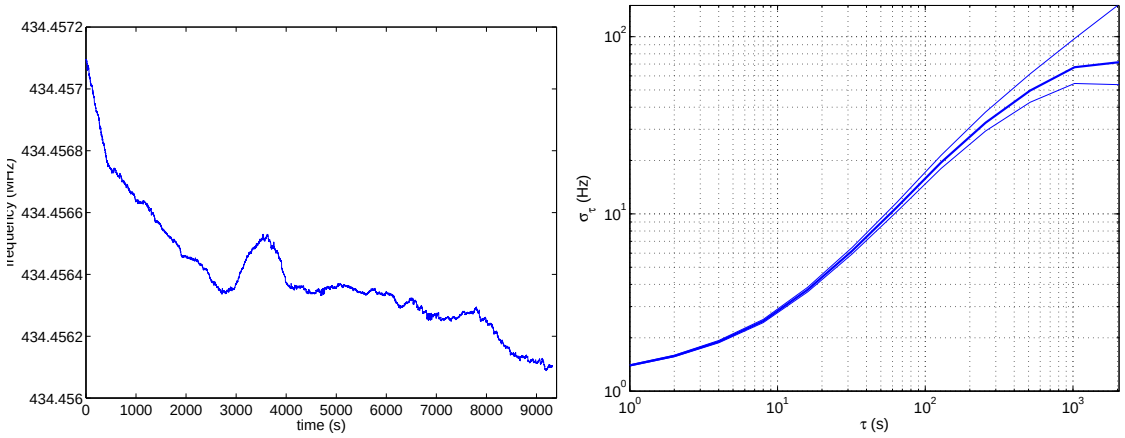

Figure 3.6: Left: evolution with time of the frequency of the oscillator around 434 MHz. Right: Allan deviation, displaying a 1 Hz short term stability (2.10^{-9} relative stability) and increasing with longer integration times due to the thermal drift. Experiment performed by B. François and P. Grosclaude.

3.4 Effects of physical quantities on the sensor behavior

As the principal effect of the disturbing parameters consist in changing the phase velocity of the acoustic propagation, the frequency or the flight time of respectively resonator or delay lines records the useful information for measurement purposes. However, for a given geometry

of the electrode of the interdigitated transducer, any acoustic velocity variation necessarily yields an evolution of the reflection condition of the gratings, and hence a change of the reflected power detected by the interrogation electronics if the reflection coefficient evolves [269, 270]. Thus, a sensor must be designed to operate best in the *middle of its application range* rather than at its rest state as observed during device manufacturing.

Furthermore, characterizing the coupled influence of each physical quantity on the other parameters of the sensor is necessary to identify the number of resonators to be included in the sensor (which quantity to measure) and their coupled behavior. As an example of such study, we have attempted to detect changes of the temperature coefficient of SAW resonators as a function of applied stress (Fig. 3.7). These measurements seem to indicate that the temperature coefficient of the quartz resonator is independent of applied load, provided the resonator remains free to operate in all space directions: the only curve departing from the general trend is the no-load curve, with a discrepancy with the other curves attributed to the lack of application of the load (which also acts as a heat sink) rather than to an intrinsic effect on the quartz constants (Fig. 3.7).

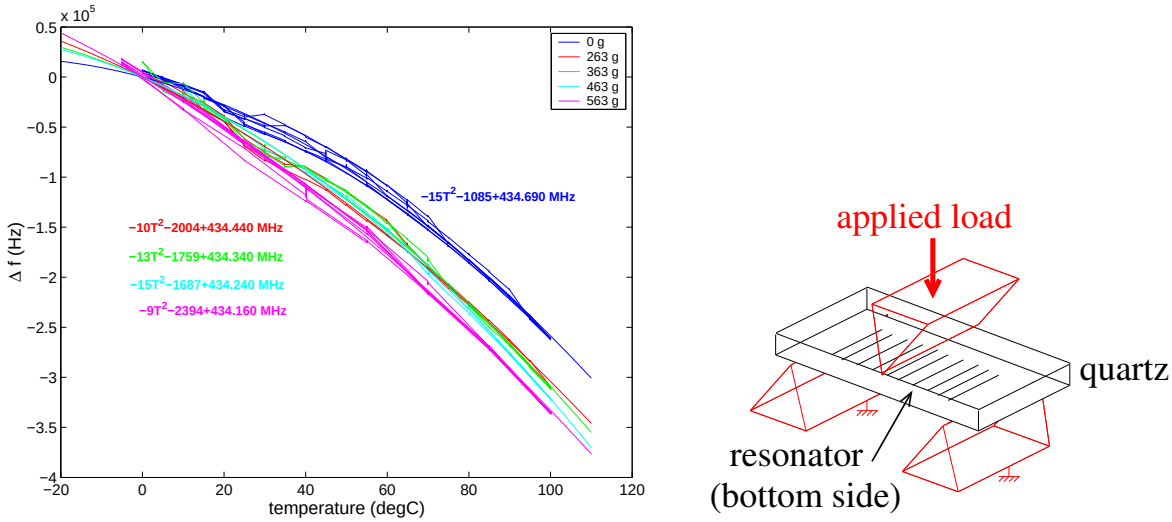

Figure 3.7: Left: experimental assessment of the independence of the temperature coefficient of frequency of a SAW quartz resonator versus applied stress. Right: schematic of the experimental setup. Load (from 0 to 563 g) is applied to an AT-cut quartz resonator while the temperature is swept from 0 to 100 ^{o}C. The full $|S_{11}|$ curves are recorded and post-processed to identify the resonance frequency.

3.5 Experimental validation using RF prototyping tools

Considering the few quantitative data available in the literature concerning the interrogation range and accuracy of the various strategies related to resonators, we have implemented on a rapid prototyping tool (Universal Software Radio Peripheral – USRP [1] – running the

[1] http://www.ettus.com/

GNURadio software [2]) some of these strategies in order to asses their performances.

We will here focus on a comparison of the strategies for identifying the characteristics of SAW resonators, specifically designed for temperature measurement (Fig. 3.8). These devices are the most difficult to monitor using the USRP due to the short switching time between the end of the emission and acquisition steps. The application of this tool to identify the propagation delay of acoustic delay lines was already presented by our group elsewhere [271].

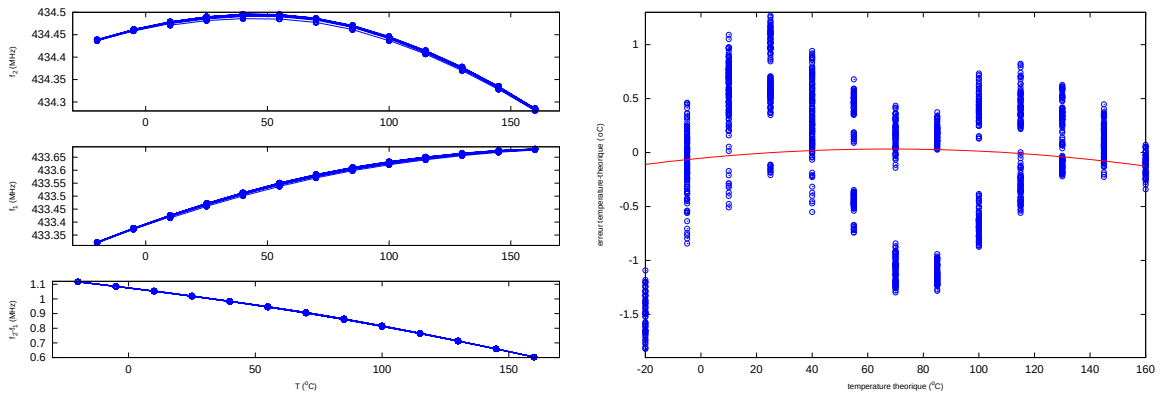

Figure 3.8: Left: calibration curves of the frequency of each independent resonance (top and middle) as a function of temperature, and (bottom) the temperature dependence of the frequency difference. Right: the remaining error after fitting the frequency difference curve from a second order polynomial fit, removing the values of the polynom from each measurement and converting the residual value to a temperature systematic bias. The red curve on the right figure is a second order polynomial fit of the temperature, well below the $\pm 0.5^o$C error.

The USRP provides a reconfigurable hardware platform including FPGA-controlled fast (64 Msamples/s) digital-to-analog (DAC) and analog to digital (ADC) converters. The software controlled radio frequency outputs or inputs are frequency-translated to various radiofrequency bands using I/Q modulators and demodulators provided as removable daughter boards. We are here especially interested in translating the RF signal to the 434 MHz band. Hence, an initial part of the digitally programmable software radio consists in generating I and Q coefficients in the FPGA (either locally or transferred through an USB bus), which will then be shifted through the appropriate hardware (I/Q modulator and PLL-generated carrier frequency) to the wanted signal to the right frequency band. Similarly, during the demodulation step, the amplified received signal is mixed with a local PLL-generated RF oscillator to bring the modulated signal in basedband lower than 64 MHz, for sampling and recording by fast ADCs controlled by the same FPGA. The resulting data are transferred to the personnal computer through the USB link for processing.

The software we use for quickly switching on and off the emission for sampling the RADAR-like signal is based on the Python `usrp_radar_mono.py` script generating the control signals for the embedded `usrp_radar_mono.rbf` FPGA configuration script.

[2] http://gnuradio.org/trac

We have tested the wideband, frequency sweep strategy with 40 μs long emitted pulse (spectral width 25 kHz, *i.e.* narrower than the typically 43 kHz width of the resonator, so that the resonance frequency accuracy is limited by the Q of the resonator rather than the pulse width: Fig. 3.9) centered on frequencies separated by 13.3 kHz. On the other hand, the Fourier transform strategy (Fig. 3.10) was demonstrated with 1 μs long pulses, so that the two resonances within the 434 MHz ISM band were loaded by the RF signal. The global sampling duration is not representative of an embedded application since programming a new frequency step (an operation needs 128 steps to sweep the whole ISM band in the narrowband strategy) is time consuming with the USRP on the one hand, and on the other hand the computational power of a fast modern personal computer is more than enough to perform the Fourier transform of the sampled signal, but a challenging application in the embedded world of low power microprocessors.

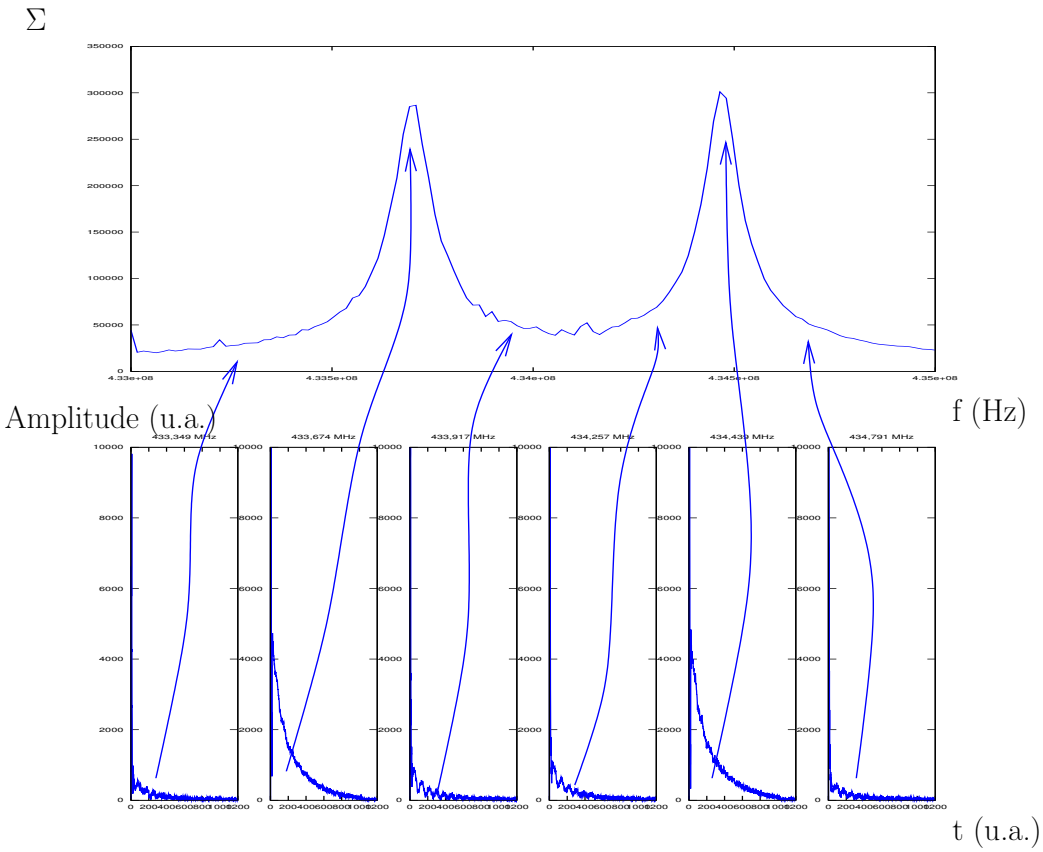

Figure 3.9: Basic principle of the narrowband interrogation method: the closer to the resonance frequency the emitted pulse, the larger the echo observed 1 μs after shutting down the emission.

Using the same kind of polynomial fit of the returned magnitude signal on the one hand, and of the resonances in the spectrum extracted from the Fourier transform on the other hand, the accuracy as a function of the number of averaged measurements (Allan deviation) is found to be similar (Fig. 3.11) for both methods. Hence, selecting one strategy or the other is mostly a matter of compliance with radiofrequency emission regulations, ability to develop

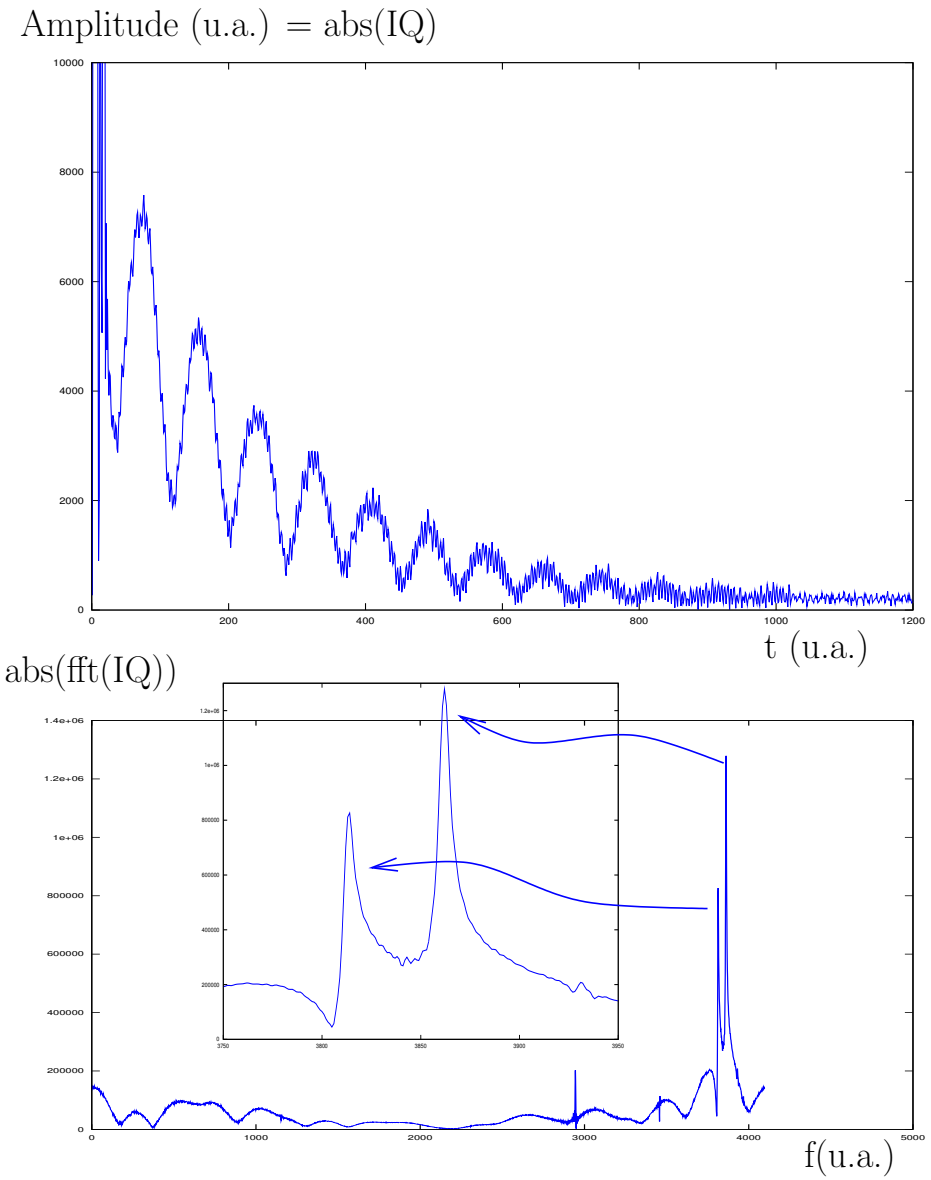

Figure 3.10: Basic principle of the wideband interrogation method: the beat signal between the responses of both resonators is visible in the time-domain sampled signal. The Fourier transform of this acquired signal provides an identification of the two resonance frequencies and hence the ability to perform a differential measurement.

on DSP or low-power microcontroller, and generating a versatile radiofrequency source (here a Direct Digital Syhtesizer – DDS – or an I/Q modulator) as opposed to generating widely spaced apart, short pulses as found in low cost digital radiofrequency emitters commercially available.

3.5.1 RADAR-like electronics

The strategy we have just presented is included in the wider class of instruments known as monostatic RADARs: a single, fixed antenna is used to both emit and receive the radiofrequency signal. The short pulses or, in the case of delay line interrogation, chirp pulses, are generated by an oscillator which is briefly fed to the antenna using a fast switch which also defines the isolation between emission and reception circuits. The interrogation range of such RF electronics is defined by the isolation between the emission and reception stages. As an illustration of the performance of the frequency-sweep embedded interrogation unit we have designed, Fig. 3.12 displays the standard deviation of the measured frequency (single-resonance measurement at 434 MHz) as a function of insertion loss defined as double the value (two way path) of a variable attenuator located between the antenna and the resonator.

An alternate solution to pulses which generates a narrower signal is the continuous wave (CW) RADAR. In this case, the spectral width is only associated with the source sweep rate rather than with the pulse duration. We have implemented such a strategy in which an I/Q modulator monitors the relative phase and magnitude of the coupled channel of a splitter to which the monostatic antenna is connected with reference to the (attenuated) reference signal generated by the RF source. The main issue with this strategy is nulling the signal at the input of the I/Q demodulator so as to be able to increase the gain at the output of the detector and hence increase the interrogation range. Unfortunately, the best isolation we could achieve between the direct (reference) signal and the returned (coupled) signal is 30 dB, more than 30 dB worse than the isolation obtained using switches in series to isolate the emission and reception channels in the former method.

Finally, based on reverse engineering a Mala RAMAC ground penetrating RADAR, we have observed than an alternative strategy to the use of a stable, programmable radiofrequency source consists in using an avalanche transistor to feed an antenna with a high voltage ($\pm$350 V) pulse. The duration of the pulse is solely associated with the impedance of the antenna: a high voltage capacitor is slowly loaded through a resistor from a high voltage power supply, and the duration it takes to release the energy in the load antenna when the avalanche transistor is triggered is defined by the resonance frequency of the antenna. Furthermore, the number of oscillations in the emitted signal is defined by the matching between the transistor output and the antenna input (through a transformer or balun): a matching condition will yield a single pulse, while the poorer the matching the more oscillations are observed. Hence, tuning the number of oscillations to reach the optimum value of the number of finger pairs in a delay line is feasible by detuning the balun. This configuration is used in a bistatic configuration since the high gain receiver must be protected against the high voltage generated at the emitting antenna. We are currently developing this kind of electronics design in our own readers, as well as tuning commercially available RADAR systems to use readily available instruments to probe acoustic sensors.

3.5.2 Enhanced interrogation strategies

We demonstrate the conversion of frequency modulation to amplitude modulation by radiofrequency resonators as means of accurately determining the resonance frequency of wireless passive sensors [272]. The frequency-modulated emitted radiofrequency pulses are generated by a pulsed RADAR for probing a passive acoustic sensor. The sharp sign transition of the amplitude modulated received signal provides a signal on which a feedback loop is controlled to monitor the resonance signal. The strategy is demonstrated using a fully software implementation on generic hardware described previously and published in [273].

We have demonstrated the working principles of a frequency sweep wireless network analyzer for identifying the resonance frequency of acoustic resonators used as sensors [273]. The full software implementation of the strategy allows for innovative strategies such as frequency hopping or adaptative frequency interrogation schemes as defined by the microcontroller defining the frequency generated by the radiofrequency Direct Digital Synthesizer (DDS). Beyond identifying the resonance frequency of an acoustic sensor through the maximum returned power, we here demonstrate the use of another functionality of the DDS, namely the ability to generate a frequency modulated (FM) signal by sweeping an internal RAM filled with user defined values defining the generated frequency. We demonstrate the gain in resonance frequency accuracy achieved by working on a *signed phase signal* for keeping a feedback loop close a null-returned signal through the software implementation on the previously described hardware.

Basic principles

A resonator acts, through its transfer function, as a frequency modulation to amplitude modulation converter. Hence, by exciting a narrowband resonator away from its resonance frequency with a signal frequency modulated at rate of ω, the returned signal is an amplitude modulated at ω. At resonance frequency, where the first order polynomial development of the transfer function becomes null and the second order coefficient becomes dominant, the frequency modulation at ω becomes an amplitude modulation at ω, with a contribution at ω close to zero. Above the resonance frequency, the frequency modulation at ω again becomes an amplitude modulation at ω, but this time with a 90^o phase shift of the amplitude modulation with respect to the frequency modulation signal compared to the case before the resonance frequency (Fig. 3.13).

Implementation: openloop characterization

We implemented this strategy using the hardware described earlier [273], as a full software implementation:

- the internal RAM of the Direct Digital Synthesizer is filled with values describing the sine-shaped evolution of the emitted frequency, *i.e.* a frequency modulated emission.

The frequency modulation deviation – also known as the modulation index – is set by programming the RAM with values spanning the wanted deviation. The speed at which this RAM is swept, defined by a programmable internal counter, defines the modulation carrier.

- while the FM signal is continuously emitted, the switches connecting the antenna alternately to the emission circuitry and reception circuitry is controlled by the same microcontroller used to program the DDS.
- the power-detector is periodically sampled as the switches are programmed since the frequency modulated signal has been converted to an amplitude modulated signal.

The received signal is then bandpass filtered at ω, with removal of the DC component. We observe however that the received signal is offset by a value function of the received power: at resonance frequency, the ω component is removed (since it is converted to a solely 2ω component) but a background offset induces additional signal processing: the average value is subtracted in order to keep the resulting average at mid-scale of the analog-to-digital converter scale.

Furthermore, the modulation frequency carrier and excursion must be set according to some quantitative analysis. The excursion is the parameter easiest to define: it must be wide enough for the signal to significantly sweep the resonance (*i.e.* at least a few kHz) without being larger than the width at half height, *i.e.* less than f_0/Q with $f_0 \simeq 434$ MHz the resonance frequency of the sensor an $Q \simeq 10000$ its quality factor. The carrier frequency must be set considering that each responses sampling must be performed assuming a quasi-static emitted signal loading the resonator. Considering the resonator parameters we just provided, and since the decay time of a resonator is Q/π periods, each sampling step requires loading the resonator during $3\tau = Q/(\pi \times f_0) = 22\ \mu$s. The same delay is needed during signal reception. In order for the resonator to observe a quasi-static signal, we use a modulation carrier $\frac{1}{10} \times \frac{1}{2\tau} \simeq 4.5$ kHz. The received signal is sampled using a timer-defined periodic analog-to-digital conversion. The maximum allowed sampling speed, due to the other computational requirements, is 16 kHz: the returned signal is recorded at the rate of 4 to 5 points per period. We sample 10 periods for an accurate estimate of the returned signal amplitude. Hence, each frequency sampling – and hence resonance frequency feedback control loop update – requires about 2.2 ms.

The frequency demodulation would be expected to be limited to a magnitude information since the timer defining the dates at which the received signal is sampled is not synchronized with the timer of the DDS defining how its internal RAM is swept. However, since the same microcontroler triggers the start of the RAM sweep, we can identify which sampled signal has been recorded as what instantaneous frequency was emitted. Hence, we can extract a phase information, and generate a *signed* feedback signal (Fig. 3.14).

The notch in the magnitude signal is replaced by a signed information which evolves linearly close to the resonance. While a notch is difficult to track since it requires, for best accuracy, a fine frequency tracking of the magnitude minimum, the linear signed magnitude signal is usable for a feedback.

Hence, we can select which samples are used for detecting the amplitude at maximum frequency modulation deviation, and extract the signed feedback signal for feeding a proportional controller.

Closed loop frequency control

Full digital electronics implementation, with the reference modulation signal implicit within the sweep of the look-up-table of the frequency synthesizer. The band pass filter aims at removing the DC component of the received signal and keep only the signal at ω: the average received signal provides a rough estimate of the resonance frequency during an initial sweep. Once the received average power is maximum, the control on the filtered signal keeps the emitted signal centered on the resonance frequency with a standard deviation of 25 Hz, limited by the stability of the resonator. We have demonstrated sub-10 Hz stability with a resonator attached to a heat-sink.

Hence, we have demonstrated a strategy for interrogating acoustic resonators based on the nulling of an amplitude modulated signal resulting from the conversion of the frequency modulated emitted signal to an amplitude modulation by the transfer function of the resonator. A closed loop control of the emitted carrier frequency keeps the modulation frequency component of the returned signal minimum: this strategy results in a 10-fold improvement of the resonance frequency identification with respect to a fixed frequency-step magnitude envelope sampling and fit. This gain in resolution results however in a longer interrogation time since the modulation frequency must be slow with respect to the response time of the resonator, defined by its quality factor. Furthermore, the closed loop strategy of tracking the zero-phase condition makes the use of this strategy difficult when the sensor is only intermittently visible (e.g. rotating or moving object).

3.6 Novel acoustic sensor designs

As seen from the above discussion, some parameter optimization might be suitable to improve the accuracy of the measurement and the interrogation. As long as we consider narrowband transducers, we have seen that the most significant parameter is the quality factor since it defines how accurately the resonance frequency position can be defined, as well as the decay time. Since the acoustic quality factor is always much greater than the dielectric quality factor of the environment, the acoustic response can be sorted from the background clutter for identifying the acoustic signal. However, the signal to noise ratio – and hence detection range – is improved with longer detection delay (allowing for the clutter to decay significantly) and hence higher quality factor.

Another parameter of interest is the increase of the working frequency. At the moment, although the sensor is less than a cubic centimeter in dimensions, the associated antenna are ideally 35 (dipole) or 18 (monopole) cm-long. Increasing the working frequency proportionally reduces the antenna dimensions, but most significantly allows for interesting strategy such as

directional antennas, phased arrays, beam steering which are impossible to use considering the 434 MHz band wavelength. As mentioned previously, increasing the frequency by N reduces the response time by N^2 for a given technology (assuming a constant $Q \times f$ factor), hence the need to developed innovative strategies for high quality factor, high frequency transducers. Current approaches include the classical HBAR approach, with an emphasis on keeping the ability to model the behaviors of such devices by using exclusively monocrystaline materials. FBAR are also of interest but more fragile and require additional etching steps to create the membrane.

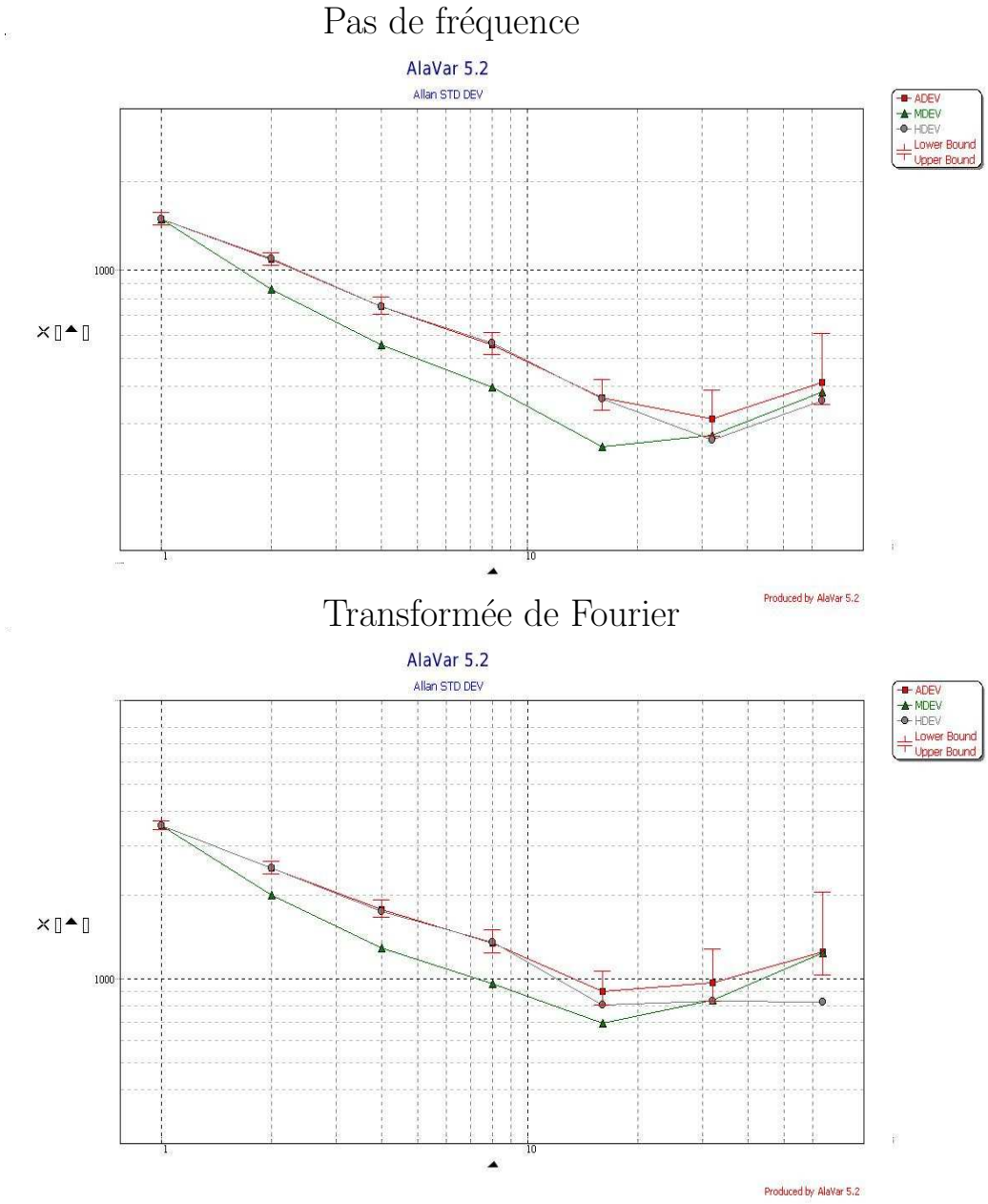

Figure 3.11: Allan deviation of the frequency sweep (top) and Fourier transform (bottom) methods. In both cases the short term (one sample) standard deviation is in the kHz range, with a slightly worse performance of the Fourier transform strategy. After 16 averages, both strategies exhibit sub-kHz performance, typically 200 Hz for the frequency sweep strategy and 500 Hz for the Fourier transform strategy. Beyond 16 sample integration time, the Allan deviation rises due to long term drift of the physical quantity under investigation: 16 averages is an optimum compromise between low noise, while keeping reactive to changes of the quantity being measured. Abscissa are the integration time in number of recorded samples, ordinates are the Allan deviation in Hz.

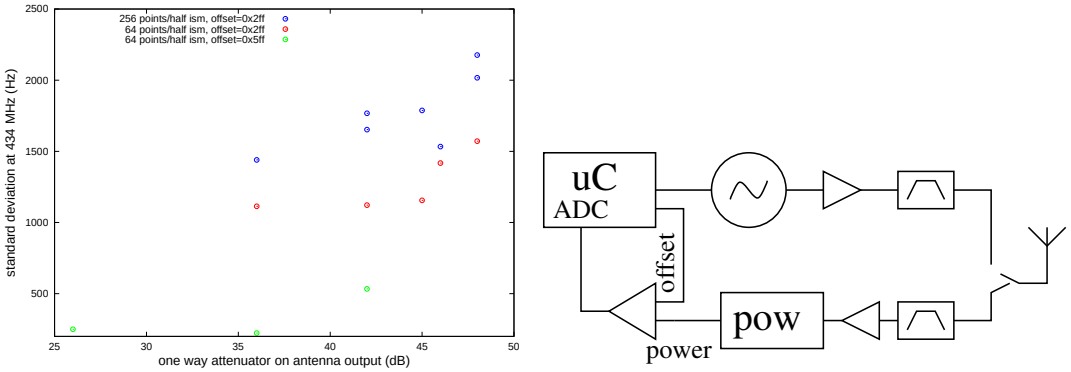

Figure 3.12: Standard deviation of the frequency measurement at 434 MHz as a function of the attenuator value at the output of the antenna: the two-way RF budget is thus twice the value of this attenuator. Below 30 dB, the standard deviation stabilizes at 150 Hz since the digital automatic gain control included in the embedded electronics tunes the output power to keep the received signal within an optimum range. One important parameter is an offset – generated by a Digital to Analog Converter (DAC) on the embedded board – to subtract a constant voltage from the power detector. This offset is dependant on the impedance connected to the antenna output, and hence on the RF environment of the sensor. This offset value has been here optimized for best performances with a fixed attenuator on the antenna output, a favorable environment hardly representative of a real application environment. Although a wireless link will probable not perform well for such high attenuations (poor signal above 42 dB), the standard deviation observed below 42 dB is representative of our wireless experiments. Unpublished data.

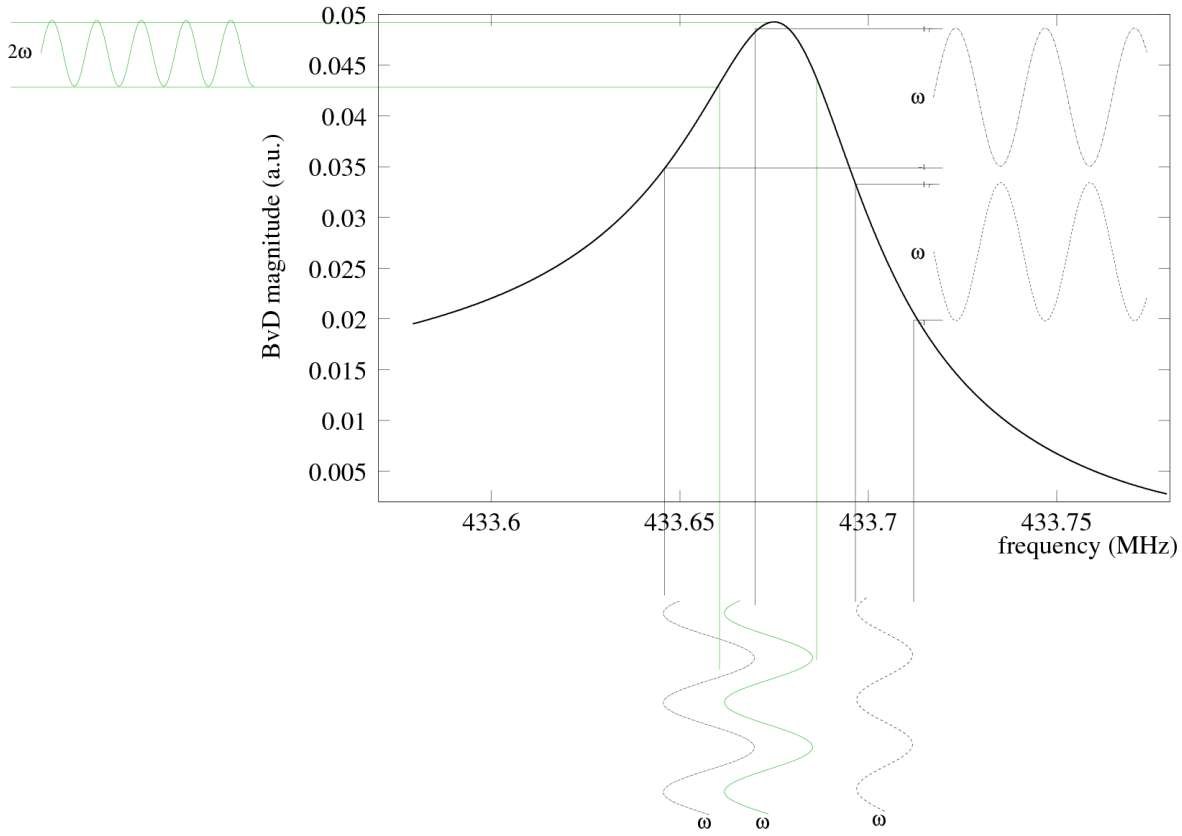

Figure 3.13: Frequency to amplitude modulation through the transfer function of the resonator: at resonance, the contribution at modulation pulsation ω vanishes and the sole contribution to the returned signal is at multiples of 2ω. From left to right: when the slope of the transfer function is rising, the emitted frequency modulated signal is recovered as an amplitude modulated signal. At resonance frequency, the contribution at ω vanishes. When the slope of the transfer function is negative, the emitted signal at modulation frequency ω is received as an amplitude modulated signal at ω but with *phase inversion*.

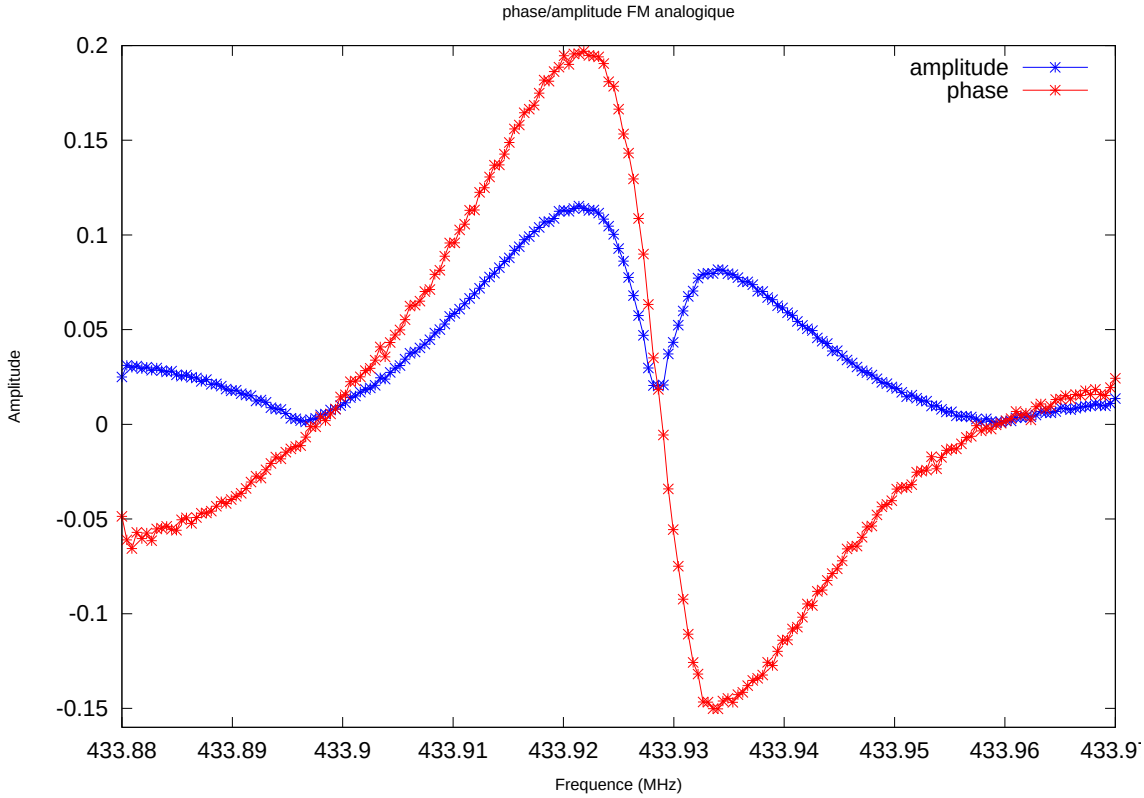

Figure 3.14: Openloop characterization of the magnitude of the amplitude modulated signal at ω, and signed magnitude (phase). The signed (red) amplitude is equal to the magnitude signal (blue) with the additional information of the received amplitude modulated signal with respect to the emitted modulation signal. The feedback control aims at keeping the phase information (red curve) close to 0. Unpublished data.

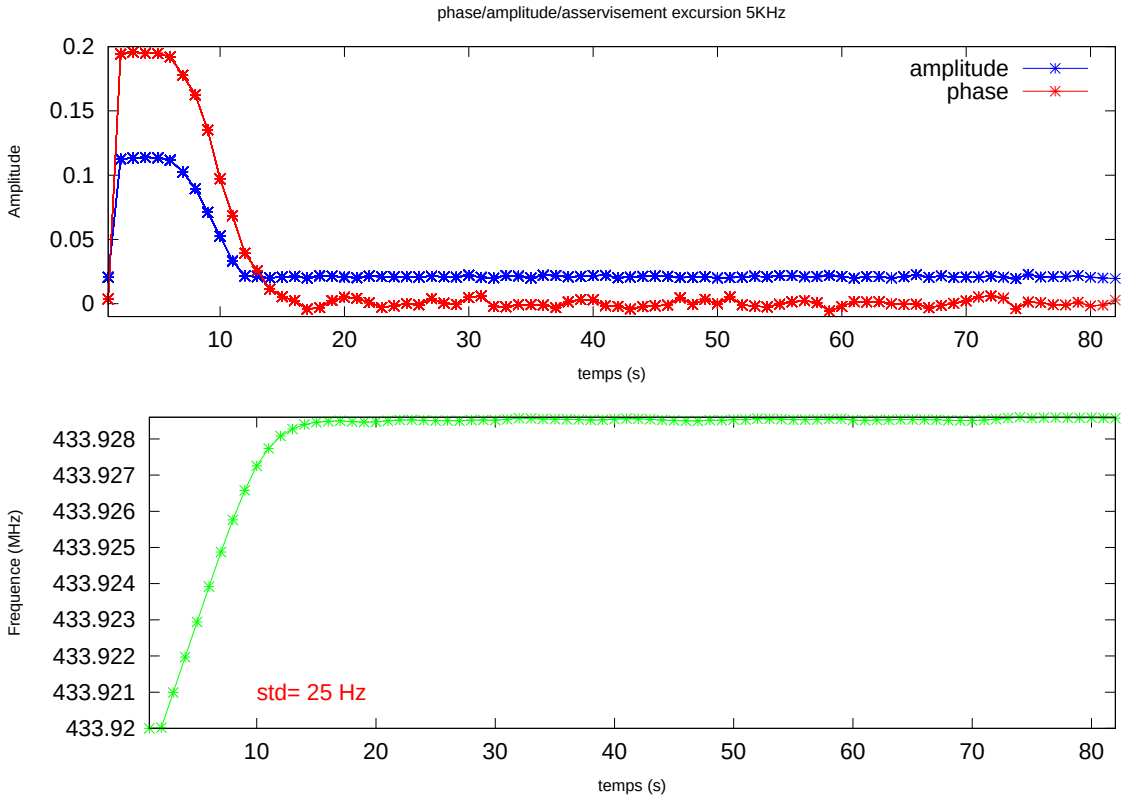

Figure 3.15: Closed loop control of the frequency in order to minimize the component of the amplitude modulated signal at ω. Unpublished data.

Chapter 4

Embedded electronics for mobile applications

> "They recognized the effective use of electronics to be as much about mechanical packaging as about circuit design."
> *E.C. Hall, Journey to the Moon – the history of the Apollo guidance computer (AIAA, 1996)*

This chapter discusses developments concerning embedded digital systems. Why focus on digital, while RF components generally work at frequencies well above the clock rate of most digital components ? The keyword is *flexibility*. While analog computers are well known for their speed and robustness, digital computers are not affected by noise (unless a bit flips state due to some external effect such as ionizing radiation), but most significantly can be reprogrammed to perform different operations depending on the task being requested (computation, communication, storage) without any new hardware re-design. However, developing digital system induces new challenges: what is the latency between a received signal and the associated action ? Are all the functionalities of an operating system needed for the simple tasks we are interested in ? What are the alternatives between low level assembly language development and resource-hungry operating systems ? These are some of the questions we have tackled and provided some answers for our particular application, namely the programming and sequencing of RADAR-like electronics.

4.1 Teaching: embedded systems and sensors

The first aspect of the industrial application of the sensors developed in this presentation is to be able to provide a customer with a full solution including the (acoustic, optical or scanning probe) transducer, signal processing hardware and software, digital acquisition and storage and, if absolutely needed, graphic interface. While the former part of this list is original, the digital acquisition and user interface aspects are hardly research, but basic understanding

is needed in most of them for the completion of a usable instrument in an environment not necessarily dedicated to radiofrequency electronics or optics. Hence the need to develop basic knowledge which, if not publishable as research topics, are nevertheless worth transferring to students and more generally to the public interested in understanding how the instruments (a.k.a small home appliance) they use in their daily life works and can be best modified to suit everyone's needs. Since we already have developed the signal processing aspects and embedded electronics hardware in the previous chapters, we will here focus on the embedded software and on the associated development tools.

Additionally, some time and effort have been dedicated to transferring the knowledge acquired during embedded device development – and most significantly about digital programmable instruments and the associated software and operating systems – towards master level students and the general public [274, 275, 276, 277, 278, 279, 280, 281, 282, 283, 284, 285, 286, 287, 288, 289, 290, 291, 292, 293]. Although mostly dedicated to the French speaking reader [294, 295, 296, 297, 298, 213], some international conference presentations [299, 300] and journal publications [301, 302, 29, 218] were the opportunity to widen the audience.

I am convinced that the use of opensource tools for developing software for embedded device is a useful strategy for transferring students some *methods* rather than some dedicated knowledge on a few proprietary software. I have tested this strategy for the second year now, completing at ENSMM [1] – the engineering school hosting our laboratory – a 36 hour (12 hour teaching, 24 hour labs) course on developing embedded devices. As part of this course

1. we developed custom hardware with peripherals meeting our teaching needs and available lab-equipment – for example the lack of oscilloscope and function generator in the lab classes were compensated for by the use of the sound-card of personal computers for generating signals needed for applied signal processing courses. While the time spend developing and building these boards is not included in the estimated price of the boards, working on sample components allowed the fabrication of a dozen boards for a fraction of the price of a single commercial teaching board. This reduced price, and intimate understanding of the working of the tools used for teaching, means that the boards can evolve as quickly as the accessible technology, without need to delay renewal of the teaching equipment as a function of available funding, often yielding the use of obsolete processor or development environment which were bought several years earlier. These devices are used in my own embedded device development course as well as by my colleagues at university teaching digital electronics,

2. we provide the student with a live CD running GNU/Linux and including all the software needed to perform the lab classes. With such short teaching sessions and lack of practical knowledge, providing all the software needed to reproduce at home the experiments performed in the classes (another reason for using personal computer sound cards as function generators) at least provides the tools – if not the will – to deepen the understanding on the topics discussed in the class.

3. Furthermore, we emphasize on the fact that the opensource GNU Compiler Collection is a *generic compiler* providing support for multiple languages on *most digital computing*

[1] MicroMechanics Engineering School, http://www.ens2m.fr

platforms, from 8-bit to 64-bit processors. Hence, the emphasis is not so much on the use of a particular implementation of GCC for a given processor (in our teaching sessions, the 16-bit MSP430 and ARM7, and 32-bit Coldfire running uClinux), but rather on the means to generate a cross-compilation toolchain which can be adapted to any board equipped with any kind of processor.

Hence, the general philosophy behind the selection of opensource software as development tools is that the user should only be limited in his selection of the platform on which he will implement a given algorithm according to the required processing resources or power consumption, rather than by the available development tools. Hence, I have restricted my approach of embedded hardware programming to opensource, universal compilers which allow the user to change hardware architecture when needed, and correct compiler bugs [2] when observed without relying on an utopic customer support from a commercial vendor. Hence, the strategy focusing on using the GNU Compiler Collection (`gcc`) as a teaching tool is to emphasize that engineering creativity should be restricted only by knowledge and available hardware, thus teaching users how to best use the available tools rather than being limited by funding of proprietary tools.

Furthermore, beyond the topic of academic (formal) teaching, I believe that extending some themes of the research activities towards lab experiments accessible to students and more generally to the general public, with instruments accessible to most users, is an interesting way to analyze in-depth our working methods [218, 29, 301]. Beyond the expensive, dedicated lab instruments we daily use for prototyping experiments, our environment is full of interesting interfaces to exploit towards uses not necessarily originally imagined but nevertheless interesting to our own purpose. The opensource software and hardware ideas – using and contributing to the concept – is obviously central to such considerations.

4.2 Embedded devices

From the aforementioned description, one might be led to believe that we have acquired experience in embedded devices for use by a non-specialist audience. An humbling experience has been the French national National Research Agency (ANR) HydroSensorFLOWS project devoted to monitoring the climatic and hydrologic behavior of a polar glacier using automated instruments. As part of this project, the Time and Frequency department of FEMTO-ST, claiming experience in embedded system developments, has been committed to develop automated digital cameras for grabbing high resolution pictures of the glacier 3 times a day over a time span of 3 years from 10 different points of view. The apparently trivial task of automating the capture of 10 Mpixels images in a polar environment happened to be rather challenging but provided ample opportunities to demonstrate our ability to answer a simple technical requirement in an hostile environment. Two interesting quotes provide inspiration

[2] http://gcc.gnu.org/bugzilla/show_bug.cgi?id=10834 and http://gcc.gnu.org/bugzilla/show_bug.cgi?id=16634 describe a mistake in stack handling during interrupt management routine generation, a problem which was rather slowly solved by the ARM-compiler community but whose detailed documentation provided workarounds in the mean time. The issue seems solved with `arm-gcc-4.3.3`.

for such a project: *They recognized the effective use of electronics to be as much about mechanical packaging as about circuit design* [303] and *It has become fashionable to denigrate the computers of the past with phrases like "we flew to the moon with less computing power than I have on my wristwatch" [...] Simply focusing on memory size, or the computer's speed, misses the important engineering accomplishment of the Apollo computer. [...] It never failed in flight.* [304, p.124].

Our first approach, claiming to develop a fully automated digital camera including an operating system for acquiring the image, storage on non-volatile medium and possible radiofrequency link transfer, proved to be interesting but failed in terms of performances. Any optical system, and especially a digital camera, is not only a digital electronics device but most significantly the associated hardware including optical alignment, moisture tight enclosure and lightweight mechanics. Furthermore, the use of a general purpose operating system (uClinux port to the MMU-less Coldfire processor used for this application) is simply not compatible with a low power application with such a low cyclic ratio of 15-second switch on time every 4-hours when the boot time of the operating system is several tens of seconds.

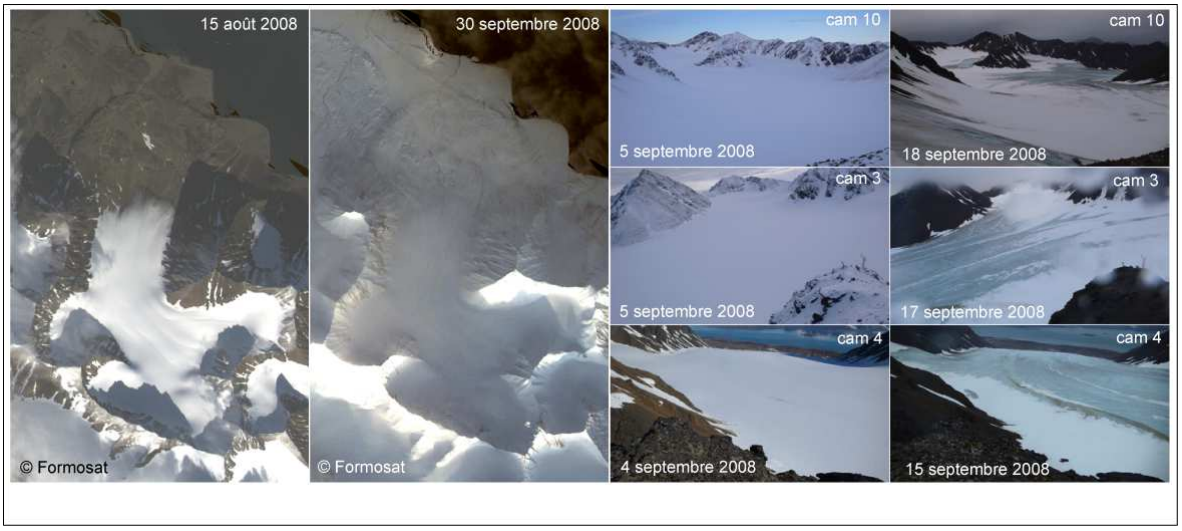

Figure 4.1: Example of the complementarity in terms of pixel size and time resolution of the satellite imaging and ground-based automated digital camera [305].

We ended up solving the hardware issue using a dedicated low-power microcontroller added to a commercial high resolution, high grade optical system digital camera. However, solving the hardware issue proved to be only a minor part of the challenge, with the additional requirement to develop a portable [3] graphics interface usable outdoors on a laptop under direct sunlight illumination, and resisting the harsh environment conditions of a glacier located above the arctic circle.

Let us emphasize that the technical success of this endeavor has been possible thanks to the unusual motivation of the program leader to reach a *scientific goal* of monitoring

[3] from a philosophical point of view, a development on a non-unix system was not possible, but the end-user needed a Microsoft Windows compatible application

over a long term duration the evolution of this polar glacier, whatever technical satisfaction was to be gained from the electronic instrument development: the objective were unusual in the aspects that we were not requested to develop innovative instruments – only using well known concepts would answer the reliability needs of the challenging environment – nor were we requested to look for further funding rather than focusing on the scientific results (Fig. 4.1). This true (as opposed to politically motivated) interaction of various fields – geography, hydrology, physics and engineering – generated a motivating environment. Gathering data is only part of the challenge, since processing such a huge amount of informations and defining which parameter to extract from such a rich database as high resolution pictures is time consuming. We have attempted to implement various automated signal processing technique such as automatic motion detection (using 2D cross correlation), automated classification for identifying usable pictures, finding missing pictures when the camera failed, matching scalar datasets (temperature maps) and the state of the glacier as seen on the pictures (Figs. 4.2 and 4.3).

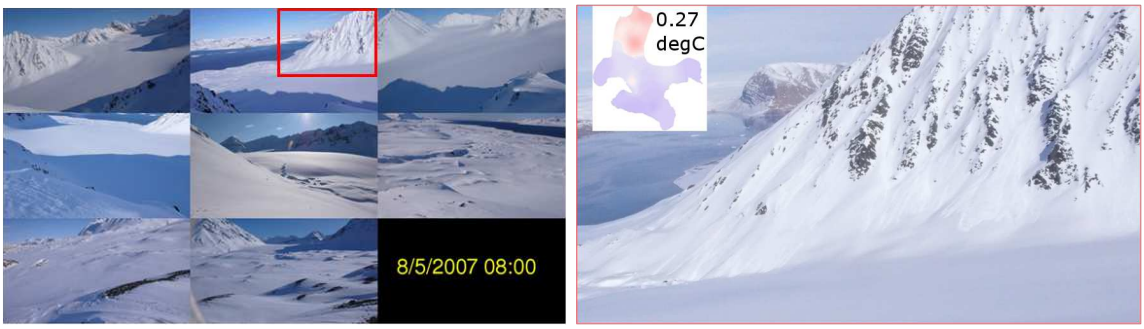

Figure 4.2: Top left: mosaic of pictures taken at the same time by 8 automated digital camera located around the glacier basin under investigation. Top right: the use of high resolution digital camera allows for zooming on regions of interest, here a slope for analyzing the snow cover and dynamics of snow accumulation from the slopes to the glacier.

4.3 Digital RF electronics for versatile interrogation units

The interrogation units we develop to probe acoustic devices – whether acoustic delay lines, resonators through a wireless link, or ultrasonic probes – are all centered around a digital frequency synthesizer (usually Analog Device's AD9954) controlled by a powerful microcontroler. This strategy provides a *flexible environment* for prototyping many algorithms beyond the simple continuous frequency sweep. As an example, we have adapted to this interrogation scheme a frequency modulated strategy as described in the WO/2008/015129 patent [4], as was described in details earlier (section 3.5.2).

The resulting development boards combine the flexibility of the software-radio approach demonstrated earlier on the USRP, while targeting a dedicated frequency band and lower manufacturing cost and power consumption to be compatible with a larger scale fabrication

[4]available at http://www.wipo.int/pctdb/en/wo.jsp?wo=2008015129

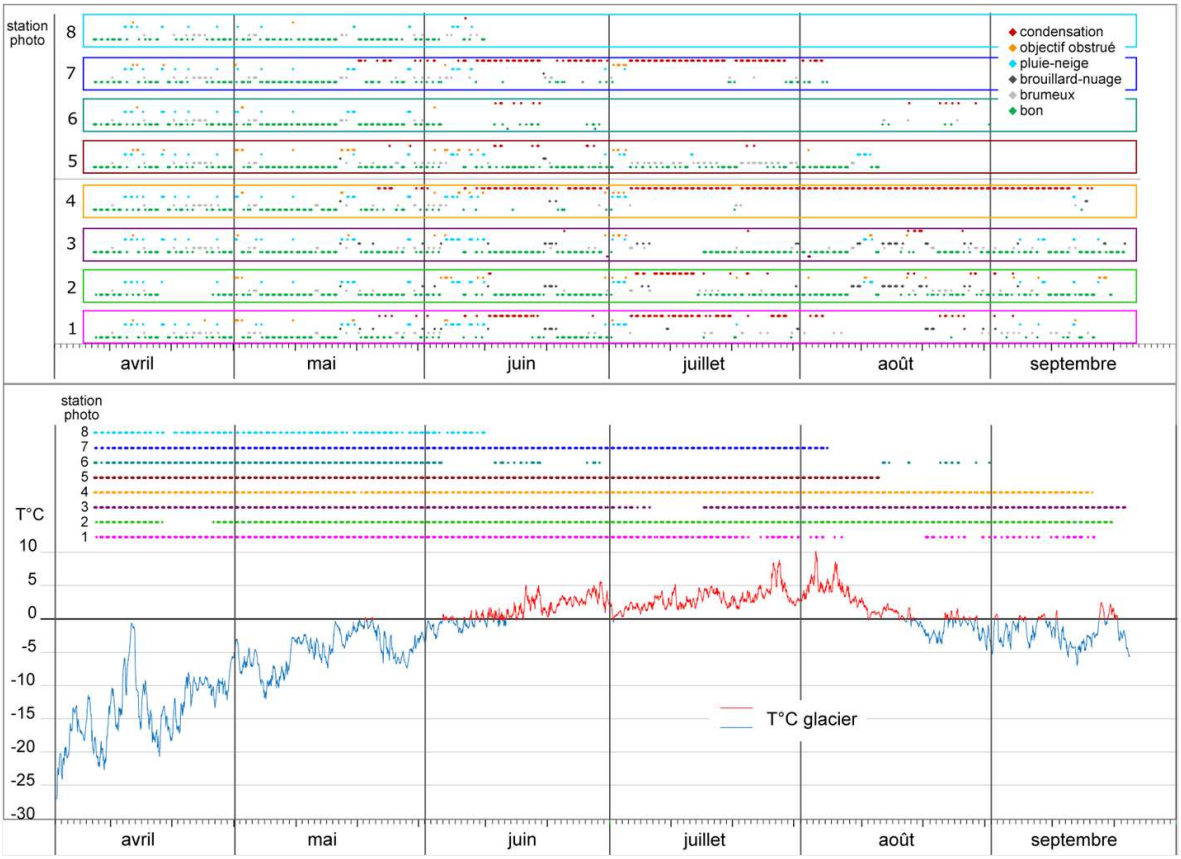

Figure 4.3: Reliability analysis of the 8 cameras located from spring to autumn in Spitsbergen. The top graph classifies the causes of failure (the green dots are usable pictures, other causes of unusable pictures are distributed between poor weather – blue to grey – and failure of the cameras – orange and purple). The bottom graph displays the number of usable pictures, color coded for each camera, and the mean glacier temperature in an attempt to correlate temperature transitions close to the dew point and camera failure. While 1778 usable pictures were recorded during the march to september 2007 duration (out of an expected 4032), only 11 satellite images were provided [306].

for demonstration purposes. However, the combination of digital and RF electronics for embedded systems is arguably the field of applied electronics evolving fastest these last years, requiring a constant update of the technology used for implementing algorithms. On the other hand, the constant increase of the computing power while keeping constant the electrical power consumption provides the means for implementing algorithm that would either have needed a few years ago either powerful desktop computers, or post-processing. One example of such improvement – beyond dedicated chips for tasks such as music algorithm decoding or compression, or non-volatile mass storage – is the software implementation of intercorrelation strategies after sampling baseband radiofrequency signals. Similarly, Fourier transform strategies which until recently required dedicated hardware (Digital Signal Processor for example) are now accessible to higher grade 32-bit microcontrollers [307].

As an example of a universal method for stabilizing the reference clock of digital systems

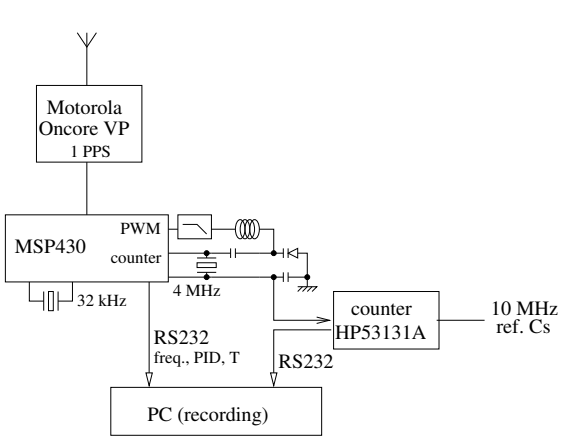

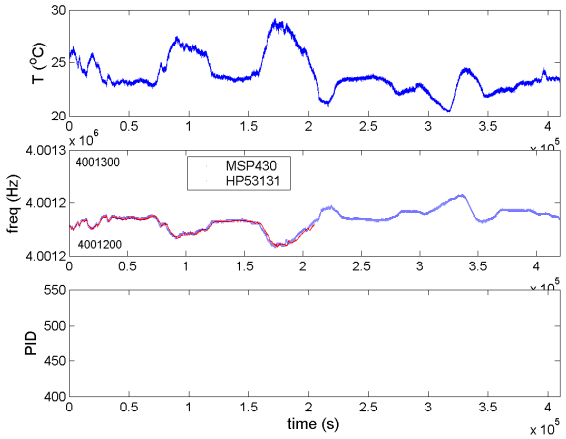

Figure 4.4: Left: schematic setup of the microcontroller clock control loop using the GPS 1 PPS signal as reference. A commercial HP53131 frequency counter clocked on a cesium reference is used for qualifying the performance of the system. Right: frequency fluctuation measured by the Input Capture timer of the microcontroller, and by the commercial counter, as a function of time (middle curve) in a 100 Hz full scale graphics. In this case, no feedback loop control is applied and the frequency shifts with temperature (top graph).

to prevent long term drift due to the physical environment on the quartz resonator, we have implemented a feedback loop of the core digital system clock on the GPS 1 PPS (1 Pulse Per Second) signal. While this strategy is well known and the GPS provides a convenient, low cost high accuracy (150 ns per second or 150 ppb) reference signal stable on the long term, our focus here was to implement the feedback control strategy on microcontrollers with no additional component other than the GPS receiver. As an example, Fig. 4.4 focuses on the practical implementation of the control and characterization of the resulting stability on a Texas Instruments MSP430 microcontroller. This particular chip is well suited for this task since it runs on two quartz resonator, one low frequency resonator clocks the digital processing unit while a high frequency (up to 8 MHz) quartz resonator clocks the peripherals. Hence, even in case the feedback control loop brings the high frequency resonator away from its oscillation condition, the core is still clocked and can correct the unsuitable parameter. The basic strategy, applicable to any recent microcontroller, is to use one internal timer in Input Capture mode to count the number of oscillations of the RF quartz between two 1 PPS pulses. Since the rough frequency is known, overflow does not matter since only the lower bits of the counter are useful for stabilizing the quartz resonator frequency: even 16 bits counters are useful for such an application. A proportional feedback loop generates a voltage on a Digital to Analog converter output (or, in this example, in a Pulse Width Modulated output which is the low-pass filtered) for controlling the capacitance of a varicap diode connected to one side of the quartz resonator (Fig. 4.5). The resulting frequency pulling due to the voltage-controlled capacitor acts as a closed loop feedback signal. Using this strategy, we demonstrate the stabilization to within ± 1 Hz at 4 MHz of a quartz resonator on the long term, using a strategy quite reminiscent, if not overly simplified, of atomic clocks.

This strategy is generally applicable to any digital RF system requiring long term stability, with minimal additional hardware other than a GPS receiver and a clear view of the sky for

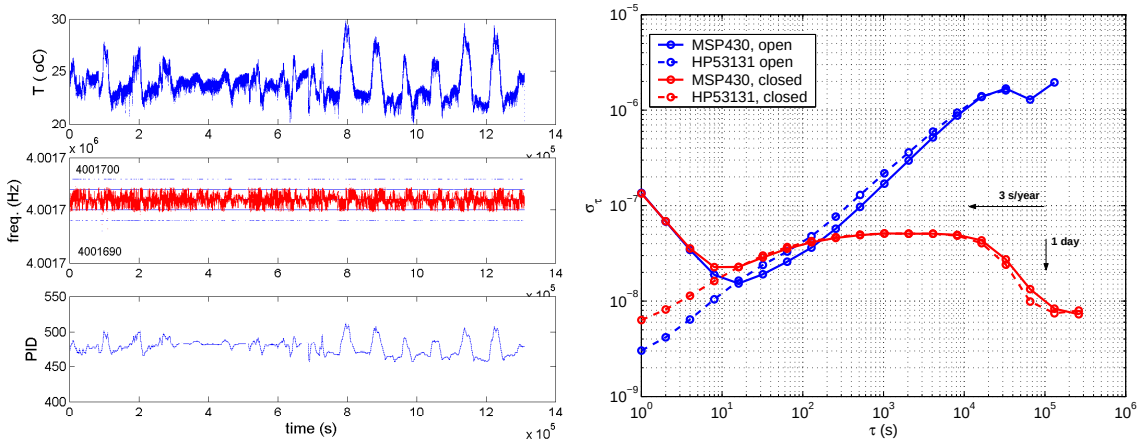

Figure 4.5: Left: applying the feedback loop control, the 4 MHz clock is stabilized to within ±1 Hz, limited by the crude direct counter strategy imposed by the nature of the high stability reference (the 1 PPS signal acting as a precise gate time). Right: Allan deviation analysis, exhibiting the few 10^{-8} stability at 10 s consistent with 1 Hz at 4 MHz, the poor performance of the direct counter on the short term (as opposed to the high performance of the reciprocal counter), the consistent measurements of the microcontroller timer and the HP53131 for integration times longer than 10 s, and most significantly the elimination of the long term frequency drift since the Allan deviation stabilizes above 10 s when the feedback loop is closed.

the receiver antenna. Furthermore, the use of the control signal provides, as was discussed earlier in acoustic delay line measurements, an alternative measurement technique of the influence of the environment on the quartz resonator. Here, the PID control signal reflects the temperature fluctuations during the experiment. More generally, the feedback control signal provides a means of measuring the physical parameter while keeping the working setpoint of the transducer fixed: one interesting aspect of this strategy is that the linearity of the sensor is defined by the control element (here the linearity of the frequency pulling of the varicap diode as a function of applied voltage) rather than by the transducer. Hence, even a non-linear transducer working at a fixed setpoint might provide a linear response, a useful strategy when the phase to frequency relationship of an acoustic delay line departs from linearity due to interference effects for example.

4.4 FPGA for real time processing

General purpose microcontrollers provide sufficient computing power, always limited at some point by the finite speed of the clock sequencing the operations of the core. As a couple of examples where general purpose microcontrollers are unsuitable: the generation of 10 ns pulses for 100 MHz GPR or ultrasonic probe, or control of massively parallel (several tens) arrays of microsystems [15]. In those cases, we are considering the direct implementation of algorithms as logic gate matrices in Field Programmable Gate Arrays. Furthermore, such architectures are reconfigurable depending on the need: on given electronic circuit can be

adapted to several needs, with only a reprogramming step but no time consuming routing and manufacturing of new RF boards. The drawback of such a strategy is the heavy power consumption of these circuits, which are nevertheless in our applications of the same order of magnitude as the power consumption of low noise and monolithic RF amplifiers.

The practical implementation of these strategies rely on a board sold by the French Armadeus Systems company, combining a general purpose ARM-based processor running GNU/Linux, and a 200 kgates FPGA. Both components are connected on-board by fast busses (shared address, data and control busses between the CPU and FPGA) allowing efficient data transfer between the both processing units, removing the communication bandwidth bottleneck often met when designing such systems. Furthermore, thanks to this strategy, FPGA development focuses on embedding custom algorithms or hardware (e.g. fast counters) in the FPGA, while the user interface and less-time critical such as post-processing are implemented under GNU/Linux, with the invaluable access to the operating system abstraction layers and libraries.

Rather than following the trend of generating translation tools between high-level language subsets (Matlab, C) and VHDL for implementing algorithms as logic gate matrices, we are interested in developing a toolbox of efficient, dedicated components for basic signal and image processing. The purpose is here not to recycle software already available for general purpose computers, but to target the real time processing of data which would otherwise need post-processing for extracting the needed information. Real time processing means that the resulting informations extracted from the measurement (whether matrix of microsystems or images gathered from optical sensors) can be incorporated in a real time feedback loop for controlling the system under investigation rather than simpling observing its state in an openloop configuration. Such instruments should open paths towards new applications of real-time visual control which would either nowadays require large and power-hungry computing infrastructures – preventing mobile applications – or would simply not be feasible.

This topic is a central aspect of the latest orientations of my research activities, and is the subject of a PhD grant request for the 2010-2013 period, shared with the Armadeus Systems company, for real time artificial vision based on the implementation of image processing algorithms in FPGAs.

Chapter 5

Conclusion and perspectives

As a summary of the developments discussed in this document, I have focused on demonstrating a core competence in using RF acoustic devices for sensing application, and to implement peripheral technologies meeting the needs of acoustic sensor exploitation. The latter include such instrumental techniques as scanning probe microscopy, evanescent wave optical setups, radiofrequency electronics and embedded digital computing devices. From a software point of view, the acquired signal are both processed to extract as much information as possible from the measuements, and compared to models whose understanding is however restricted to the user perspective (as opposed to the developer).

Beyond the research and industrial aspects of these developments, I have illustrated some need to share these core competences either with a wider, general public audience, and while teaching master level students. Such skills are fundamental when interacting with non-engineers partners, as was for example with the glaciologist and hydrologist team of the Sensor-Flows project in the Arctic region.

I have concluded each section with some perspective on the work I expect to complete in each field I have discussed:

- developing robust bio-chemical transducers for thin film characterization to provide tools to identify the constants to be included in biochemical sensor models remains a priority, with the two extension paths already in process with the combination of acoustic transducers with white-light SPR and shear force scanning probe microscopy. More generally, the objective is combining multiple physical sensing mechanisms on a same thin film layer in order to acquire as many measurements as coupled variables defining the properties of the layer,
- improved wireless sensors, possibly shifting from resonators to delay lines, whose rich features provide more flexibility in selecting some property (measurement, identification) and wider playground for implementing signal processing techniques well known in the RADAR in ultrasonic imaging community. From an application perspecive, environmental monitoring of buried sensors – temperature and strain sensors in ice and

permafrost – are of interest for basic reseach and towards practical, civil engineer, applications.

- finally, developing new competences towards reconfigurable, fast digital hardware implemented in FPGAs will provide the needed tools for real time signal processing and providing embedded hardware meeting the requirements of the above-mentioned basic developments toward a practical use in laboratories not dedicated to radiofrequency development.

Most of this work would not have been possible without the support and help of the students I had the opportunity to work with after obtaining my PhD. Amongst the most significant contribution:

- the team I joined in IMEC (Leuven, Belgium) as a postdoctoral fellow hosted 3 PhD students whose work I supported, including some work concerning electrodeposition and impendance spectroscopy which fitted nowhere in this document, ending up not being suitable for neither optical nor acoustic transducers [308] (K. Bonroy obtained her PhD from KU Leuven in 2005, F. Frederix obtained his PhD from KU Leuven in 2004, and L. Francis obtained his PhD from UC Louvain in 2006.
- similarly, after returning to France, I supported the work of a PhD student concerning the data acquisition, instrumentation and signal processing on some work concerning aging of dielectrics for high voltage insulation. Again, the associated publication hardly relates with any of the work presented here [309] (É. Mboungou obtained his PhD from Franche-Comté University in Besançon in 2006)
- finally, since being hosted by the time and frequency department of FEMTO-ST, I supervised the work on packaging acoustic sensors refered several times throughout this document, but also a PhD student from the computer science department working on embedded sensor nodes for wireless sensor network. While my interest in this topic is closely related to the instrumentation activity concerning environmental monitoring in Spitsbergen, the computer science approach to such problems is solely on the higher abstraction level software implementation of the appropriate data communication and storage algorithms. L. El Fissi obtained her PhD in 2009, while E. CapoChichi will defend his PhD at the computer science department in 2010.

Bibliography

[1] T. Vo-Dinh and B. Cullum. Biosensors and biochips: advances in biological and medical diagnostics. *Fresnius J. Anal. Chem.*, 266:540–551, 2000. 6

[2] G. Harsámyi. *Sensors in biomedical applications*. Technomic publishing company, Lancaster, Pennsylvania, 2000. 6

[3] A. Chaubey and B.D. Malhotra. Mediated biosensors. *Biosensors and bioelectronics*, 17:441–456, 2002. 6

[4] F.W. Scheller, C.G. Bauer, A. Makower, U. Wollenberger, A. Warsinke, and F.F. Bier. *Biomolecular Sensors*, chapter Immunoassays using enzymatic amplification electrodes. Taylor & Francis, London, 2002. 6

[5] W. Göpel and P. Heiduschka. Interface analysis in biosensor design. *Biosensors and bioelectronics*, 10:853–883, 1995. 7

[6] S.F. D'Souza. Immobilization and stabilization of biomaterials for biosensor applications. *Applied biochemistry and biotechnology*, 96:225–238, 2001. 7

[7] B. Catimel, J. Rothacker, and E. Nice. The use of biosensors for microaffinity purification: an integrated approach to proteomics. *J. Biochem. Biophys. Methods*, 49:289–312, 2001. 7

[8] S. Mittler-Neher, J. Spinke, M. Liley, G. Nelles, M. Weisser, R. Back, G. Wenz, and W. Knoll. Spectroscopic and surface-analytical characterization of self-assembled layers on au. *Biosensors and bioelectronics*, 10:903–916, 1995. 7

[9] F. Frederix, K. Bonroy, W. Laureyn, G. Reekmans, A. Campitelli, W. Dehaen, and G. Maes. Enhanced performance of an affinity biosensor interface based on mixed self-assembled monolayers of thiols on gold. *Langmuir*, 19:4351–4357, 2003. 7

[10] C. Zhou. Constructing novel interface layers towards the realization of high performance biosensors. *PhD Thesis, K.U. Leuven, Belgium*, 2006. 7

[11] J.D.N. Cheeke, N. Tashtoush, and N. Eddy. Surface acoustic wave humidity sensor based on the changes in the viscoelastic properties of a polymer film. volume 1, page 449, 1996. 8

[12] P. Gould. Nanoparticles probe biosystems. *Materials Today*, 7(2), february 2004. 8

[13] R. de Palma. Surface engineering: immunosensor interfaces, magnetic biosensors and magnetic nanoparticles. 2007. 8

[14] X. Su, F.T. Chew, and S.F.Y. Li. Design and application of piezoelectric quartz-crystal based immunoassay. *Analytical Sciences*, 16:107–114, 2000. 8

[15] H.P. Lang, M. Hegner, and C. Gerber. Cantilever array sensors. *Materials Today*, pages 30–36, April 2005. 9, 70

[16] J. Fritz, M.K. Baller, H.P. Lang, H. Rothuizen, P. Vettiger, E. Meyer, H.-J. Güntherodt, C. Gerber, and J.K. Gimzewski. Translating biomolecular recognition into nanomechanics. *Science*, 288:316–318, 2000. 9

[17] J. Tamayo, A.D.L. Humphris, A.M. Malloy, and M.J. Miles. Chemical sensor and biosensors in liquid environment based on microcantilevers with amplified quality factor. *Ultramicroscopy*, 86:167–173, 2001. 9

[18] R. Raiteri, G. Nelles, H.-J. Butt, W. Knoll, and P. Skládal. Sensing biological substances based on the bending of microfabricated cantilevers. *Sensors and Actuators B*, 61:213–217, 1999. 9

[19] R. Raiteri, M. Grattarola, H.-J. Butt, and P. Skládal. Micromechanical cantilever-based biosensors. *Sensors and Actuators B*, 79:115–126, 2001. 9

[20] G. Wu, R.H. Datar, K.M. Hansen, T. Thundat, R.J. Cote, and A. Majundar. Bioassay of prostate-specific antigen (psa) using microcantilevers. *Nature Biotechnology*, 19:856–860, 2001. 9

[21] R. Raiteri, M. Grattarola, and R. Berger. Micromechanics senses biomolecules. *Sensors and Actuators B*, 05(01):22–29, 2002. 9

[22] G. Kovacs, G.W. Lubking, M.J. Vellekoop, and A. Venema. Love waves for (bio)chemical sensing in liquids. In *IEEE ultrasonics symposium*, pages 281–285, 1992. 9

[23] E. Gizeli. *Biomolecular Sensors*, chapter Acoustic transducers. Taylor & Francis, London, 2002. 9, 13

[24] O. Tamarin, C. Déjous, D. Rebière, J. Pistré, S. Comeau, D. Moynet, and J. Bezian. Study of acoustic Love wave devices for real time bacteriophage detection. *Sensors and Actuators B*, 91(1-3):275–284, 2003. 9

[25] O. Tamarin, S. Comeau, C. Déjous, D. Moynet, D. Rebière, J. Bezian, and J. Pistré. Real time device for biosensing: design of a bacteriophage model using Love acoustic waves. *Biosensors and Bioelectronics*, 18(5-6):755–763, 2003. 9

[26] P. Mazein, C. Zimmermann, D. Rebière, C. Déjous, J. Pistré, and R. Planade. Dynamic analysis of love waves sensors responses: application to organophosphorus compounds in dry and wet air. *Sensors and Actuators B*, 95:51–57, 2003. 9

[27] D.B. Leeson. Simple model of feedback oscillator noise spectrum. *Proc. IEEE*, page 329, Feb. 1966. 10

[28] E. Rubiola. *Phase noise and frequency stability in oscillators*. 2009. 10, 46

[29] J.-M Friedt and E. Carry. Introduction to the quartz tuning fork. *American Journal of Physics*, pages 415–422, May 2007. 10, 35, 64, 65

[30] J.-M. Friedt, L. A. Francis, and S. Ballandras. Thickness and viscosity of organic thin films probed by combined surface acoustic love wave and surface plasmon resonance. September 2005. 10

[31] C. Zhou, J.-M. Friedt, A. Angelova, K.-H. Choi, W. Laureyn, F. Frederix, L. A. Francis, A. Campitelli, Y. Engelborghs, and G. Borghs. Human immunoglobulin adsorption investigated by means of quartz crystal microbalance dissipation, atomic force microscopy, surface acoustic wave, and surface plasmon resonance techniques. *Langmuir*, 20(14):5870–5878, June 2004. 11

[32] L. Huang, G. Reekmans, D. Saerens, J.-M Friedt, F. Frederix, L. Francis, S. Muyldermans, A. Campitelli, and C. Van Hoof. Prostate-specific antigen immunosensing based on mixed self-assembled monolayers, camel antibodies and colloidal gold enhanced sandwich assays. *Biosensors & Bioelectronics*, 21(3):483–490, September 2005. 11

[33] L. El Fissi, J.-M. Friedt, F. Chérioux, and S. Ballandras. Amine functionalized su-8 layer guiding love mode surface acoustic wave. *Sensors and Actuators B*, 2009. 11

[34] L. El Fissi, J.-M. Friedt, B. Belgacem, F. Chérioux, and S. Ballandras V. Luzet. Fabrication and packaging technologies of love-wave-based microbalance for fluid analysis. *Procedia Chemistry*, (1):52–55, 2009. 11

[35] T. Nomura and M. Iijima. Electrolytic determination of nanomolar concentrations of silver in solution with a quartz crystal microbalance. *Analytica Chimica Acta*, 131:97–102, 1981. 11

[36] E. Hwang and Y. Lim. Construction of a low noise electrochemical quartz crystal microbalance. *Bull. Korean Chem. Soc.*, 17:39–42, 1996. 11

[37] G.L. Dybwad. A sensitive new method for the determination of adhesive bonding between a particle and a substrate. *J. Appl. Phys.*, 58(7):2789–2790, 1985. 11

[38] G. Sauerbrey. Verwendung von schwingquarzen zur wägung dünner schichten und zur mikrowägung. *Zeitschrift für Physik*, 155:206–222, 1959. 11

[39] M. Muratsugu, F. Ohta, Y. Miya, T. Hosokawa, S. Kurosawa, N. Kamo, and H. Ikeda. Quartz crystal microbalance for the detection of microgram quantities of human serum albumin: relationship between the frequency change and the mass of protein adsorbed. *Anal. Chem.*, 65:2933–2937, 1993. 11

[40] M. Rodahl and B. Kasemo. On the measurement of thin liquid overlayers with the quartz-crystal microbalance. *Sensors and Actuators A*, 54:448–456, 1996. 11, 12

[41] M. Rodahl, P. Dahlqvist, F. Höök, and B. Kasemo. *Biomolecular Sensors*, chapter The quartz crystal microbalance with dissipation monitoring. Taylor & Francis, London, 2002. 11

[42] D.A. Buttry and M.D. Ward. Measurement of interfacial processes at electrode surfaces with the electrochemical quartz crystal microbalance. *Chem. Rev.*, 92:1355–1379, 1992. 11, 33

[43] A. Janshoff, H.-J. Galla, and C. Steinem. Piezoelectric mass-sensing devices as biosensors – an alternative to optical biosensors ? *Angew. Chem. Intl.*, 39:4004–4032, 2000. 11

[44] R. Schumacher, J.G. Gordon, and O. Melroy. Observation of morphological relaxation of copper and silver electrodes in solution using a quartz microbalance. *J. Electroanal. Chem.*, 216:127–135, 1987. 11

[45] R. Schumacher. The quartz crystal microbalance: a novel approach to the in-situ investigation of interfacial phenomena at the solid/liquid junction. *Angew. Chem. Int. Ed. Engl.*, 29:329–343, 1990. 11

[46] M. Urbakh and L. Daikhin. Influence of the surface morphology on the quartz crystal microbalance reponse in a fluid. *Langmuir*, 10:1836–2841, 1994. 11

[47] M. Urbakh and L. Daikhin. Roughness effects on the frequency of a quartz-crystal resonator in contact with a liquid. *Physical Review B*, 49(7):4866–4870, 1994. 11

[48] L. Daikhin and M. Urbakh. Effect of surface film structure on the quartz crystal microbalance response in liquids. *Langmuir*, 12:6354–6360, 1996. 11, 18

[49] L. Daikhin, E. Gileadi, G. Katz, V. Tsionsky, M. Urbakh, and D. Zagidulin. Influence of roughness on the admittance of the quartz crystal microbalance immersed in liquids. *Anal. Chem.*, 74:554–561, 2002. 11

[50] M. Huand, D. Shen, L.M. Chow, and M. Yang. Correlations of the impedance parameters ad conductivity and permittivity of liquid and gel phases in a series piezoelectric quartz crystal sensor. *Sensors and Actuators B*, 72:21–27, 2001. 11

[51] S. Ghafouri and M. Thompson. Interfacial properties and the response of the transverse acoustic wave device in electrolyes. *Electroanalysis*, 12(5):326–336, 2000. 11

[52] R. Etchenique and T. Buhse. Anomalous behaviour of the quartz crystal microbalance in the presence of electrolytes. *Analyst*, 125:785–787, 2000. 11

[53] V. Tsionsky, G. Katz, E. Gilaedi, and L. Daikhin. Admittance studies of the eqcm on rough surfaces. the double layer region. *Journal of Electroanalytical Chemistry*, 524-525:110–119, 2002. 11

[54] G. McHale, R. Lücklum, M.I. Newton, and J.A. Cowen. Influence of viscoelasticity and interfacial slip on acoustic wave sensors. *Journal of Applied Physics*, 88(12):7304–7312, 2000. 11

[55] K.K. Kanazawa and J.G. Gordon. Frequency of a quartz microbalance in contact with liquid. *Anal. Chem.*, 57(8):1770–1771, 1985. 11

[56] A. Arnau, T. Sogorb, and Y. Jiménez. Circuit for continous motional series resonant frequency and motional resistance monitoring of quartz crystal resonators by parallel capacitance compensation. *Rev. Sci. Instrum.*, 73:2724–2737, 2002. 11

[57] D.W. Dye. The piezo-electric quartz resonator and its equivalent electrical circuit. *Proc. Phys. Soc. London*, 38:399–458, 1925. 11

[58] K.S. Van Dyke. The electrical network equivalent of a piezoelectric resonator. *Phys. Rev.*, 25:895, 1925. 11

[59] K.K. Kanazawa. Mechanical behaviour of films on the quartz microbalance. *Faraday Discuss.*, 107:77–90, 1997. 12

[60] M. Rodahl, F. Höök, C. Fredriksson, C.A. Keller, A. Krozer, P. Brzezinski, M. Voinova, and B. Kasemo. Simultaneous frequency and dissipation factor QCM measurements of biomolecular adsorption and cell adhesion. *Faraday Discuss.*, 107:229–246, 1997. 12

[61] S. Kurosawa, D.-S. Han, J.-W. Park, H. Aizawa, M. Yoshimoto, C. Nakamura, J. Miyake, and S.-M. Chang. Gas sensor using high-frequency quartz crystal microbalance. In *Proceedings of the 2001 IEEE International Frequency Control Symposium and PDA Exhibition*, pages 462–464, 2001. 12

[62] J.-M. Friedt, K.H. Choi, F. Frederix, and A. Campitelli. Simultaneous atomic force microscope and quartz crystal microbalance measurements: Methodology validation using electrodeposition. *Journal of the Electrochemical Society*, 150(10):H229–H234, 2003. 13, 16, 18

[63] J.C. Andle and J.F. Vetelino. Acoustic wave biosensors. In *IEEE ultrasonics symposium*, pages 451–460, 1995. 13

[64] M. Rapp, T. Wessa, and H.J. Ache. Modification of commercially available low-loss SAW devices towards an immunosensor for in-situ measurements in water. In *IEEE ultrasonics symposium*, pages 433–436, 1995. 14

[65] B.A. Auld. *Acoustic Fields and Waves in Solids*. 1990. 14

[66] A.J. Ricco, S.J. Martin, G.C. Frye, and T.M. Niemczyk. Acoustic plate mode devices as liquid phase sensors. In *IEEE Solid-State Sensor and Actuator Workshop*, pages 23–26, 1988. 14

[67] G. McHale, M.I. Newton, and F. Martin. Theoretical mass sensitivity of love wave and layer guided acoustic plate mode sensors. *Journal of Applied Physics*, 91(12):9701–9710, 2002. 14

[68] E. Gizeli, M. Liley, and C.R. Lowe. Detection of supported lipid layers by utilising the acoustic love waveguide device: application to biosensing. In *Transducers'95*, pages 521–523, 1995. 14

[69] B. Jakoby. Analysis and optimization of love wave liquid sensors. *IEEE Transactions on ultrasonics, ferroelectrics,and frequency control*, 45(5):1293–1302, 1998. 14

[70] J. Du and G.L. Harding. A multilayer structure for love-mode acoustic sensors. *Sensors and Actuators A*, 65:152–159, 1998. 14, 17

[71] E. Gizeli. Study of the sensitivity of the acoustic waveguide sensor. *Anal. Chem.*, 72:5967–5972, 2000. 14, 17

[72] J. Freudenberg, M. von Schickfus, and S. Hunklinger. A saw immunosensor for operation in liquid using a sio_2 protective layer. *Sensors and Actuators B*, 76:147–151, 2001. 14

[73] K. Saha, F. Bender, A. Rasmusson, and E. Gizeli. Probing the viscoelasticity and mass of a surface-bound protein layer with an acoustic waveguide device. *Langmuir*, 19(4):1304–1311, 2003. 14

[74] K. Saha, F. Bender, and E. Gizeli. Comparative study of IgG binding to proteins g and a: Nonequilibrium kinetic and binding constant determination with the acoustic waveguide device. *Anal. Chem.*, 75(4):835–842, 2003. 14, 16

[75] A. Royer and E. Dieulesaint. *Ondes élastiques dans les solides, tome 2*. 1999. 14

[76] C.K. Campbell. *Surface acoustic wave devices for mobile and wireless communications*. 1998. 14

[77] B. Jakoby and M.J. Vellekoop. Viscosity sensing using a love-wave device. *Sensors and Actuators A*, 68:275–281, 1998. 16

[78] A.J. Ricco, S.J. Martin, and T.E. Zipperian. Surface acoustic wave gas sensor based on film conductivity changes. *Sensors and Actuators*, 8:319–333, 1985. 16

[79] G.L. Harding, J. Du, P.R. Dencher, D. BArnett, and E. Howe. Love wave acoustic immunosensor operating in liquid. *Sensors and Actuators A*, 61:279–286, 1997. 16

[80] L. El Fissi, J.-M. Friedt, and S. Ballandras. Modeling the rf acoustic behaviour of love-wave sensors loaded with organic layers. pages 484–487, 2007. 17

[81] J.-M. Friedt, L. Francis, K.-H. Choi, and A. Campitelli. Combined atomic force microscope and acoustic wave devices: Application to electrodeposition. *Journal of Vacuum Science and Technology A*, 21(4):1500–1505, 2003. 18, 34

[82] J. Bargon, S. Braschoß, J. Flörke, U. Herrmann, L. Klein, J.W. Loergen, M. Lopez, S. Maric, A.H. Parham, P. Piacenza, H. Schaefgen, C.A. Schalley, G. Silva, M. Schlupp, H. Schwierz, F. Vögtle, and G. Windscheif. Determination of the ripening state of emmental cheese via quartz microbalances. *Sensors and Actuators B*, 95:6–19, 2003. 18

[83] E. Rubiola. On the measurement of frequency and its sample variation with high resolution counters. *Rev. Sci. Instrum.*, 76(5):054703, May 2005. 20

[84] S. Dawkins, J.J. McFerran, and A.N. Luiten. Considerations on the measurement of the stability of osillators with frequency counters. pages 759–764, 2007. 20

[85] G.R. Fowles. *Introduction to modern optics*. Dover Publications, New-York, 1975. 23

[86] P.B Johnson and R.W. Christy. Optical constants of nobel metals. *Phys. Rev. B*, 6(12):4370–4379, 1972. 23, 32

[87] P.B Johnson and R.W. Christy. Optical constants of transition metals: Ti, v, cr, mn, fe, co, ni and pd. *Phys. Rev. B*, 9(12):5056–5070, 1974. 23

[88] E.D. Palik, editor. *Handbook of optical constants of solids (2 volumes)*. Academic Press, New York, 1991. 23, 32

[89] M. Liley. *Biomolecular Sensors*, chapter Optical transducers. Taylor & Francis, London, 2002. 23

[90] R.W. Glaser. *Biosensors and their applications*, chapter Surface plasmon resonance biosensors. Kluwer Academic/Plenum publishers, 2000. 23

[91] B. Ivarsson and M. Malmqvist. *Biomolecular Sensors*, chapter Surface plasmon resonance: development and use of BIACORE instruments for biomolecular interaction analysis. Taylor & Francis, London, 2002. 23

[92] E. Kretschmann and H. Raether. Radiative decay of nonradiative surface plasmon excited by light. *Z. Naturforschung*, 23A:2135, 1968. 23

[93] H. Raether. *Surface plasmons*, chapter Surface plasmons on smooth surfaces. Springer-Verlag, 1988. 23, 24

[94] R.P.H. Kooyman, H.E. de Bruijn, R.G. Eenink, and J. Greve. Surface plasmon resonance as a bioanalytical tool. *journal of molecular structure*, 218:345–350, 1990. 23

[95] H.E. de Bruijn, B.S.F. Alternburg, R.P.H. Kooyman, and J. Greve. Determination of thickness and dielectric constant of thin transparent dielectric layers using surface plasmon resonance. *Optics Communications*, 82(5, 6):425–432, 1991. 23

[96] H.E. de Bruijn, R.P.H. Kooyman, and J. Greve. Choice of metal and wavelength for surface-plasmon resonance sensors: some considerations. *Applied Optics*, 31(4):440–442, 1992. 23

[97] T. Akimoto, S. Sasaki, K. Ikebukuro, and I. Karube. Effect of incident angle of light on sensitivity and detection limit for layers of antibody with surface plasmon resonance spectroscopy. *Biosensors & Bioelectronics*, 15:355–362, 2000. 23, 24

[98] U. Kreibig and M. Vollmer. *Optical properties of metal clusters*. Springer-Verlag, Berlin, 1995. 23, 25

[99] P. Guédon. *Étude de systèmes optiques pour l'analyse directe, en temps réel et en parallèle, d'interactions biomoléculaires*. Doctorat de l'université Paris VI, France, 2000. 23

[100] B.P. Nelson, A.G. Frutos, J.M. Brockman, and R.M. Corn. Near-infrared surface plasmon resonance measurements of ultrathin films. *Anal. Chem.*, 71:3928–3940, 1999. 23

[101] J.D. Swalen, J.G. Gordon, M.R. Philpott, A. Brillante, I. Pockrand, and R. Santo. Plasmon surface polariton dispersion by direct optical observation. *Am. J. Phys.*, 48(8):669–672, 1980. 23

[102] R.C. Jorgenson and S.S. Yee. A fiber-optic chemical sensor based on surface plasmon resonance. *Sensors and Actuators B*, 12:213–220, 1993. 23

[103] K.A. Peterlinz and R. Georgiadis. In situ kinetics of self-assembly by surface plasmon resonance spectroscopy. *Langmuir*, 12:4731–4740, 1996. 23

[104] H. Knobloch, G. von Szada-Borryszkowski, S. Woigk, A. Helms, and L. Brehmer. Dispersive surface plasmon microscopy for the characterization of ultrathin organic films. *Appl. Phys. Lett.*, 69(16):2336–2337, 1996. 23

[105] R.A. Innes and J.R. Sambles. Optical characterization of gold using surface plasmon-polaritons. *J. Phys. F*, 17:277–287, 1987. 23

[106] E. Fontana, R.H. Pantell, and M. Moslehi. Characterization of dielectric-coated, metal mirrors using surface plasmon spectroscopy. *Applied Optics*, 27(16):3334–3340, 1988. 23

[107] Z. Salamon, H.A. Macleod, and G. Tollin. Surface plasmon resonance spectroscopy as a tool for investigating the biochemical and biophysical properties of membrane protein systems. *Biochimica and biophysica acta*, 1331:117–152, 1997. 24

[108] K.-F Giebel, C. Bechinger, S. Herminghaus, M. Riedel, P. Leiderer, U Weiland, and M. Bastmeyer. Imaging of cell/substrate contacts of living cels with surface plasmon resonance. *Biophysical Journal*, 76(1):509–516, January 1999. 24

[109] P. Orfanides, T.F. Buckner, M.C. Buncick, and T.L. Ferrell. Demonstration of surface plasmon resonance in metal island films and the effect of the surrounding medium – an undergraduate experiment. *Am. J. Phys.*, 68(10):936–942, 2000. 25

[110] P. Mulvaney. Not all that's gold does glitter. *MRS Bulletin*, 26(12):1009–1014, 2001. 25

[111] F. Kim, J.H. Song, and P. Yang. Photochemical synthesis of gold nanorods. *J. Am. Chem. Soc.*, 124:14316–14317, 2002. 25

[112] H. Xu and M. Käll. Modeling the optical response of nanoparticle-based surface plasmon resonance sensors. *Sensors and Actuators B*, 87:244–249, 2002. 25

[113] S. Lal, S.L. Westcott, R.N. Taylor, J.B. Jackson, P. Nordlander, and N.J. Halas. Light interaction between gold nanoshells plasmon resonance and planar optical waveguides. *J. Phys. Chem. B*, 106(22):5609–5612, 2002. 25

[114] E.S. Kooij, H. Wormeester, E.A.M. Brouwer, E. van Vroonhoven, A. van Silfhout, and B. Poelsema. Optical characterization of thin colloidal gold films by spectroscopic ellipsometry. *Langmuir*, 18(11):4401–4413, 2002. 25

[115] M. Born and W. Wolf. *Principles of optics*, chapter Optics of metals. Cambridge university Press, 1999. 25

[116] B.M.I. van der Zande, M.R. Böhmer, L.G.J. Fokkink, and C. Shönenberg. Aqueous gold sols of rod-shaped particles. *J. Phys. Chem. B*, 101:852–854, 1997. 25

[117] S.-S. Chang, C.-W. Shih, C.-D. Chen, W.-C. Lai, and C.R.C. Wang. The shape transition of gold nanorods. *Langmuir*, 15(3):701–709, 1999. 25

[118] C.L. Haynes and R.P. Van Duyne. Nanosphere lithography: a versatile nanofabrication tool for studies of size-dependent nanoparticle optics. *J. Phys. Chem. B*, 105:5599–5611, 2001. 25

[119] M. Himmelhaus and H. Takei. Cap-shaped gold nanoparticles for an optical biosensor. *Sensors and Actuators B*, 63:24–30, 2000. 25

[120] Y. Lu, Y. Yin nd Z.-H. Li, and Y. Xia. Synthesis and self-assembly of $au@sio_2$ core-shell colloids. *NanoLetters*, 2(7):785–788, 2002. 25

[121] T. Okamoto, I. Yamaguchi, and T. Kobayashi. Local plasmon sensor with gold colloid monolayers deposited upon glass substrates. *Optics Letters*, 25(6):372–374, 2000. 25

[122] N. Nath and A. Chilkoti. Interfacial phase transition of an environmentally responsive elastin biopolymer adsorbed on functionalized gold nanoparticles studied by colloidal surface plasmon resonance. *J. Am. Chem. Soc.*, 123:8197–8202, 2001. 25

[123] N. Nath and A. Chilkoti. A colorimetric gold nanoparticle sensor to interrogate biomolecular interactions in real time on a surface. *Anal. Chem.*, 74:504–509, 2002. 25

[124] N. Nath and A. Chilkoti. Creating "smart" surfaces using stimuli responsive polymers. *Advanced Materials*, 14(17):1243–1247, 2002. 25

[125] S.-F. Cheng and L.-K. Chau. Colloidal gold-modified optical fiber for chemical and biochemical sensing. *Anal. Chem.*, 75:16–21, 2003. 25

[126] J.C. Riboh, A.J. Haes, A.D. McFarland, C.R. Yonzon, and R.P. Van Duyne. A nanoscale optical biosensor: real-time immunoassay in physiological buffer enabled by improved nanoparticle adhesion. *J. Phys. Chem. B*, 107(8):1772–1780, 2003. 25

[127] M. Watanabe and K. Kajikawa. An optical fiber biosensor based on anomalous reflection of gold. *Sensors and Actuators B*, 89:126–130, 2003. 25

[128] T. Okamoto and I. Yamaguchi. Optical absorption study of the surface plasmon resonance in gold nanoparticles immobilized onto a gold substrate by self-assembly technique. *J. Phys. Chem. B*, 2003. 25

[129] F. Frederix, J.-M. Friedt, K.-H. Choi, W. Laureyn, A. Campitelli, D. Mondelaers, G. Maes, and G. Borghs. Biosensing based on light absorption of nanoscaled gold and silver particles. *Analytical Chemistry*, 75(24):6894–6900, 2003. 25

[130] B. Lin, J. Qiu, J. Gerstenmeier, P. Li, H. Pien, J. Pepper, and B. Cunningham. A label-free optical technique for detecting small molecule interactions. *Biosensors and Bioelectronics*, 17:827–834, 2002. 25

[131] P. Grossel, J.-M. Vigoureux, and F. Baïda. Nonlocal approach to scattering in a one-dimensional problem. *Phys. Rev. A*, 50:3627–3637, 1994. 26, 32

[132] E. Stenberg, B. Persson, H. Roos, and C. Urbaniczky. Quantitative determination of surface concentration of protein with surface plasmon resonance using radiolabeled proteins. *Journal of colloid and interface science*, 143(2):513–526, 1991. 26, 30, 31

[133] R.M.A. Azzam and N.M. Bashra. *Ellipsometry and polrized light*. Elsevier Science, 1987. 26

[134] G. Wang, M. Rodahl, M. Edvardsson, S. Svedhem, G. Ohlsson, F. Höök, and B. Kasemo. A combined reflectometry and quartz crystal microbalance with dissipation setup for surface interaction studies. *Rev. Sci. Instrum.*, 79:075107, 2008. 26

[135] B.J. Luff, J.S. Wilkinson, J. Piehler, U. Hollenbach, J. Ingenhoff, and N. Fabricius. Integrated optical mach-zehnder biosensor. *J. of Lightwave Technology*, 16(4):583–592, April 1998. 26

[136] W. Lukosz. Integrated optical chemical and direct biochemical sensors. volume 29, pages 37–50, october 1995. 27

[137] M. Weisser, B. Menges, and S. Mittler-Neher. Refractive index and thickness determination of monolayers by multi mode waveguide coupled surface plasmon resonance. *Sensors and Actuators B*, 56:189–197, 1999. 27

[138] J. Čtyroký, J. Homola, P.V. Lambeck, S. Musa, H.J.W.M. Hoekstra, R.D. Harris, J.S. Wilkinson, B. Usievich, and N.M. Lyndin. Theory and modelling of optical waveguide sensors utilising surface plasmon resonance. *Sensors and Actuators B*, 54:66–73, 1999. 27

[139] J.C. Abanulo, R.D. Harris, A.K. Sheridan, J.S. Wilkinson, and P.N. Bartlett. Waveguide surface plasmon resonance studies of surface reactions on gold electrodes. *Faraday Discuss.*, 121:139–152, 2002. 27

[140] J. Vörös, J.J. Ramsden, G. Csúcs, I. Szendrö, S.M. De Paul, M. Textor, and N.D. Spencer. Optical grating coupler biosensors. *Biomaterials*, 23:3699–3710, 2002. 27

[141] R. Cush, J.M. Cronin, W.J. Stewart, C.H. Maule, J. Molloy, and N.J. Goddard. The resonant miror: a novel optical biosensor for direct sensing of biomolecular interactions. *Biosensors & bioelectronics*, 8:347–353, 1993. 27

[142] R.J. Davies and P.R. Edwards. *Biomolecular Sensors*, chapter IAsys: the resonant mirror biosensor. Taylor & Francis, London, 2002. 27

[143] B. Kasapbasioglu amd P. Hesketh, W.C. Hanly, G.J. Maclay, and R. Nowroozi-Esfahani. An impedance based ultra-thin platinum island film glucose sensor. *Sensors and Actuators B*, 13-14:749–751, 1993. 28

[144] S. Hardeman, T. Nelson, D. Beirne, M. DeSilva, P.J. Hesketh, G.J. Maclay, and S.M. Gendel. Sensitivity of novel ultrathin platinum film immunosensors to buffer ionic strength. *Sensors and Actuators B*, 24-25:98–102, 1995. 28

[145] P. Bataillard, F. Gardies, N. Jeffrezic-Renault, and C. Martelet. Direct detection of immunospecies by capacitance measurements. *Anal. Chem.*, 60:2374–2379, 1988. 28

[146] C. Berggren and G. Johansson. Capacitance measurements of antibody-antigen interactions in a flow system. *Anal. Chem.*, 69:3651–3657, 1997. 28

[147] M. Dijksma, B. Kamp, J.C. Hoogvliet, and W.P. van Bennekom. Development of an electrochemical immunosensor for the direct detection of interferon-γ at the attomolar level. *Anal. Chem.*, 73:901–907, 2001. 28

[148] P. Sarkar, P.S. Pal, D. Ghosh, S.J. Setford, and I.E. Tothill. Amperometric biosensors for detection of the prostate cancer marker (psa). *International Journal of Pharmaceutics*, 238:1–9, 2002. 28

[149] B. Drake, C.B. Prater, A.L. Weisenhorn, S.A.C. Gould, T.R. Albrecht, C.F. Quate, D.S. Cannell, H.G. Hansma, and P.K. Hansma. Imaging crystals, polymers, and processes in water with the atomic force microscope. *Science*, 243:1586–1589, 1989. 28

[150] J. Davies, C.J. Roberts, A.C. Dawkes, J. Sefton, J.C. Edwards, T.O. Glasbey, A.G. Haynes, M.C. Davies, D.E. Jackson, M. Lomas, K.M. Shakesheff, S.J.B. Tendler, M.J. Wilkins, and P.M. Williams. Use of scanning probe microscopy and surface plasmon resonance as analytical tools in the study of antibody-coated microtiter wells. *Langmuir*, 10:2654–2661, 1994. 29

[151] K.D. Jandt. Atomic force microscopy of biomaterials surfaces and interfaces. *Surface Science*, 491:303–332, 2001. 29

[152] K. H. Choi, J.-M Friedt, F. Frederix, A. Campitelli, and G. Borghs. Simultaneous atomic force microscope and quartz crystal microbalance measurement. *Applied Physics Letters*, 81(7), 2002. 29, 33

[153] R. Wigren, H. Elwing, R. Erlandsson, S. Welin, and I. Lundström. Structure of adsorbed fibrinogen obtained by scanning force microscopy. *FEBS Letters*, 280(2):225–228, 1991. 29

[154] P. Cacciafesta, A.D.L. Humphris, K.D. Jandt, and M. Miles. Human plasma fibrinogen adsorption on ultraflat titanium oxide surfaces studied with atomic force microscopy. *Langmuir*, 16(21):8167–8175, 2000. 29

[155] P.S. Sit and R.E. Marchant. Surface-dependent differences in fibrin assembly visualized by atomic force microscopy. *Surface science*, 491:421–432, 2001. 29

[156] M.L. Wallwork, J. Kirkham, J. Zhang, D.A. Smith, S.J. Brookes, R.C. Shore, S.R. Wood, O. Ryu, and C. Robinson. Binding of matrix proteins to developing enamel crystals: an atomic force microscopy study. *Langmuir*, 17:2508–2513, 2001. 29

[157] M. Bergkvist, J. Carlsson, and S. Oscarsson. A method for studying protein orientation with atomic force microscopy using relative protein volumes. *J. Phys. Chem. B*, 105:2062–2069, 2001. 29

[158] P. Zhang and W. Tan. Atomic force microscopy for the characterization of immobilized enzyme molecules on biosensor surfaces. *Fresenius J. Anal. Chem.*, 369:302–307, 2001. 29

[159] A. Perrin, V. Lanet, and A. Theretz. Quantification of specific immunological reactions by atomic force microscopy. *Langmuir*, 13:2557–2563, 1997. 29

[160] Y.F. Dufrêne, T.G. Marchal, and P.G. Rouxhet. Influence of substratum surface properties on the organization of adsorbed collagen films: in situ characterization by atomic force microscopy. *Langmuir*, 15:2871–2878, 1999. 29

[161] V.M. De Cupere and P.G. Rouxhet. Collagen films adsorbed on native and oxidized poly(ethylene terephtalate): morphology after drying. *Surface Science*, 491:395–404, 2001. 29

[162] I. Revenko, Y. Tang, and J.P. Santerre. Surface structure of polycarbonate urethanes visualized by atomic force microscopy. *Surface Science*, 491:346–354, 2001. 29

[163] P. Cacciafesta, K.R. Hallam, A.C. Watkinson, G.C. Allen, M.J. Miles, and K.D. Jandt. Visualization of human plasma fibrinogen adsorbed on titanium implant surfaces with different roughness. *Surface Science*, 491(21):405–420, 2001. 29

[164] F.A. Denis, P. Hanarp, D.S. Sutherland, J. Gold, C. Mustin, P.G. Rouxhet, and Y.F. Dufrêne. Protein adsorption on model surfaces with controlled nanotopography and chemistry. *Langmuir*, 18:819–828, 2002. 29

[165] K. Hu and A.J. Bard. In situ monitoring of kinetics of charged thiol adsorption on gold using an atomic force microscope. *Langmuir*, 14:4790–4794, 1998. 29

[166] M.M. Stevens, S. Allen, M.C. Davies, C.J. Roberts, E. Schacht, S.J.B. Tendler, S. VanSteenkiste, and P.M. Williams. The development, characterization, and demonstration of a versatile immobilization strategy for biomolecular force measurements. *Langmuir*, 18:6659–6665, 2002. 29

[167] R.D. Piner, S. Hong, and C.A. Mirkin. Improved imaging of soft materials with modified afm tips. *Langmuir*, 15:5457–5460, 1999. 29

[168] J.-B.D. Green and G.U. Lee. Atomic force microscopy with patterned cantilevers and tip arrays: force measurements with chemical arrays. *Langmuir*, 16:4009–4015, 2000. 29

[169] M.A. Cooper, F.N. Dultsev, T. Minson, P.V. Ostanin, C. Abell, and D. Kleenerman. Direct and sensitive detection of a human virus by rupture event scanning. *Nature Biotech.*, 19(9):833–837, 2001. 29

[170] S. Kidoaki and T. Matsuda. Adhesion forces of the blood plasma proteins on self-assembled monolayer surfaces of alkanethiolates with different functional groups measured by atomic force microscope. *Langmuir*, 15:7639–7646, 1999. 29

[171] Z. Wei, C. Wang, Z. Wang, D. Liu, and C. Bai. Topography investigation of water layer and self-assembled monolayers with ots-modified afm tips. *Surface and interface analysis*, 32:275–277, 2001. 29

[172] J.-B.D. Green, A. Idowu, and S.S.F. Chan. Modified tips: molecules to cells. *Materials Today*, 02:22–29, 2003. 29

[173] D.J. Pena, M.P. Raphael, and J.M. Byers. "dip-pen" nanolithography in registry with photolithography for biosensor development. *Langmuir*. 29

[174] J.J. Davis, C.M. Halliwell, H.A.O. Hill, G.W. Canters, M.C. van Amsterdam, and M.P. Verbeet. protein adsorption at a gold electrode studied by *in situ* scanning tunnelling microscopy. *New. J. Chem.*, pages 1119–1123, 1998. 29

[175] J. Kwak and A.J. Bard. Scanning electrochemical microscopy. apparatus and two-dimensional scans of conductive and insulating substrates. *Anal. Chem.*, 61:1794–1799, 1989. 29, 34

[176] D.O. Wipf. *Scanning electrochemical microscopy*, chapter Instrumentation, pages 17–74. Marcel Dekker, Inc., New York, 2001. 29

[177] O.E. Hüsser, D.H. Craston, and A.J. Bard. Scanning electrochemical microscopy. *Journal of the Electrochemical Society*, 136(11):3222–3229, 1989. 29

[178] C.C. Williams and H.K. Wickramasinghe. Scanning chemical potential microscope: A new technique for atomic scale surface investigation. *J. Vac. Sci. Tech. B*, 9(2):537–540, 1991. 29

[179] Y.E. Korchev, Y.A. Negulyaev, C.R.W. Edwards, I. Vodyanoy, and M.J. Lab. Functional localization of single active ion channels on the surface of a living cell. *Nature cell biology*, 2:616–618, 2000. 29

[180] O.D. Uitto and H.S. White. Scanning electrochemical microscopy of membrane transport in the reverse imaging mode. *Anal. Chem.*, 73(3):533539, 2001. 29

[181] B.D. Bath, H.S. White, and E.R. Scott. *Scanning electrochemical microscopy*, chapter Imaging molecular transport across membranes, pages 343–396. Marcel Dekker, Inc., New York, 2001. 29

[182] B.R. Hooroks and G. Winstokk. *Scanning electrochemical microscopy*, chapter Biological systems, pages 445–520. Marcel Dekker, Inc., New York, 2001. 29

[183] D. Johannsmann. Viscoelastic analysis of organic thin films on quartz resonators. *Macromol. Chem. Phys.*, 200(3):501–516, 1999. 30

[184] F. Höök, B. Kasemo, T. Nylander, C. Fant, K. Scott, and H. Elwing. Variations in coupled water, viscoelastic properties, and film thickness of Mefp-1 protein film during adsorption and cross-linking: a quartz crystal microbalance with dissipation monitoring, ellipsometry, and surface plasmon resonance study. *Anal. Chem.*, 73:5796–5804, 2001. 30, 31

[185] F. Höök, J. Vörös, M. Rodahl, R. Kurrat, P. Böni, J.J. Ramsden, M. Textor, N.D. Spencer, P. Tengvall, J. Gold, and B. Kasemo. A comparative study of protein adsorption on titanium oxide surfaces using in situ ellipsometry, optical waveguide lightmode spectroscopy, and quartz crystal microbalance/dissipation. *Colloids and Surfaces B*, 24:155–170, 2002. 30

[186] C. Kößlinger, E. Uttenthaler, S. Drost, F. Aberl, H. Wolf, G. Brink, A. Stanglmaier, and E. Sackmann. Comparison of the qcm and the spr method for surface studies and immunological applications. *Sensors and Actuators B*, 24-25:107–112, 1995. 30

[187] T.P. Vikinge, K.M. Hanson, P. Sandström, B. Liedberg, T.L. Lindahl, I. Lundström, P. Tengvall, and F. Höök. Comparison of surface plasmon resonance and quartz crystal microbalance in the study of whole blood and plasma coagulation. *Biosensors & Bioelectronics*, 15:603–613, 2000. 30

[188] A. Laschitsch, B. Menges, and D. Johannsmann. Simultaneous determination of optical and acoustic thicknesses of protein layers using surface plasmon resonance spectroscopy and quartz crystal microweighing. *Applied Physics Letters*, 77(14):2252–2254, 2000. 30

[189] L.E. Bailey, D. Kambhampati, K.K. Kanazawa, W. Knoll, and C.W. Franck. Using surface plasmon resonance and the quartz crystal microbalance to monitor in situ the interfacial behavior of thin organic films. *Langmuir*, 18:479–489, 2002. 30

[190] A. Domack and D. Johannsmann. Shear birefringence measurements on polymer thin films deposited on quartz resonators. *J. Appl. Phys.*, 83(3):1286–1295, 1998. 30

[191] B. Liedberg, C. Nylander, and I. Lundström. Surface plasmon resonance for gas detection and biosensing. *Sensors and Actuators*, 4:299–304, 1983. 30

[192] R.J. Marsh, R.A.L. Jones, and M. Sferrazza. Adsorption and displacement of a globular protein on hydrophilic and hydrophobic surfaces. *Colloids and Surfaces B*, 23(1):31–42, 2002. 30

[193] F. Caruso, D.N. Furlong, K. Ariga, I. Ichinose, and T. Kunitake. Characterization of polyelectrolyteprotein multilayer films by atomic force microscopy, scanning electron microscopy, and fourier transform infrared reflectionabsorption spectroscopy. *Langmuir*, 14:4559–4565, 1998. 30

[194] J.-M Friedt, L. Francis, G. Reekmans, R. De Palma, A. Campitelli, and U.B. Sleytr. Simultaneous surface acoustic wave and surface plasmon resonance measurements: electrodeposition and biological interactions monitoring. *Journal of Applied Physics*, 95(4):1677–1680, 2004. 30

[195] L. Francis, J.-M. Friedt, C. Zhou, and P. Bertrand. In situ evaluation of density, viscosity and thickness of adsorbed soft layers by combined surface acoustic wave and surface plasmon resonance. *Analytical Chemistry*, 78(12):4200–4209, 2006. 31

[196] L. Nieba, A. Krebber, and A. Plückthun. Competition BIAcore for measuring true affinities: large differences from values determined from binding kinetics. *Analytical Biochemistry*, 234:155–165, 1996. 31

[197] P.A. van der Merwe and A.N. Barclay. Analysis of cell-adhesion molecule interactions using surface plasmon resonance. *current opinion in immunology*, 8(2):257–261, 1996. 31

[198] D.E. Aspnes, E. Kingsbron, and D.D. Bacon. Optical properties of Au: sample effects. *Phys. Rev. B*, 21(8):3290–3300, April 1980. 32

[199] X. Chen, K.M. Shakesheff, M.C. Davies, J. Heller, C.J. Roberts, S.J.B. Tendler, and P.M. Williams. Degradation of a thin polymer film studied by simultaneous *in situ* atomic force microscopy and surface plasmon resonance analysis. *J. Phys. Chem.*, 99:11537–11542, 1995. 32

[200] K. H. Choi, J.-M. Friedt, F. Frederix, A. Campitelli, and G. Borghs. Simultaneous atomic force microscope and quartz crystal microbalancemeasurement. *Applied Physics Letters*, 81(7):1335–1337, 2002. 32

[201] J.-M Friedt, K. H. Choi, L. Francis, and A. Campitelli. Simultaneous atomic force microscope and quartz crystal microbalance measurements: interactions and displacement field of a qcm. *Japanese Journal of Applied Physics*, 41(6A):3974–3977, 2002. 32

[202] A. Bund, O. Schneider, and V. Dehnke. Combining AFM and EQCM for the *in situ* investigation of surface roughness effects during electrochemical metal depositions. *Phys. Chem. Chem. Phys.*, 4:3552–3554, 2002. 32

[203] O. Hayden, R. Bindeus, and F.L. Dickert. Combining atomic force microscope and quartz crystal microbalance studies for cell detection. *Meas. Sci. Technol.*, 14:1876–1881, 2003. 32

[204] J.-M Friedt, K. H. Choi, L. Francis, and A. Campitelli. Simultaneous atomic force microscope and quartz crystal microbalance measurements: interactions and displacement field of a qcm. *Japanese Journal of Applied Physics*, 41(6A):3974–3977, 2002. 33

[205] K.-H. Choi, J.-M. Friedt, W. Laureyn, F. Frederix, A. Campitelli, and G. Borghs. Investigation of protein adsorption with simultaneous measurements of atomic force microscope and quartz crystal microbalance. *Journal of Vacuum Science and Technology B*, 21(4):1433–1436, 2003. 33

[206] K. Karrai and R.D. Grober. Piezoelectric tip-sample distance control for the near field optical microscopes. *Applied Physics Letters*, 66(14):1842–1844, 1995. 34

[207] H. Edwards, L. Taylor, W. Duncan, and A.J. Melmed. Fast, high-resolution atomic force microscopy using a quartz tuning fork as actuator and sensor. *J. Appl. Phys.*, 82(3):980–984, 1997. 34

[208] Y.E. Korchev, J. Gorelik M.J. Lab, E.V. Sviderskaya, C.L. Johnston, C.R. Coombes, I. Vodyanov, and C.R.W. Edwards. Cell volume measurement using scanning ion conductance microscopy. *Biophysical Journal*, 78:451–457, 2000. 34

[209] M. Todorovic and S. Schultz. Magnetic force microscopy using a nonoptical piezoelectric quartz tuning fork detection design with applications to magnetic recording studies. *Journal of Applied Physics*, 83(11):6229–6231, 1998. 34

[210] D.W. Pohl, U.C. Fischer, and U.T. Dürig. Scanning near-field optical microscopy (SNOM). *Journal of Microscopy*, 152(3):853–861, 1988. 34

[211] Y.E. Korchev, M. Raval, M.J. Lab, J. Gorelik, C.R.W. Edwards, T. Rayment, and D. Klenerman. Hybrid scanning ion conductance and scanning near-field optical microscopy for the study of living cells. *Biophysical Journal*, 78:2675–2679, 2000. 34

[212] N.F. van Hulst, J.-A Veerman, M.F. Garciía-Parajó, and L.K. Kuipers. Analysis of individual (macro)molecules and proteins using near field optics. *Journal of Chemical Physics*, 18(112):7799–7810, 2000. 34

[213] J.-M Friedt and E. Carry. Introduction au diapason à quartz. *Bulletin de l'Union des Physiciens*, December 2005. 35, 64

[214] J.-M Friedt, E. Carry, Z. Sadani, B. Serio, M. Wilm, and S. Ballandras. Quartz tuning fork vibration amplitude as a limitation of spatial resolution of shear force microscopes. April 2005. 35

[215] P. Sandoz, J.-M Friedt, and E. Carry. In-plane rigid-body vibration mode characterization with a nanometer resolution by stroboscopic imaging of a microstructured pattern. *Review of Scientific Instruments*, 78:023706, 2007. 35

[216] P. Sandoz, J. M. Friedt, and E. Carry. In-plane displacement measurement with subpixel resolution: application to vibration characterization of a shear-force scanning probe. June 2007. 35

[217] P. Sandoz, E. Carry, J.-M. Friedt, and S. Ballandras. Digital image processing for measuring 2d vibration amplitudes with subpixel resolution: application to the quartz tuning fork. May 2007. 35

[218] P. Sandoz, J.-M. Friedt, E. Carry, B.Trolard, and J. Garzon Reyes. Frequency domain characterization of tuning-fork mechanical vibrations by vision and digital image processing. *American Journal of Physics*, 77(1):20–26, 2009. 35, 64, 65

[219] P.Sandoz, J.-M Friedt, and E. Carry. Vibration amplitude of a tip-loaded quartz tuning fork during shear force microscopy scanning. *Rev. Sci. Instrum.*, 79(8), august 2008. 35

[220] W.H. Rensen, N.F. van Hulst, and S.B. Kämmer. Imaging soft samples in liquid with tuning fork based shear force microscopy. *Applied Physics Letters*, 77(10):1557–1559, 2000. 35

[221] L.Reindl, G.Scholl, T.Ostertag, W.Ruile, H. Scherr, C.C.W. Ruppel, and F.Schmidt. Wireless remote identification and sensing with saw devices. In *Sensor*, pages 161–166, 1997. 37

[222] L. Reindl, G. Scholl, T. Ostertag, A. Pohl, and R. Weigel. Wireless remote identification and sensing with saw devices. In *Proc. IEEE 1998 MMT/AP International Workshop on Commercial Radio Sensor and Communication Techniques*, pages 83–96, 1998. 37

[223] A. Stelzer, G. Schimetta, L. Reindl, A. Springer, and R. Weigel. Wireless saw sensors for surface and subsurface sensing applications. In *SPIE Proceedings – Subsurface ans Surface Sensing Technologies and Applications III*, volume 4491, pages 358–366, 2001. 37, 38

[224] J. H. Kuypers, M. Esashi, D. A. Eisele, and L. M. Reindl. 2.45 ghz passive wireless temperature monitoring system featuring parallel sensor interrogation and resolution evaluation. In *IEEE Ultrasonics Symposium*, pages 1453–1458, 2006. 37

[225] R.M. White and F.W. Voltmer. Direct piezoelectric coupling to surface acoustic waves. *Applied Physics Letters*, 7(12):314–316, december 1965. 38

[226] Y. Dong, W. Cheng, S. Wang, Y. Li, and G. Feng. A multi-resolution passive saw chemical sensor. *Sensors and Actuators B*, 76:130–133, 2001. 38

[227] T. Nomura, A. Saitoh, and H. Tokuyama. Wireless sensor using surface acoustic wave. In *WCU*, pages 935–938, 2003. 38

[228] G. Scholl, F. Schmidt, T. Ostertag, L. Reindl, H. Scherr, and U. Wolff. Wireless passive SAW sensor systems for industrial and domestic applications. In *IEEE International frequency control symposium*, pages 595–601, 1998. 38

[229] A. Springer, R. Weigel, A. Pohl, and F. Seifert. Wireless identification and sensing using surface acoustic wave devices. *Mechatronics*, 9:745–756, 1999. 38

[230] F. Schmidt, O. Sczesny, L. Reindl, and V. Mhgori. Remote sensing of physical parameters by means of passive surface acoustic wave devices ("ID-TAGS"). In *IEEE Ultrasonics Symposium*, pages 589–592, 1994. 38

[231] W.E. Bulst, G. Fischerauer, and L. Reindl. State of the art in wireless sensing with surface acoustic waves. *IEEE Transactions on Industrial Electronics*, 48(2):265–271, April 2001. 38

[232] G. Bruckner, R. Hauser, A. Stelzer, L. Maurer, L. Reindl, R. Teichmann, and J. Biniasch. High temperature stable saw based tagging system for identifying a pressure sensor. In *Proceedings of the 2003 IEEE International Frequency Control Symposium and PDA Exhibition, Jointly with the 17th European Frequency and Time Forum*, pages 942–947, 2003. 38

[233] L.M. Reindl and I.M. Shrena. Wireless measurement of temperature using surface acoustic waves sensors. *IEEE transactions on utrasonics, ferroelectrics, and frequency control*, 51(11):1457–1463, november 2004. 38

[234] S. Schuster, S. Scheiblhofer, L. Reindl, and A. Stelzer. Performance evaluation of algorithms for saw-based temperature measurement. *IEEE transactions on utrasonics, ferroelectrics, and frequency control*, 53(6):1177–1185, june 2006. 38

[235] R. Fachberger, G. Bruckner, R. Hauser, and L. Reindl. Wireless SAW based high-temperature measurement systems. 2006. 38

[236] H. Scherr, G. Scholl, F. Seifert, and R. Weige. Quartz pressure sensor based on saw reflective delay line. In *IEEE Ultrasonics Symposium*, pages 347–350, 1996. 38

[237] A. Pohl, G. Ostermayer, L. Reindl, and F. Seifert. Monitoring the tire pressure at cars using passive saw sensors. In *IEEE Ultrasonics Symposium*, 1997. 38

[238] A. Pohl and L. Reindl. Measurement of physical parameters of car tires using passive saw sensors. In *Advanced Microsystems for Automotive Applications Conference*, pages 250–262, 1998. 38

[239] H. Oh, W. Wang, K. Lee, I. Park, and S.S. Yang. Sensitivity improvement of wireless pressure sensor by incorporating a SAW reflective delay line. *International journal on smart sensing and intelligent systems*, 1(4):940–954, december 2008. 38

[240] A. Pohl, R. Steindl, and L. Reindl. The "intelligent tire" utilizing passive SAW sensors – mesurement of tire friction. *IEEE transactions on instrumentation and measurement*, 48(6):1041–1046, december 1999. 38

[241] J. Beckley, V. Kalinin, M. Lee, and K. Voliansky. Non-contact torque senseor based on saw resonators. In *IEEE International Frequency Control Symposium and PDA Exhibition*, pages 202–213, 2002. 38

[242] M. Dierkes and U. Hilleringmann. Telemetric surface acoustic wave sensor for humidity. *Advances in Radio Science*, 1:131–133, 2003. 38

[243] S. Schneid and H. Gieseler. Evaluation of a new wireless temperature remote interrogation system (TEMPRIS) to measure product temperature during freeze drying. *AAPS PharmaSciTech*, 9(3):729–739, september 2008. 38

[244] W. Buff, M. Rusko, M. Goroll, J. Ehrenpfordt, and T. Vandahl. Universal pressure and temperature SAW sensor for wireless applications. In *IEEE Ultrasonics Symposium*, pages 359–362, 1997. 39

[245] W. Buff, S. Klett, M. Rusko, J. Ehrenpfordt, and M. Goroli. Passive remote sensing for temperature and pressure using SAW resonator devices. *IEEE transactions on ultrasonics, ferroelectrics, and frequency control*, 45(5):1388–1392, september 1998. 39

[246] X Q. Bao, W. Burfhand an V.V. Varadan, and V.K. Varadan. SAW temperature sensor and remote reading system. In *IEEE Ultrasonics Symposium*, pages 583–585, 1987. 40

[247] A.Pohll, F.Seifert, L.Reind, G.Scholl, T. Ostertag, and W.Pietschl. Radio signals for saw id tags and sensors in strong electromagnetic interference. In *IEEE Ultrasonics Symposium*, pages 195–198, 1994. 40

[248] L. Reindl, G. Scholl, T. Ostertag, C.C.W. Ruppel, W.-E. Bulst, and F. Seifert. Saw devices as wireless passive sensors. In *IEEE Ultrasonics Symposium*, pages 363–367, 1996. 40

[249] A. Pohl and L. Reindl. Measurement of physical parameters of car tires using passive saw sensors. *Advanced Microsystems for Automotive Applications Conference*, pages 250–262, march 1998. 40

[250] F. Seifert, A. Pohl, R. Steindl, L. Reindl, M.J. Vellekoop, and B. Jakoby. Wirelessly interrogable acoustic sensors. *Joint Meeting EFTF-IEEE IFCS*, pages 1013–1018, 1999. 40

[251] L. Reindl. Wireless passive saw identification marks and sensors. *2nd Int. Symp. Acoustic Wave Devices for Future Mobile Communication Systems*, pages 1–15, march 2004. 40

[252] R.W. Brocato. Passive wireless sensor tags. *Sandia Report*, pages 1–20, march 2006. 40

[253] C.T. Allen, K. Shi, and R.G. Plumb. Characterization of a cooperative target for ground penetrating radar. 40

[254] A. Pohl, G. Ostermayer, L. Reindl, and F. Seifert. Spread spectrum techniques for wirelessly interrogable passive saw sensors. *IEEE Fourth International Symposium on Spread Spectrum Techniques and Applications*, pages 730–735, 1996. 42

[255] A. Springer, M. Huemer, L. Reindl, C.C. W. Ruppel, A. Pohl, F. Seifert, W. Gugler, and R. Weigel. A robust ultra-broad-band wireless communication system using saw chirped delay lines. *IEEE transactions on microwave theory and techniques*, 46(12):745–756, december 1998. 42

[256] W. Buff, F. Plath, 0. Schmeckebier, M. Rusko, T. Vandahl, H. Luck, F. Möller, and D.C. Malocha. Remote sensor system using passive saw sensors. In *IEEE Ultrasonics Symposium*, pages 585–588, 1994. 44

[257] U. Rösler, W. Ruile, K.Ch. Wagner, T.W. Johannes, G. Scholl, and R. Weigel. Energy distribution in a quartz resonator. In *IEEE Ultrasonics Symposium*, pages 1–4, 1996. 44

[258] A. Pohl, G. Ostermayer, and F. Seifert. Wireless sensing using oscillator circuits locked to remote high-q saw resonators. *IEEE transactions on ultrasonics, ferroelectrics, and frequency control*, 45(5):1061–1168, september 1998. 44

[259] T. Osterag and S. Kunzmann. Batteryless tire pressure monitoring systems with bulk acoustic resonators. *IQ-mobil Gmbh*, pages 1–9, september 2003. 44

[260] Y. Wen, P. Li, J. Yang, and M. Zheng. Detecting and evaluating the signals of wirelessly interrogational passive saw resonator sensors. *IEEE sensors journal*, 4(6), DECEMBER 2004. 44

[261] V. Kalinin. Influence of receiver noise properties on resolution of passive wireless resonant saw sensors. In *IEEE Ultrasonics Symposium*, volume 3, pages 1452–1455, 2005. 44

[262] M. Hamsch, R. Hoffmann, W. Buff, M. Binhack, and S. Klett. An interrogation unit for passive wireless saw sensors based on fourier transform. *IEEE transactions on ultrasonics, ferroelectrics, and frequency control*, 51(11):1449–1456, november 2004. 44

[263] C. Rauscher, V. Janssen, and R. Minihold. Fundamentals of spectrum analysis. In *Rohde & Schwartz*, 2001. 44

[264] S. Segars, K. Clarke, and L. Gourdge. Embedded control problems, thumb and the ARM7TDMI. *IEEE Micro*, pages 22–30, 1995. 46

[265] I.D. Avramov. The rf-powered surface wave sensor oscillator – a successful alternative to passive wireless sensing. In *IEEE International Frequency Control Symposium and PDA Exhibition Jointly with fhe 17 European Frequency and Time Forum*, pages 911–917, 2003. 46

[266] R. Matsuzakia and A. Todoroki. Wireless strain monitoring of tires using electrical capacitance changes with an oscillating circuit. *Sensors and Actuators A*, 119:323–331, 2005. 46

[267] T.E. Parker and G.K. Montress. Precision surface-acoustic-wave (saw) oscillators. *IEEE transactions on ultrasonics, ferroelectrics and frequency control*, 35(3):342–364, May 1988. 46

[268] T. Sadek and P.M. Smith. Low voltage saw oscillator. In *CCECE 2004 - CCGEI 2004*, pages 246–249, 2004. 47

[269] D. Hermelin, W. Daniau, J. Garcia, S. Ballandras, B. Belgacem, and M. Bruniaux. Analysis of inhomogeneous stress distribution in surface acoustic wave resonators. In *IEEE Frequency Control Symposium*, pages 81–84, 2008. 48

[270] D. Hermelin, W. Daniau, S. Ballandras, and B. Belgacem. Fabrication of surface acoustic wave wireless pressure sensor. In *IEEE Frequency Control Symposium joint with 22nd European Frequency and Time Forum*, pages 96–99, 2009. 48

[271] J.-M Friedt, T. Rétornaz, G. Martin, T. Laroche, J.-P. Simonnet, E. Carry, and S. Ballandras. Surface acoustic wave resonators as passive buried sensors. April 2009. 49

[272] S. Ballandras, G. Martin, and L. Fagot-Revurat. Method of remote interrogation of passive sensors. 2009. 53

[273] J.-M Friedt, C. Droit, G. Martin, and S. Ballandras. A wireless interrogation system exploiting narrowband acoustic resonator for remote physical quantity measurement. *Rev. Sci. Instrum.*, 2010. 53

[274] J.-M Friedt and G. Goavec-Merou. Interfaces matérielles et os libres pour nintendo ds : Dslinux et rtems. *GNU/Linux Magazine France Hors Série*, (43), august 2009. 64

[275] J.-M Friedt and E. Carry. Développement sur processeur à base de cœur ARM7 sous GNU/linux. *GNU/Linux Magazine France*, (117):40–59, June 2009. 64

[276] S. Guinot and J.-M Friedt. Gnu/linux sur playstation portable. *GNU/Linux Magazine France*, (114):30–40, Mars 2009. 64

[277] J.-M Friedt. Affichage et traitement de données au moyen de logiciels libres. *GNU/Linux Magazine France*, (111), December 2008. 64

[278] J.-M Friedt. Analyse des étiquettes d'identification par radiofréquence (rfid). *GNU/Linux Magazine France Hors Série*, (39), November-December 2008. 64

[279] J. Garcia and J.-M Friedt. Communication asynchrone et interface graphique portables sous qt. *GNU/Linux Magazine France Hors série*, (38), august 2008. 64

[280] T. Rétornaz and J.-M Friedt. Instrumentation scientifique reconfigurable. *GNU/Linux Magazine France Hors série*, (38), august 2008. 64

[281] J.-M. Friedt, A. Masse, and F. Bassignot. Les microcontroleurs msp430 pour les applications faibles consommations – asservissement d'un oscillateur sur le gps. *GNU/Linux Magazine France*, (98), October 2007. 64

[282] J.-M. Friedt. Géolocalistion de photographies numériques. *GNU/Linux Magazine France*, (96), July/August 2007. 64

[283] G. Weisenhorn, E. Pamba Capo-Chichi, and J.-M. Friedt. Communications de données et d'images issues de la carte fox par bluetooth. *GNU/Linux Magazine France*, (95), June 2007. 64

[284] J.-M Friedt. Introduction à la programmation sur PlayStation Portable. *GNU/Linux Magazine France*, (92), March 2007. 64

[285] J.-M Friedt and E. Carry. Prises de vues automatiques. *GNU/Linux Magazine France, Hors Série*, (27), October 2006. 64

[286] J.-M Friedt and É. Carry. Acquisition et dissémination de trames gps à des fins de cartographie libre. *GNU/Linux Magazine France, Hors Série*, (27), October 2006. 64

[287] S. Guinot and J.-M Friedt. Stockage de masse non-volatile : un block device pour multimediacard. *GNU/Linux Magazine France Hors Série*, 25, April 2006. 64

[288] S. Guinot and J.-M Friedt. La réception d'images météorologiques issues de satellites : utilisation d'un système embarqué. *GNU/Linux Magazine France Hors Série*, 24, February 2006. 64

[289] J.-M Friedt and S. Guinot. La réception d'images météorologiques issues de satellites : principes de base. *GNU/Linux Magazine France Hors Série*, 24, February 2006. 64

[290] J.-M Friedt and E. Carry. Enregistrement de trames gps – développement sur microcontroleur 8051/8052 sous gnu/linux. *GNU/Linux Magazine France*, 81, February 2006. 64

[291] J.-M Friedt and S. Guinot. Programmation et interfaçage d'un microcontroleur par usb sous linux : le 68hc908jb8. *GNU/Linux Magazine France Hors Série*, 23, November/December 2005. 64

[292] J.-M Friedt and S. Guinot. Introduction au coldfire 5282. *GNU/Linux Magazine France*, 75, September 2005. 64

[293] J.-M Friedt, S. Guinot, and E. Carry. Introduction au coldfire 5272. *GNU/Linux Magazine France*, 73:26–33, June 2005. 64

[294] Projet Aurore. Lancer d'un ballon sonde. *Bulletin de l'Union de Physiciens*, July-August-September:1317–1332, 2000. 64

[295] Projet Aurore. Films accélérés : méthodes d'acquisition et traitements. *Bulletin de l'Union de Physiciens*, March(842):543–550, 2002. 64

[296] J.-M Friedt. Introduction à la microbalance à quartz : aspects théoriques et expérimentaux. *Bulletin de l'Union de Physiciens*, 97(March):429–440, 2003. 64

[297] J.-M Friedt. Cartographie du potentiel électrostatique. *Bulletin de l'Union des Physiciens*, (864):691–703, May 2004. 64

[298] J.-M. Friedt, Q. Le Masne, N. Coq, and M. Myotte. Réalisation d'un profilomètre optique : introduction à la microscopie à sonde locale. *Bulletin de l'Union des Physiciens*, (861):265–277, February 2004. 64

[299] J.-M Friedt and S. Guinot. Introduction to uclinux: low cost embedded-device development environments. July 2005. 64

[300] G. Goavec-Merou, S. Guinot, and J.-M Friedt. Developing embedded devices using opensource tools: application to handheld game consoles. 2009. 64

[301] J.-M Friedt. Realization of an optical profiler: introduction to scanning probe microscopy. *American Journal of Physics*, 72(8):1118–1125, 2004. 64, 65

[302] J.-M Friedt. Satellite image eavesdropping: a multidisciplinary science education project. *European Journal of Physics*, 26:969–984, August 2005. 64

[303] E.C. Hall. *Journey to the Moon: the istory of the apollo guidance computer*. American Institute of Aeronautics and Astronautics, 1996. 66

[304] D.A. Mindell. *Digital Apollo – Human and Machine in Spaceflight*. MIT Press, 2008. 66

[305] C. Marlin, M. Griselin, É. Bernard, É. Delangle, D. Laffly, and J.-M. Friedt. Impact of climate conditions on the hydrological reponse of a polar glacier system. 2009. 66

[306] J.-M Friedt, C. Ferrandez, G. Martin, L. Moreau, M. Griselin, E. Bernard, D. Laffly, and C. Marlin. Automated high resolution image acquisition on polar regions (east loven, spitsbergen, 79^{o}n, west greenland, 69^{o}n). 2008. 68

[307] P.H. Kamp. A cheap SDR Loran-C frequency receiver. *www.freebsd.dk/AducLoran-0.0.pdf*, pages 1–13, 2008. 68

[308] K. Bonroy, J.-M. Friedt, F. Frederix, W. Laureyn, S. Langerock, A. Campitelli, M. Sára, G. Borghs, B. Goddeeris, and P. Declerck. Realization and characterization of porous gold for increased protein coverage on acoustic sensors. *Analytical Chemistry*, 76(15):4299–4306, 2004. 74

[309] E. Mboungou, C. Mavon, J.-M. Friedt, C. Bergeon, and M. Fromm. Impact of water content on the electrical behavior of epoxy insulators. *IEEE Transactions on Dielectrics and Electrical Insulation*, 15(2):311–318, 2008. 74